A THREE-DIMENSIONAL MODEL OF ATMOSPHERIC CO_2 TRANSPORT BASED ON OBSERVED WINDS: 4. MEAN ANNUAL GRADIENTS AND INTERANNUAL VARIATIONS

Charles D. Keeling and Stephen C. Piper
Scripps Institution of Oceanography, La Jolla, California, 92093, U.S.A.

Martin Heimann
Max-Planck-Institut fur Meteorologie, Bundesstrasse 55
D-2000 Hamburg 13, FRG

Abstract. The spatial and temporal distribution of atmospheric carbon dioxide and its $^{13}C/^{12}C$ ratio have been simulated with a three-dimensional transport model which predicts variations on time scales from synoptic to annual. This paper describes the results of model simulations of the mean annual fields of CO_2, on the assumption that the carbon cycle has no time variations longer than 1 year. Interannual variations are addressed, however, by defining a series of four quasi-stationary states which characterize the average nonseasonal cycle for four historical periods: 1962, 1968, 1980, and 1984. Meridional variations predicted by the model for these periods are compared with observational data obtained from an array of stations extending from the Arctic to the South Pole. An adjustable parameter in the model controls the predicted average release of CO_2 by the tropical oceans, and another the uptake of CO_2 by the north Atlantic Ocean. These two parameters are globally adjusted to achieve an optimal fit of the model predictions to the observations of CO_2 concentration. Good fits are realized under a variety of assumptions about the strengths and locations of sources and sinks of the terrestrial biosphere, indicating that the model is not closely constrained on the basis of CO_2 concentration data alone. The model's prediction of the $^{13}C/^{12}C$ ratio of atmospheric CO_2 is acceptable, however, only if the prescribed net terrestrial biospheric exchange at high northern latitudes is overshadowed by the postulated oceanic sink in the North Atlantic. By far the largest contributor to meridional variations in both concentration and $^{13}C/^{12}C$ ratio is the combustion of fossil fuels, 95 percent of which are injected into the northern hemisphere. The build-up of CO_2 in the northern hemisphere in response to this injection is clearly seen in the comparison of the historical profiles which cover a period in which the injection doubled from 2.6 to 5.3×10^{12} kgC yr^{-1}. In contrast, the model predictions of the adjustable oceanic sources and sinks vary by less than 0.4×10^{12} kgC yr^{-1} from their mean value from one historical period to another, suggesting only relatively minor changes in these natural exchanges of CO_2 from 1962 to 1984.

1. Introduction

1.1 Methodology

Atmospheric carbon dioxide concentrations vary on time scales longer than 1 year owing to interannual imbalances between reservoirs of the carbon cycle that transfer carbon to and from the atmosphere. Some of these imbalances are natural, but others are perturbations caused by human activity, notably, but not solely, the combustion of fossil fuels. Interannual variations in atmospheric CO_2 become evident after persistent seasonal oscillations and shorter-term variations are removed from the records of observations. When such filtered records are compared for different locations, persistent spatial gradients in atmospheric CO_2 are also seen. These gradients, however, not only reflect interannual imbalances in the carbon cycle, but also reflect the interplay of seasonally varying balanced sources and sinks of atmospheric CO_2 with the seasonally varying atmospheric transport of CO_2 caused by variable winds and mixing.

Isotopic measurements aid in identifying the causes of longer-term variations in atmospheric CO_2 as they aid in the analysis of the seasonal oscillation of CO_2 [Heimann et al., this volume], because the transfers of CO_2 between the terrestrial biosphere and the atmosphere display a much stronger preference for the abundant isotope, ^{12}C, over the rare isotope, ^{13}C, than do transfers involving the oceans. As a consequence land plant carbon produces an isotopic signal distinct from that produced by oceanic carbon.

In this article we seek to explain the mean annual distribution of atmospheric CO_2 as a first approach to investigating interannual variations in the carbon cycle. Our simulation of the CO_2 distribution is carried out by means of an atmospheric tracer model, described in detail in an accompanying article by Heimann and Keeling [this volume]. In this model atmospheric CO_2 is advected by a three-dimensional time dependent wind field and is mixed vertically by convection, while fluxes of CO_2 at the earth's surface are specified on a two-dimensional grid. To simplify our analysis, we assume that fluxes representing natural atmospheric CO_2

sources and sinks, both seasonal and nonseasonal, are exactly balanced over the course of 1 year. Included in this category are the net primary productivity (NPP) and heterotrophic respiration of the terrestrial biosphere and air-sea exchange of CO_2 arising from natural processes occurring in the oceans. The natural terrestrial fluxes of CO_2 and seasonal oceanic exchange are locally balanced. Natural nonseasonal oceanic exchanges, which transfer CO_2 via the atmosphere from one oceanic region to another, are globally balanced.

Superimposed on this assumed steady state are perturbational fluxes induced by human activities. The model prescribes industrial CO_2 emissions from fossil fuel combustion and cement manufacture and several smaller perturbations:

(1) the release of CO_2 by the terrestrial biosphere owing to land use changes and deforestation which we call "biosphere destruction",
(2) stimulated uptake of CO_2 by plants owing to increasing atmospheric CO_2 or other causes, which we call "biospheric fertilization," and
(3) the air-sea exchange of CO_2 which occurs in response to these perturbations.

We consider only perturbations which vary so slowly from year to year that they may be realistically introduced into the model as constants or, in the case of industrial CO_2, as a seasonally varying but annually invariant flux. We thus ignore natural phenomena, such as El Niño events, that cause marked short-term interannual fluctuations in the carbon cycle. We take account of more slowly varying interannual imbalances, however, by simulating the cycle for selected time intervals near 1962, 1968, 1980, and 1984, as though during each interval the cycle were at steady state. The seasonal cycle in CO_2, as portrayed in the model, is prescribed with constant phasing, but with a small globally averaged increase in amplitude from one historical period to the next. The globally integrated fluxes associated with these perturbations are based on a study using a compartment model and on a data analysis, both described in the accompanying article of Keeling et al. [this volume].

Both the balanced sources and sinks, and those arising from perturbations, are divided into source components, eleven altogether. For each component the three-dimensional tracer model was run by cycling over the model year, with the atmospheric motion repeated, until the annual increase or decrease in CO_2 concentration at each grid point attained an almost constant value from year to year. The mathematical linearity of the model's transport equation permits the model solutions of the individual source components to be superimposed, so as to produce a composite model solution which serves as a prediction of the actual distribution of CO_2 concentration. From this composite we have produced the mean annual concentration fields used in the present study. Seasonal and synoptic variations are considered in an accompanying article by Heimann et al. [this volume].

The observations of atmospheric CO_2, which we compare with the model predictions, were obtained principally from an array of land-based stations which lie approximately on a north-south line within the Pacific Ocean basin from the Arctic Ocean to the South Pole (Figure 1), supplemented by samples collected on ships. We compare our model predictions directly with the observed concentrations and isotopic ratios of CO_2 with due regard to geographic location and altitude of each observing station. We thus avoid

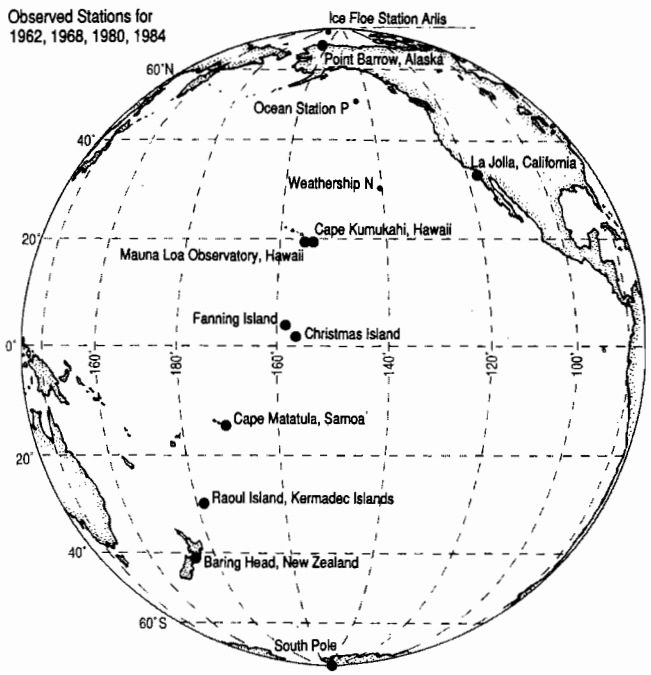

Fig. 1. Locations of air sampling stations on land and over water. Location of Ice Floe Station Arlis is approximate.

assuming that CO_2 observations at these stations are either zonally or vertically representative, as is necessary when studying the carbon cycle using one or two-dimensional transport models. We assume, however, that the shipboard data, which are widely distributed within the Pacific Ocean basin for the historical periods 1962 and 1968, apply to the longitudes of the transects connecting the land stations.

The strengths of three poorly known model source components, one seasonal and two nonseasonal, were adjusted via global factors so that the model predictions agree in a least squares sense with the atmospheric observations at selected stations. In predicting isotopic profiles no additional adjustments were made, except to specify a globally constant reference isotopic ratio. Because locally balanced seasonal source components of the model contribute to gradients in the mean annual concentration and because constant source components generate small seasonal signals, the global adjustment of the seasonal predictions to the data is not independent of the nonseasonal adjustments. As explained by Heimann and Keeling [this volume], we used an iterative procedure to produce a satisfactory convergence of the magnitudes of the three adjustable source components. The same adjustments were used in simulating the seasonal cycle of CO_2 [Heimann et al., this volume].

Three important, but poorly established, features of the tracer model had to be prescribed without adequate information. One of these is the strength of the subgridscale vertical convection representing all vertical mixing processes not explicitly resolved on the grid of the model. The original convective matrices, derived from a general circulation model, produce too small an attenuation of the seasonal cycles with height. On this account

Heimann and Keeling [this volume] reduced the matrices globally to 0.50 of their original values. As a standard case we have retained this reduced convection in simulating the mean annual field of atmospheric CO_2. As a sensitivity case we repeated each simulation with the matrices reduced to 0.25 of their original values. The three adjustable source components were refit to produce optimal agreement again of model predictions with the observations.

A second poorly established feature is the rate of exchange of CO_2 gas at the air-sea interface, expressed by a gas exchange coefficient, k_{ex}. In the standard case this coefficient is assumed to be a constant. We repeated each simulation of the oceanic source components of the model with the coefficient prescribed to vary both seasonally and spatially as a function of wind speed and sea surface temperature.

Finally, the interhemispheric exchange time of the model appears to be too large when tested with the distribution of chemically inert tracers such as krypton-85, as noted by Heimann and Keeling [this volume, subsection 3.1]. In the standard case this exchange time is determined in the model solely from the strengths of the time varying wind fields and the subgridscale vertical convection. As a sensitivity case we repeated each simulation with explicit horizontal diffusion introduced into the model, coupled to vertical convection in the same way as described by Prather et al. [1987]. Because of the nearly additive effects of air-sea exchange and horizontal diffusion on the CO_2 fields predicted for the oceanic components, we carried out further simulations in which both horizontal diffusion and variable air-sea exchange were included in the model formulation.

1.2 Previous Investigations

The main qualitative features of the earth's natural carbon cycle have been described extensively in the geochemical literature. The cycle is generally understood to encompass the interactive flows of carbon which occur between storage "pools" or "compartments" of the earth's environment in response to physical, chemical, and biological processes. Because the cycle, in its details, is exceedingly complex, attempts to describe it have tended to focus on only a limited selection of such compartments and processes.

The cycle, averaged over geological time scales, was depicted more than 30 years ago by Rankama and Sahama [1950, p. 536] and by Goldschmidt [1954, p. 533]. These authors identified highly generalized compartments such as "CO_2 in the atmosphere" and "carbonate rock" and they indicated the pathways of fluxes between such compartments. As more quantitative information has become available, the magnitudes of these fluxes and the amount of carbon stored in each compartment have been repeatedly revised [for example, by Garrels et al., 1975, p. 74].

Studies which have focused on the carbon cycle of the terrestrial biosphere or of the oceans typically have subdivided these compartments to permit more detailed descriptions. Short-term contemporary aspects of the cycle as well as aspects on geological time scales have been examined [see, for example, Bolin et al., 1979, p. 4 and Bolin, 1986, p. 94]. Matrices of coefficients have been introduced to identify a large variety of time scales and subdivisions and to facilitate mathematical modeling of the cycle, for example, by Sundquist [1985].

Until about 30 years ago studies of the carbon cycle were mainly concerned with defining average, approximately steady state, conditions. Since then, attention has gradually turned toward the analysis of perturbations, both within the cycle itself and generated externally [see, for example, Eriksson and Welander, 1956; Revelle and Suess, 1957; Broecker et al., 1971; Skirrow, 1975; Keeling et al., this volume].

In most studies of the carbon cycle the atmosphere has been treated as a single carbon pool, even if the terrestrial biosphere or oceans were subdivided. This is because the small spatial variations in mixing ratio of atmospheric CO_2 scarcely influence the strengths of the CO_2 fluxes between the air and subcompartments of the biosphere, oceans and lithosphere. Also, this neglect was almost a necessity as long as measurements of atmospheric CO_2 were only precise enough to define globally averaged values.

In the early 1960's, with more extensive and precise CO_2 data available, Junge [1962] showed that, if the atmosphere is characterized by two compartments divided at the equator, and if account is taken of the average interhemispheric difference in atmospheric CO_2 concentration, he could estimate the rate of exchange of air between the northern and southern hemisphere. The next year Bolin and Keeling [1963] addressed the mean annual spatial distribution of atmospheric CO_2 using a one-dimensional north-south model of transport. Their analysis, and a subsequent one-dimensional study by Junge and Czeplak [1968], made use of extensive atmospheric CO_2 observations which, incidentally, also comprise the first historical data set of the present study. Except for an adaptation to atmospheric CO_2 of a two-dimensional chemical pollution model briefly reported by Machta [1974], the next attempt to model atmospheric CO_2 spatially awaited the development of a comprehensive two-dimensional north-south and vertical transport model by Pearman and his coworkers [Hyson and Pearman, 1980]. In a series of papers [Hyson et al., 1980; Pearman et al., 1983; Pearman and Hyson, 1986] they repeatedly refined their model to produce ever better comparisons to the observed north-south profile in atmospheric CO_2.

Recently Keeling and Heimann [1986] reverted to the use of a one-dimensional north-south transport model to examine changes occurring in the mean annual north-south profile of atmospheric CO_2 between the years 1962 and 1980. More recently, in a preliminary version of the present study, Heimann et al. [1986] compared observations made near the year 1980 with the prediction of a three-dimensional transport model developed by Fung et al. [1983]. The model employed in the present study is identical to this previous three-dimensional model, except that the wind fields there were derived from a general circulation model (GCM) and here are based on direct observations.

1.3 Order of Presentation

Below, in section 2, we describe the source components of the model and the mean annual atmospheric CO_2 fields that the model simulates for each component. We also discuss the probable atmospheric mechanisms that produce the predicted patterns in the CO_2 fields for some of the individual source components. Then in section 3 we briefly discuss the atmospheric data used in our analyses, and in section 4 we compare the model results to these data, including an analysis of possible errors and of the sensitivity of the model predictions to such errors. In section 5 we give examples of

how the model may elucidate mechanisms underlying major oceanic and biospheric CO_2 fluxes, and in section 6 we relate the model results to general concepts of the carbon cycle. Finally, in section 7 we draw some conclusions regarding our success in modeling the carbon cycle in three dimensions.

Where appropriate we will reference the accompanying articles using abbreviations: I for Keeling et al., II for Heimann and Keeling, and III for Heimann et al. For example, I.6.4 will refer to subsection 6.4 of Keeling et al. [this volume]. Readers principally interested in the comparison of the three-dimensional model predictions with observations need not read, or may defer reading, the descriptions of model components in subsections 2.3 through 2.7, especially the lengthy description in subsection 2.3.

2. Simulated Sources and Sinks

2.1 Time Decomposition of Model Results for Concentration and Isotopic Ratio

The fully time dependent CO_2 concentration field predicted by the model is composed of a set of component fields, discussed individually below. Each composite field is expressed with respect to time, t, and location $\mathbf{x}$ ($\equiv x,y,z$ the three Cartesian space coordinates) by the function [cf. II.4.1, equation (4.2)]

$$C_{CMPS}(\mathbf{x},t) = C_o + \sum_{i=1}^{n} C_i(\mathbf{x},t) \tag{2.1}$$

where $C_i(\mathbf{x},t)$ denotes the component field (daily CO_2 concentration) corresponding to a single source component, i, and C_o denotes a constant background concentration, representing the mean annual surface concentration at the South Pole. Concentrations are expressed in parts per million of dry air by volume (ppm).

Each component field, as well as each composite field, was subsequently decomposed into four parts in order to facilitate the discussion of the simulation results in terms of the different time scales represented by the model. For the field of component i we write for this decomposition

$$C_i(\mathbf{x},t) = a_{ti} \cdot t + C_{i\,mean}(\mathbf{x}) + C_{i\,seas}(\mathbf{x},t) + C_{i\,syn}(\mathbf{x},t) \tag{2.2}$$

Here $a_{ti} \cdot t$ denotes a linear trend in time, independent of location, and $C_{i\,mean}(\mathbf{x})$ a time-independent mean annual concentration field. The final two terms represent seasonal and synoptic scale time variations, respectively, within the year of the model run. The seasonal dependency of each component is expressed by a periodic function with an annual fundamental and three harmonics. This decomposition was achieved at every gridpoint [see III.5.1].

When the model for any component is run starting with an initially uniform zero concentration field, the term $a_{ti} \cdot t$ closely approaches a single value for all grid points of the model by the fourth year of the model run. We thus take this fourth model year as being quasi-stationary. For each of the balanced sources, $a_{ti} \cdot t$ is zero within the numerical precision of the model. The composite sum, $\sum_{i=1}^{n} a_{ti} \cdot t$, was found to be 1.32 ppm yr^{-1} for the year 1980. This value reflects the specified globally integrated sum of all source components, hence it provides a global check on the numerical precision of the model calculation.

The carbon contained in, and transferred between, the atmosphere and other reservoirs of the carbon cycle consists of approximately 99 percent of the light isotope carbon-12 and 1 percent of the heavier isotope carbon-13. Owing to isotopic fractionation, the ratios of these two isotopes vary in atmospheric CO_2 as a function of time and space, as shown by the data assembled by Keeling et al. [I.2]. It would be possible to regard the atmospheric fields of the concentration of each isotope separately, both with respect to observations and to modeling predictions, but we discern more readily the influence of isotopic fractionation on the carbon cycle by considering the field of the $^{13}C/^{12}C$ ratio, especially when we consider individual component fields separately. Except for an isotopic transfer arising from the dependence of air-sea exchange of CO_2 on temperature, the $^{13}C/^{12}C$ ratio field for each model component can be computed indirectly from the concentration field using appropriate factors [see II.5, Table 8] without additional computer runs.

In accordance with standard practice in isotopic studies we express both isotopic observations and model predictions in terms of the reduced isotopic ratio

$$^{13}\delta = r/r_s - 1 \tag{2.3}$$

where r and r_s denote the $^{13}C/^{12}C$ ratio for the sample and for a standard, respectively [see II.5.1, text following equation (5.3)]. Henceforth we will omit the left subscript 13 on δ [see II.5.1 and III.5.3].

As in the case of CO_2 concentration (equation 2.1) we define a composite isotopic field of atmospheric CO_2 by

$$\delta_{CMPS}(\mathbf{x},t) = \delta_o + \sum_{i=1}^{n} \delta_i(\mathbf{x},t) \tag{2.4}$$

Analogous to equation (2.2) for CO_2 concentration, we decompose the isotopic field of each component i into four parts

$$\delta_i(\mathbf{x},t) = b_{ti} \cdot t + \delta_{i\,mean}(\mathbf{x}) + \delta_{i\,seas}(\mathbf{x},t) + \delta_{i\,syn}(\mathbf{x},t) \tag{2.5}$$

where $b_{ti} \cdot t$ denotes a linear trend of δ in time and the subscripts have the same meaning as for concentration.

The main objective of this article is to compare the individual mean annual component fields, $C_{i\,mean}(\mathbf{x})$ and $\delta_{i\,mean}(\mathbf{x})$, and the composite mean fields

$$C_{mean}(\mathbf{x}) = C_o + \sum_{i=1}^{n} C_{i\,mean}(\mathbf{x}) \tag{2.6}$$

and

$$\delta_{mean}(\mathbf{x}) = \delta_o + \sum_{i=1}^{n} \delta_{i\,mean}(\mathbf{x}) \tag{2.7}$$

with corresponding observations of atmospheric CO_2 represented by the smoothed seasonally adjusted data, $C_{obs\,rem}(\mathbf{x})$, and $\delta_{obs\,rem}(\mathbf{x})$ as derived from the original observations reported by Keeling et al. [I.2]. The time dependent terms, $C_{i\,seas}(\mathbf{x},t)$, $\delta_{i\,seas}(\mathbf{x},t)$, $C_{i\,syn}(\mathbf{x},t)$, and their composites, were addressed in the preceding article of Heimann et al. [this volume]. Observational data are lacking to consider $\delta_{i\,syn}(\mathbf{x},t)$. Henceforth, to simplify the terminology, we will refer to $C_{obs\,rem}$ and $\delta_{obs\,rem}$ as "observed C_{mean}" and "observed δ_{mean}", respectively.

2.2 *Modeling Strategy*

Our aim is to simulate the nonseasonal atmospheric CO_2 cycle as it existed during four time intervals, here called "historical periods". They each extend over two calendar years: 1961–1962, 1967–1968, 1979–1980, and 1983–1984, and are referred to elsewhere in the text as year "1962", etc. They are regarded as applying to January 1 both with respect to the model simulations and observational data, except for the year 1984 when the observational data apply to a central date of May 15 [I.2.3]. We ignore the small discrepancy of 4½ months in comparing seasonally adjusted model results with observations for this final historical period.

The natural fluxes arising from the activity of terrestrial vegetation and air-sea interaction and the spatial characteristics of the superimposed perturbation fluxes are prescribed in the model on the basis of a variety of data previously discussed [II.4.3]. They are summarized and further specified in subsections 2.3 and 2.4 below.

The global integrals of the perturbation fluxes, including their isotopic composition, are prescribed *a priori* by a carbon cycle compartment model, called the "box diffusion" model [I.5], that specifies atmospheric CO_2 and terrestrial biospheric carbon as single uniform chemical pools, while inorganic carbon in the oceans is assumed to reside in a uniform surface water layer which exchanges carbon with a vertically diffusive subsurface layer. The fluxes of carbon between these pools, arising from perturbations in the carbon cycle, are computed for the whole industrial era. These fluxes have been introduced into the three-dimensional model as time-invariant global average sources and sinks for each of the four historical periods under investigation.

Because each perturbation flux is distributed regionally with a fixed pattern irrespective of its global integral, only one computer run was needed to establish the spatial variability of the CO_2 concentration field which it produces. This field was afterwards adjusted for each historical period by a single global factor, set to be consistent with the associated flux derived from the compartment model [II.4.6, Table 6]. The corresponding isotopic field for each component was then computed, taking into account the degree of isotopic fractionation associated with that component [II.5.5, Table 8].

The model predictions for each component, $C_i(\mathbf{x},t)$ and $\delta_i(\mathbf{x},t)$, as explained in section 2.1, contain the seasonal variations used in the study of Heimann et al. [this volume] as well as predictions of the mean annual fields. It is only for convenience that these aspects of the outputs are discussed in separate articles. In the subsections that follow we briefly review the composition of each source component, the mean annual atmospheric fields which it predicts, and some immediate implications of these predictions. Additional details regarding model formulation are given by Heimann and Keeling [this volume]. The same source components are discussed by Heimann et al. [this volume] from the point of view of seasonal variations.

2.3 *Exchanges of CO_2 with the Terrestrial Biosphere*

2.3.1 Seasonal exchange. Two components in the model depict aspects of the natural, unperturbed seasonal activity of the terrestrial biosphere: one with the uptake of CO_2 by plants (net primary productivity, or "NPP"), the other with the release of CO_2 by plant decomposition (mainly heterotrophic respiration, which we will simply call "respiration"). NPP is locally specified from remote sensing data of plant growth derived from data of a radiometer mounted on an earth-orbiting satellite [II.4.3.1]. Respiration is specified as a function of monthly averaged air temperature at the surface [II.4.3.2]; its annual integral is set equal to that for NPP for each grid box of the model. An adjustable global parameter, v_{RES} [see II.4.5, equation (4.3.2)], specifies the sensitivity of respiration to temperature; it is determined by a weighted fit of the model simulated concentrations for the sum of all source components to the observed seasonal variation in CO_2 concentration at four observing stations in the northern hemisphere: Point Barrow, Alaska; Ocean Station P; La Jolla, California; and Cape Kumukahi, Hawaii.

Monthly mean NPP and respiration were initially specified as gC (grams of carbon) m^{-2} yr^{-1}. For each grid box they were then multiplied by the associated land area to produce monthly average fluxes to or from the atmosphere. The annual integrals for NPP and respiration each were assumed to change from year to year such that for 1962 both were reduced to 88.5 percent of the corresponding values for 1980, in 1968 to 92.3 percent, and in 1984, raised to 102.8 percent. These adjustments are consistent with variations in the amplitude of the seasonal cycle of atmospheric CO_2 observed at Mauna Loa Observatory, Hawaii [I.4.1]. Our assumption that the annual integrals of NPP and respiration have increased in proportion to an increase in seasonality is probably an exaggeration for the tropics or even generally, but it is a convenient basis for insuring that the model predicts the observed variation in amplitude of the seasonal cycles of atmospheric CO_2. The annual field of NPP for 1980 is shown by Heimann and Keeling [II.4.6, Figure 12].

Because of time variations prescribed in the transport terms of the model, the seasonal variations in NPP and respiration contribute appreciably to the model simulated mean annual CO_2 concentration, C_{mean}. This is illustrated in Figure 2 for the mean component field produced by the sum of NPP and respiration in the lowest atmospheric layer of the model ("level 1") in 1980. Figure 3 is a similar plot at an elevation of about 6 km (200 hPa pressure height, model "level 7").

The mean component fields of C_{mean} at the two levels are strikingly different. At the upper level, the CO_2 concentration varies mainly with latitude, generally diminishing northward. The concentration is everywhere negative with respect to the mean component concentration generated for the lowest atmospheric layer at the South Pole. In contrast the concentration near the earth's surface is generally higher than at the South Pole, especially in the northern hemisphere where the seasonal cycles of NPP and respiration are pronounced. The lower field exhibits large scale variations east-west, as well as north-south, and also shows smaller scale patches of high and low concentration over the continents. To some degree such patches also appear aloft. The contrasting concentrations in the upper and lower levels of the atmosphere can also be seen in a zonally averaged vertical north-south cross-section (Figure 4).

Seasonal variations in vertical motion at least partially explain the high CO_2 predicted near the ground and the low CO_2 aloft. During the spring and summer the sun's radiation is above average intensity. This circumstance promotes both plant growth and warming of the air near the ground. Plant growth depletes CO_2,

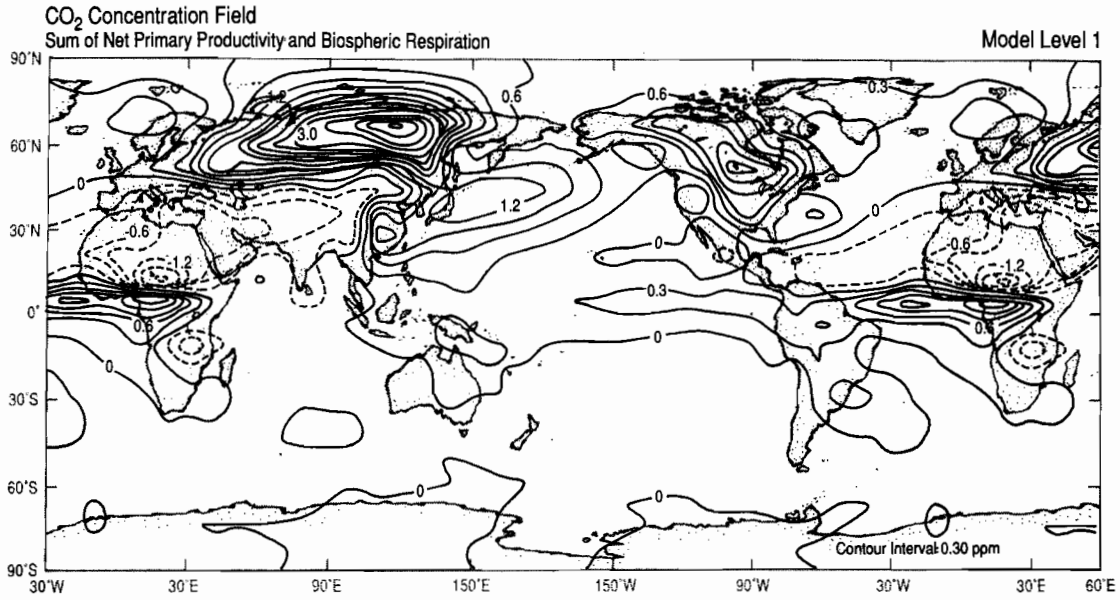

Fig. 2. Contour map of the mean annual CO_2 concentration field generated by the sum of the model source components for net primary productivity and respiration of the terrestrial biosphere for the year 1980 at model level 1 (global mean pressure 959 hPa). Contour lines are labeled in ppm. Solid lines indicate positive or zero concentration differences from that of the South Pole. Dashed lines indicate negative differences. The field from 30°W. to 60°E. is repeated as an aid to discerning patterns.

while warming promotes rising air not only locally during the daytime but generally over the continents. The air aloft, therefore, also tends to be depleted in CO_2. In autumn and winter, when the sun's radiation is below average, respiration predominates over NPP and enriches CO_2 near the ground. Also, as a result of cooling, the air near the ground tends to become more stable, often with a temperature inversion. Vertical mixing is reduced, further promoting a buildup of CO_2. Because the continents, in winter, on average tend to be cooler than the ocean surface, continental air tends to sink and be replaced laterally aloft by air previously over the oceans, air which has not been appreciably enriched in CO_2 even at the lowest levels.

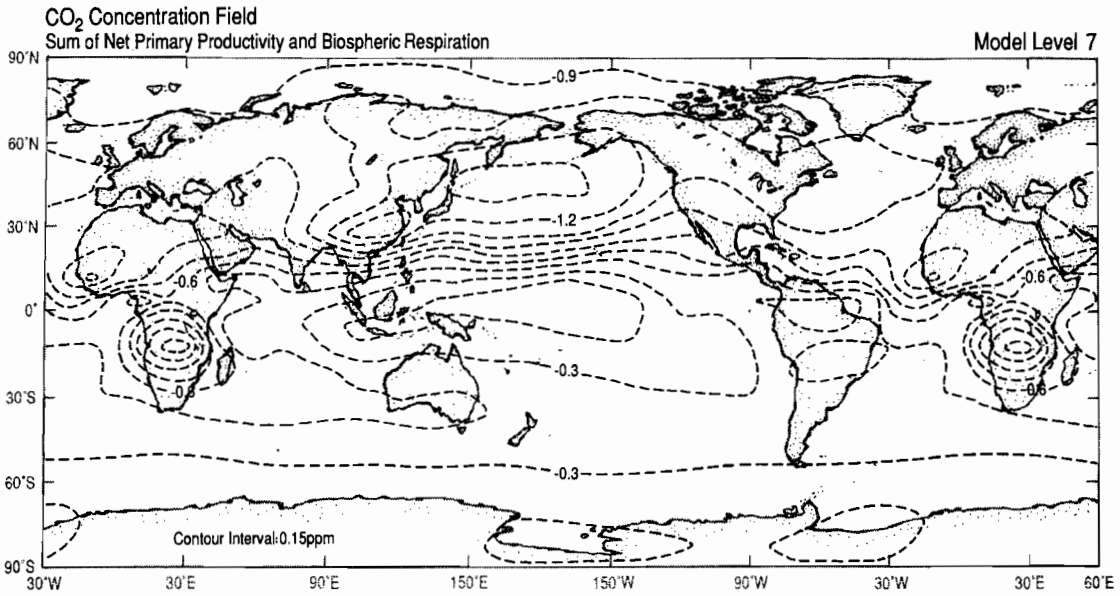

Fig. 3. Same as Figure 2 but at model level 7 (global mean pressure 201 hPa). Concentration differences are with respect to the South Pole at model level 1.

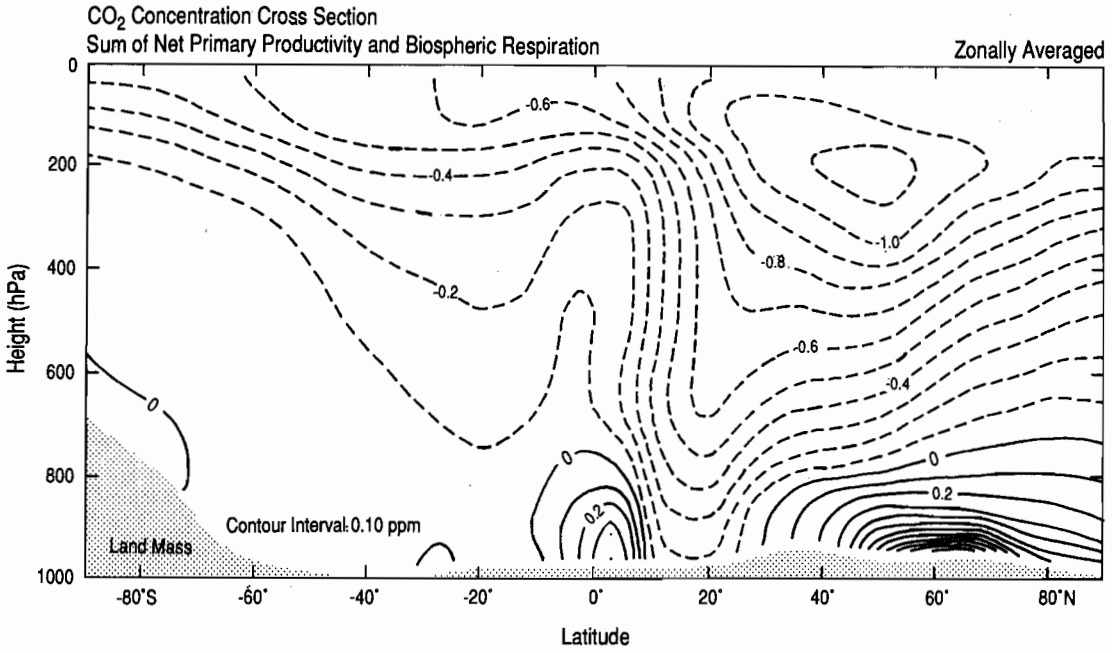

Fig. 4. Meridional-vertical cross-section of the zonally averaged mean annual CO_2 concentration field generated by the sum of the model source components for net primary productivity and respiration of the terrestrial biosphere for the year 1980 expressed as differences from the concentration at the South Pole. Contour lines are labeled in ppm. Solid and dashed lines are defined as in Figures 2 and 3.

The combination of these summer and winter effects is to promote higher CO_2 concentrations, on annual average, near the ground and lower concentrations aloft, especially over the continents. But even over the oceans the CO_2 aloft is predicted, on annual average, to be depleted in concentration because of vigorous lateral mixing with air from high altitude over the land. The vertical gradients of the annual mean field are more pronounced in the northern hemisphere where the great temperate and boreal land masses strongly support seasonal NPP and respiration.

A striking model prediction of the influence of seasonally varying vertical motion in the production of low CO_2 aloft is found near 15°S. over Africa where a pronounced patch of low CO_2 concentration appears at level 7 in association with rising air (see Figure 3). This rising air induces a divergent flow field aloft as indicated in Figure 5 by anticyclonic, divergent, upper level streamlines during the southern summer season when plants, on net, are removing CO_2 from the air near the ground and propagating low CO_2 aloft. During the opposite season, when CO_2 is high near the ground, such divergent motion is absent (Figure 6). In addition to the large scale vertical motion as inferred from the horizontal flow field, smaller scale vertical mixing exhibits a seasonal cycle, with maximum convective activity in the summer months, thus reinforcing the aforementioned transport effect.

There are close similarities between the pattern of the mean field of CO_2 at level 7 (Figure 3) and of the seasonal amplitude of CO_2 [III.5.3, Figure 20], including propagation of the feature over the south Indian Ocean. A similar, though weaker, association of minimal CO_2 with divergent, upper level air motion in the southern hemisphere summer season is seen over southern Brazil (Figure 3, near 20°S., 60°W.). In the northern hemisphere minimal CO_2 concentrations are found close to the west coast of Africa (near 15°N., 10°W.) and in a vast region extending from China eastward over the Pacific Ocean. Here, the upper level flow field is divergent during the northern hemisphere summer months (Figure 6). No such features, however, are obvious over the Americas or Australia, either in the predicted CO_2 field or in the air stream flow.

In the lower atmosphere, as shown in Figure 2, the sum of the mean component fields of NPP and respiration, predicted by the model, shows high CO_2 concentrations in regions of strong winter cooling centered in Siberia and Canada. A sharp gradient separates high concentrations over Siberia with much lower concentrations over southern Asia, approximately along a line marking the northern limit of the monsoon circulation. This subtropical region of low predicted CO_2 extends westward across Africa, southern Europe, and the Atlantic Ocean and narrowly connects to a small region of low concentration over Mexico. The latter feature extends weakly into the tropical Pacific Ocean. To the south of this extensive region of low CO_2 is a narrow, nearly east-west oriented band of high CO_2, strongly developed over the eastern Atlantic Ocean, weakly developed over South America and the Pacific Ocean, and almost completely absent over the Indian Ocean. Further to the south, we find again a zone of low surface CO_2 concentration in the subtropical region, which is, however, weaker than its northern hemisphere counterpart.

The narrow band of high CO_2 near the equator is at least partially, perhaps almost entirely, explained by the meridional component of the tropical circulation as portrayed for each season in the four panels by Heimann and Keeling [II.2, Figure 1] and as an

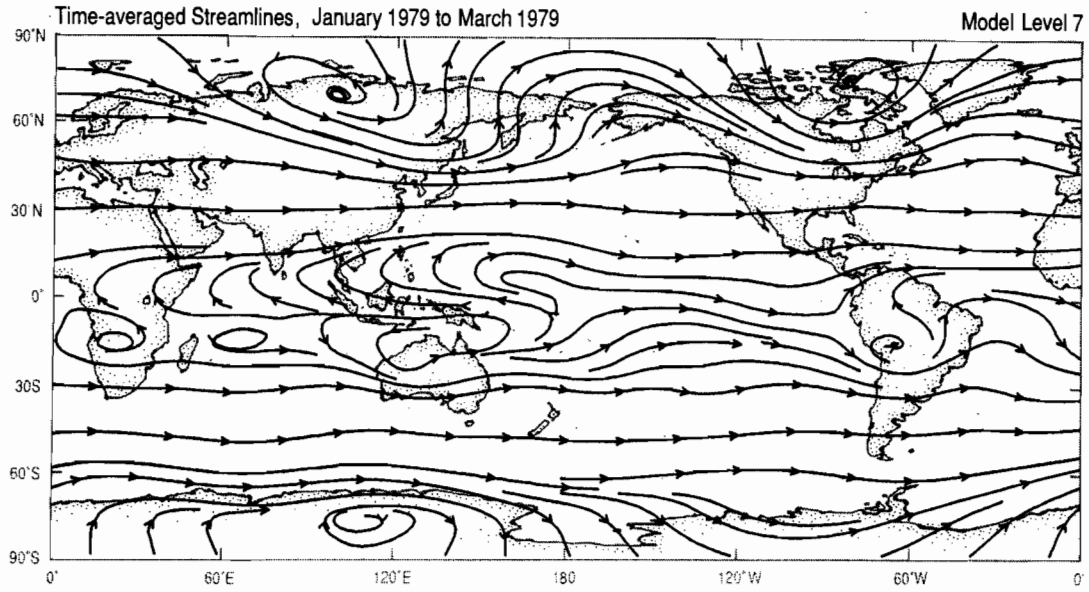

Fig. 5. Streamlines of the horizontal wind used in the three dimensional model at model level 7, averaged for January through March.

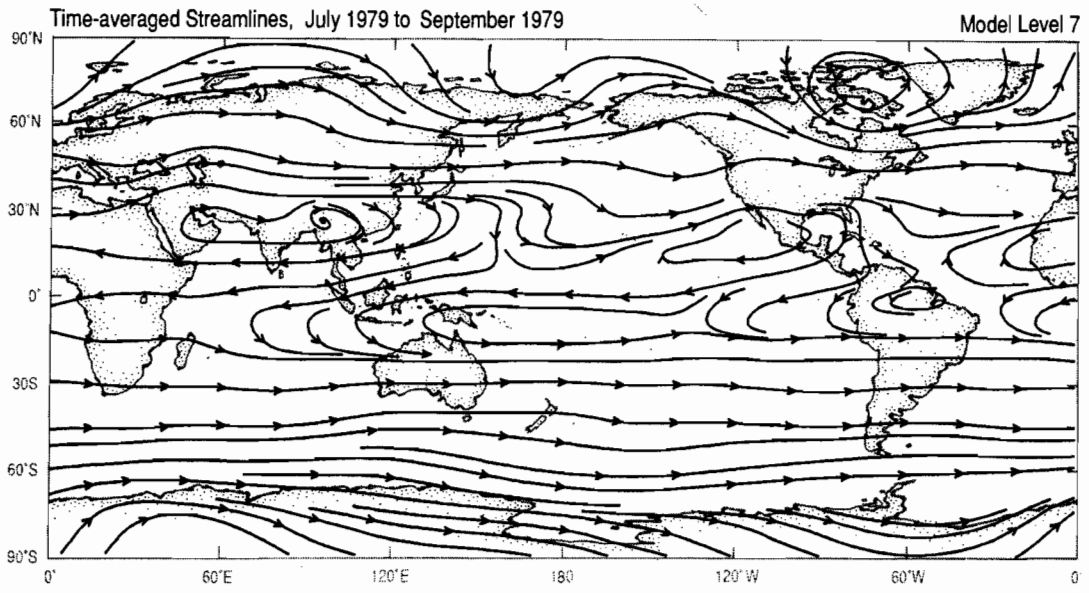

Fig. 6. Streamlines as in Figure 5 but averaged for July through September.

annual mean in Figure 7. This so-called "Hadley circulation" consists of one or two cells of rising and descending air near the equator which migrate north and south and change strength with the seasons. The interception of the fluxes produced seasonally by the terrestrial biosphere with this Hadley circulation strongly affects the mean annual concentration fields generated by seasonally varying NPP and respiration, especially over the oceans where perturbing influences of strongly heated and cooled land surfaces are minimal. In summer and winter, as explained by Heimann et al. [1986, p. 38] only one meridional cell is well developed, and this cell is oriented so that the air in its lower part is flowing towards the summer hemisphere. The winter hemisphere is relatively enriched in CO_2 because of the phase of the biospheric seasonal cycle, hence the lower branch of the cell always transports CO_2-enriched air toward the equatorial region, producing, in the lower atmosphere, a narrow zone of high predicted CO_2. But here the air

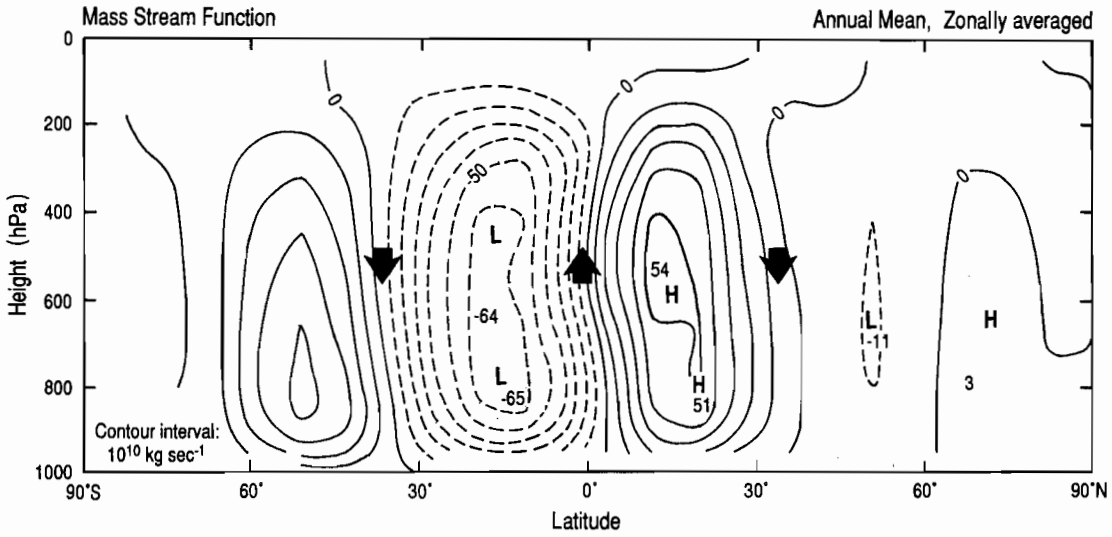

Fig. 7. Latitude-height display of zonally averaged mean annual mass stream function of the meridional circulation used in the three dimensional model of Heimann and Keeling [this volume]. Contour labels are expressed in units of 10^9 kg sec^{-1}. Solid contour lines indicate positive stream function. Negative lines indicate negative stream function.

is also rising, so that the zone of high, or at least horizontally maximal, CO_2 also appears aloft, as seen in Figures 3 and 4.

According to the model, the Hadley circulation also produces an overall accumulation of CO_2 in the southern hemisphere related to the seasonal biosphere, as was already noted by Pearman and Hyson [1980] in a two-dimensional tracer model study. The observed seasonal signal in CO_2 decreases upward, because it is generated by NPP and respiration only at the ground and is attenuated by turbulent mixing and vertical air currents aloft, as already described (see also references cited by Heimann et al. [III.1]). During the winter, therefore, the air aloft tends to be lower in CO_2 concentration than is the air near the surface, whereas in the summer it is higher aloft, although only slightly so over land owing to prevailing rising air. Since the air in the upper part of the Hadley cell in both summer and winter flows in the opposite direction to that near the ground, a process analogous to direct current rectification of an alternating signal is set up in each hemisphere.

Furthermore, the seasonal oscillation in atmospheric CO_2 is observed to be much more pronounced in the northern hemisphere than in the southern. Therefore the oscillation in CO_2 concentrations in the northern hemisphere predominates in the signal rectification process. During the northern winter the lower part of the Hadley cell transports high CO_2 southward, while in the northern summer the upper part of the Hadley cell transports high CO_2 southward. The return flows in each season, in contrast, are nearly the same owing to the small seasonal signal in the southern hemisphere; these northward flows, therefore, only slightly affect the southward transport of CO_2.

When averaged vertically and zonally, the annual mean concentration field produced by the sum of NPP and respiration in the northern hemisphere is depleted in CO_2 by approximately 0.4 ppm, as shown by the lower curve in Figure 8. In contrast the northern hemispheric zonal vertical average near the ground (upper curve in the figure) is enriched. Near the north-south axis of the Pacific Ocean, along the line of our observing stations for CO_2, the predicted profile at level 1 (upper curve in Figure 9) is influenced regionally by patches of high concentration extending eastward from Siberia and westward from Canada, but, in common with the

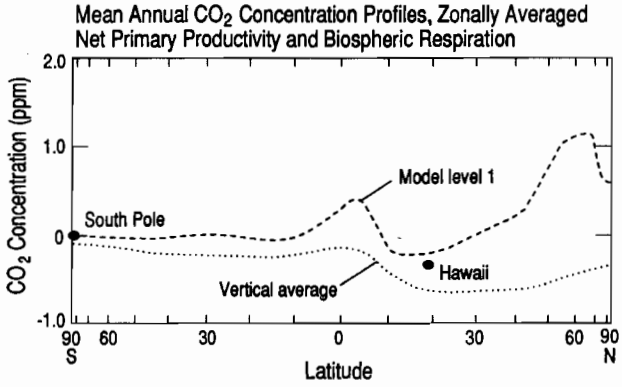

Fig. 8. Zonally averaged north-south profiles of the mean annual CO_2 concentration field, in ppm (by volume), generated by the sum of the model source components for net primary productivity and respiration of the terrestrial biosphere for the year 1980. Concentrations are expressed as departures from the concentration generated for the South Pole at model level 1. The profiles are plotted versus the sine of latitude so that the scale is proportional to the area on a sphere. Curves are shown for model level 1 and for vertically averaged concentration. Dots indicate the model generated concentrations for Mauna Loa Observatory, Hawaii (19.53°N.), and the South Pole.

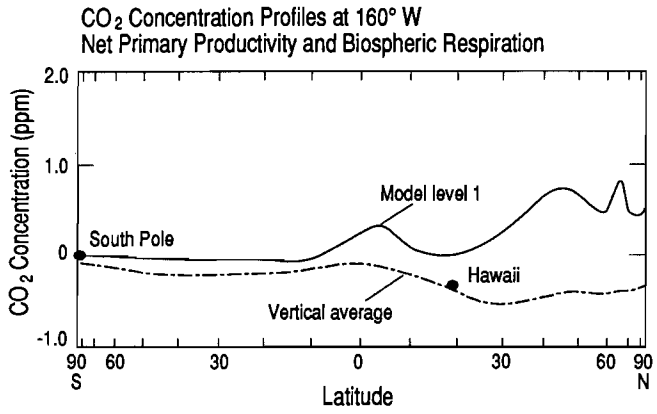

Fig. 9. Same as Figure 8, except that profiles are at 160°W.

zonal average at level 1 (upper curve in Figure 8), is generally higher in the northern hemisphere. Also, the vertically averaged CO_2 concentration of the field near the center of the Pacific Ocean (lower curve in Figure 9), in common with the vertically and zonally averaged profile (lower curve in Figure 8), is generally lower in the northern hemisphere.

The model predicts that the concentration at Mauna Loa Observatory (assumed to be at level 4, with an average pressure of 634 hPa) is nearly the same as the vertical average at that location (see Figure 9), and also nearly the same as the zonal average (see Figure 8). The predicted concentration at Mauna Loa is 0.32 ppm less than at the South Pole. This difference from the South Pole value is distinctly smaller than the two-dimensional model prediction of Pearman and Hyson [1980, p. 4461] of 0.92 ppm. These authors do not furnish data to indicate predicted CO_2 gradients elsewhere, but presumably the Mauna Loa-South Pole gradient is typical of the average interhemispheric gradient in their model as well as in ours. Thus predictions of the influence of the seasonal biosphere on atmospheric CO_2 are quantitatively different for these two models, but the models are in agreement that the vertically and zonally averaged component field should be lower in the northern hemisphere.

The relatively low predicted CO_2 concentrations in the northern subtropics, shown as a trough in north-south cross-section (both curves of Figure 8) and seen at level 1 from the Americas eastward to the Indian subcontinent (Figure 2) are also explained largely by the Hadley circulation. In the northern winter when air, on average, descends over the northern continents, it also descends over the oceans in the northern flank of the Hadley cell between about 15 and 30°N. [II.2, Panel 1 of Figure 1]. Here the descending air is part of a flow coming from the upper levels of the southern hemisphere air mass where the CO_2 concentration is relatively low, in contrast to the air further north, which has resided for some time in the northern hemisphere. To some degree this descending air reduces the CO_2 concentration at all levels.

In the summer the direction of flow in the cell is reversed [II.2, Panel 3 of Figure 1] so that the air first arrives in the zone between 15° and 30°N. as a northward flow in the lower atmosphere. To a considerable extent this air has come from the southern hemisphere, carrying with it a relatively high CO_2 concentration generated by the seasonal biosphere in the southern hemisphere. However, during its northward flow, where it passes over land after reaching the northern hemisphere, it becomes depleted by vegetation that is then enjoying its maximum growing season. For this reason the predicted CO_2 depletion is strongest north of the South American and African continents (see Figure 2) which have extensive northern tropical vegetation. The effect extends as far east as India because of the northeastward flow of the Asian summer monsoon air. As the air near the northern limit of the Hadley cell ascends from the lower atmospheric layers, the zonal winds tend to spread the effect, so that at the elevation of Mauna Loa Observatory the depletion is zonally nearly homogeneous.

We have discussed the CO_2 transport processes associated with the seasonal activity of the biosphere at some length because of their general importance to the overall mean annual field and to illustrate the possible interactions of seasonally varying CO_2 sources and sinks with seasonally varying atmospheric transport. We will not discuss other seasonally varying source components in similar detail, but the reader should be aware that similar kinds of interactions are involved with these components.

2.3.2 Nonseasonal perturbed exchanges: destruction and fertilization. Losses of carbon from the terrestrial biosphere caused by anthropogenic changes in land use and deforestation (which we call "biospheric destruction") are prescribed in the three-dimensional model according to a country-by-country analysis by Houghton et al. [1987]. This analysis is based on estimates of the net flux of carbon from establishment and abandonment of croplands, from harvest and regrowth of forests, and from the release of CO_2 by oxidation of wood products. In a few areas, especially in Europe, the estimated flux is negative, i.e., the biosphere absorbs CO_2 owing to a predominance of reforestation or establishment of cropland. For the year 1980 the authors estimated a global net release of 1.791×10^{12} kgC yr^{-1}. We assumed that the loss or gain of carbon within each country is proportional to the annual integral of NPP, leading to the distribution in annual CO_2 release shown by Heimann and Keeling [II.4.6, Figure 13]. The release occurs largely in the tropics. For other times, not considered by Houghton et al. [1987], we estimated the global net release rate by a Gaussian function in time with two adjustable parameters, which were chosen so that the compartment model of Keeling et al. [I.5] approximately reproduces the rise in atmospheric CO_2 since the year 1740. The releases of CO_2 for individual grid boxes were prorated on the basis of these global estimates to those established for 1980 by Houghton et al. [1987].

The compartment model includes a biospheric growth factor such that, for a given increase in atmospheric CO_2 concentration from a presumed preindustrial concentration of 277 parts per million by volume (ppm), there results a fractional increase in NPP equal to 41 percent of the fractional increase in CO_2 (a growth factor, β_a, of 0.41). The aforementioned Gaussian function was adjusted with this growth provision included. Indeed, without this provision, it is not possible to obtain a reasonable fit to the atmospheric CO_2 data over the past 200 years without making improbable assumptions about the uptake of CO_2 by the oceans [I.5]. The global compartment model for the year 1980 predicts a global uptake of CO_2 by the biosphere of 2.1038×10^{12} kgC [I.5, Table 12]. We include this global flux in the three-dimensional model as a model source component which we call "biospheric fertilization."

Lacking direct evidence as to how growth stimulation might vary regionally and seasonally, we assume that stimulation in 1980 occurred in direct proportion to annual NPP without seasonality.

This assumption leads to the distribution in annual CO_2 uptake shown by Heimann and Keeling [II.4.6, Figure 12]. For other times we assumed the same regional pattern, i.e., the uptakes for the individual grid boxes were prorated on the basis of the global integrals as in the case of biospheric destruction. The predicted globally integrated uptakes for the four historical periods are listed by Heimann and Keeling [II.4.6, Table 6].

For the historical periods of 1962 and 1968 the release of carbon from biospheric destruction, according to the predictions of the compartment model, exceeds the uptake by stimulation of growth, i.e., a net overall loss of biospheric carbon, whereas for 1980 and 1984 the biosphere gains carbon. The predicted cross-over from net loss to net gain occurred in 1972.

Although we estimate the global strength of biospheric fertilization by means of a growth factor tied to the CO_2 increase in the air, we do not unconditionally accept the hypothesis that plant growth is stimulated by rising concentration of atmospheric CO_2. Any enhancement of plant growth connected with human activity, such as more efficient agriculture, could have contributed to an apparent positive growth factor. Effects might be indirect, for example promotion of higher NPP owing to gradual global warming of the atmosphere linked to fossil fuel CO_2 emissions. Even global changes in climate not linked to human activities could be reflected in a nonzero growth factor, if the changes accidentally have been more or less proportional to the rise in atmospheric CO_2 concentration.

Biospheric destruction, based on the study of Houghton et al. [1987], is modeled to occur mainly in the tropics, with high intensity fluxes and resulting zones of high CO_2 concentration in southeastern Asia, Indonesia, South America, and central Africa (Figure 10). The north-south variation in the CO_2 concentration field predicted for this component in 1980 is peaked near the equator and declines monotonically towards both geographic poles (Figure 11). In contrast the greatest loss in atmospheric CO_2 from

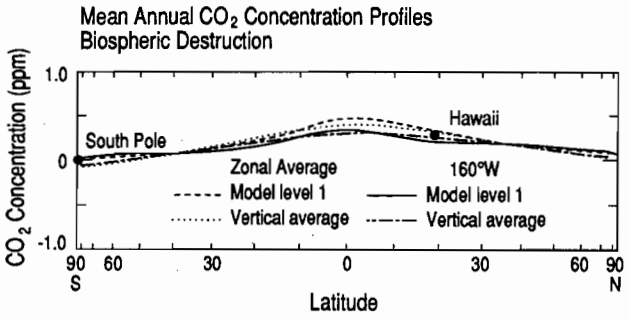

Fig. 11. North-south profiles of the mean annual CO_2 concentration field, in ppm (by volume), generated by the model source component for biospheric destruction of 1.7910×10^{12} kgC yr^{-1}. The component is distributed according to Heimann and Keeling [this volume, Figure 13] and is for the year 1980. The four curves are as defined in Figures 8 and 9.

biospheric fertilization in 1980 is predicted to occur in the temperate and boreal latitudes of the northern hemisphere where the zonal fraction of productive land area is highest (Figures 12 and 13). The combined effect of the two biospheric perturbation fluxes is predicted to produce almost monotonically northward decreasing CO_2 concentration (Figure 14).

2.4 *Exchanges of CO_2 with the Surface Ocean*

2.4.1 Introduction. The instantaneous flux of CO_2 gas exchanged at the ocean surface [II.4.4, equation (4.20)] is modeled by a bulk formula

$$F_{ex} = k_{ex}(\Delta pCO_2) \tag{2.8}$$

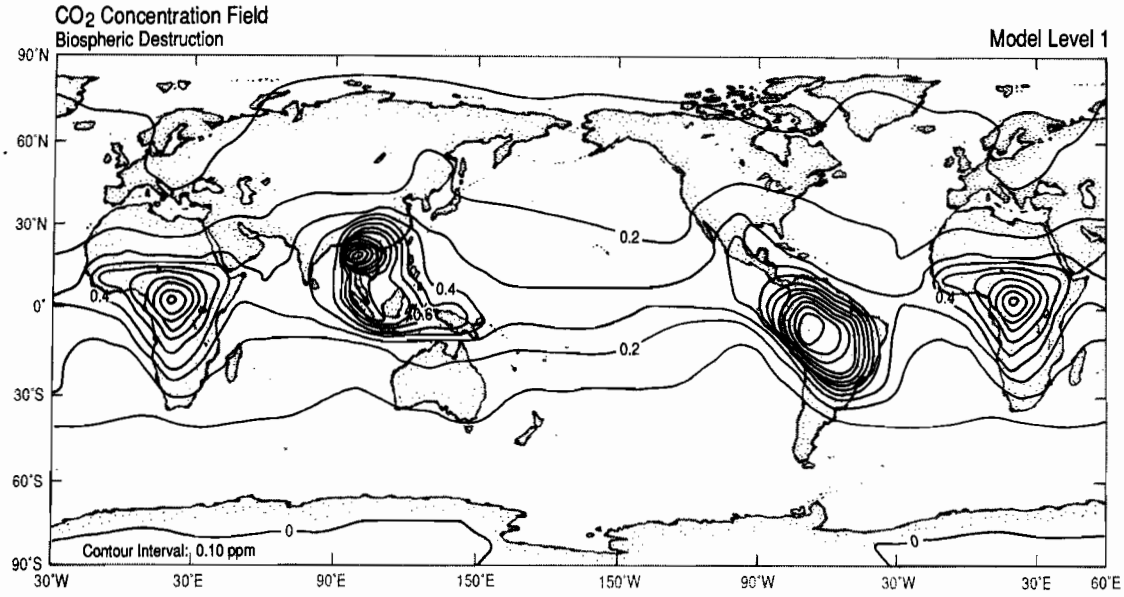

Fig. 10. Contour map of the mean annual CO_2 concentration field generated by the model source component for biospheric destruction for the year 1980 at model level 1. Format is the same as for Figure 2.

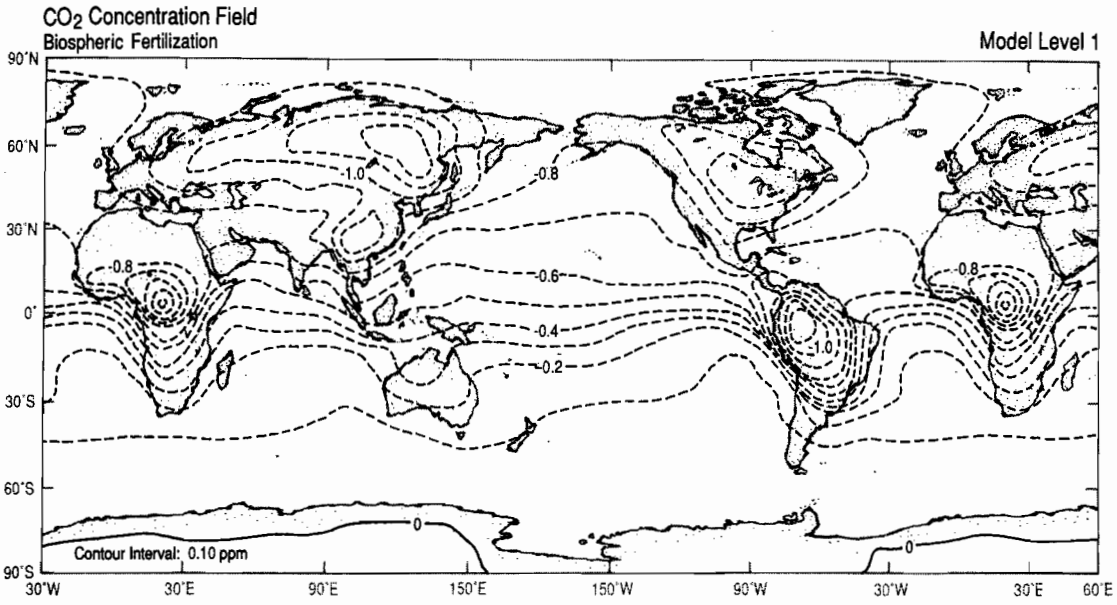

Fig. 12. Contour map of the mean annual CO_2 concentration field generated by the model source component for biospheric fertilization for the year 1980 at model level 1. Format is the same as Figure 2.

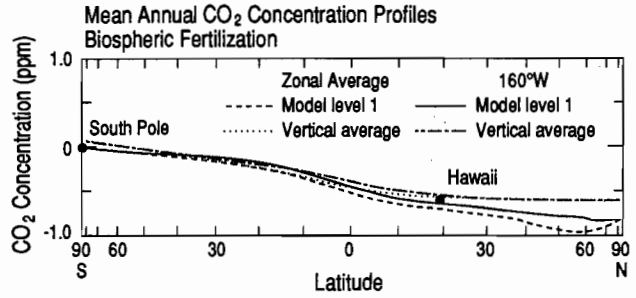

Fig. 13. North-south CO_2 concentration profiles, as in Figure 11, but for biospheric fertilization of 2.1037×10^{12} kgC yr^{-1}. The source component is for the year 1980 and is distributed according to Heimann and Keeling [II.4.6, Figure 14].

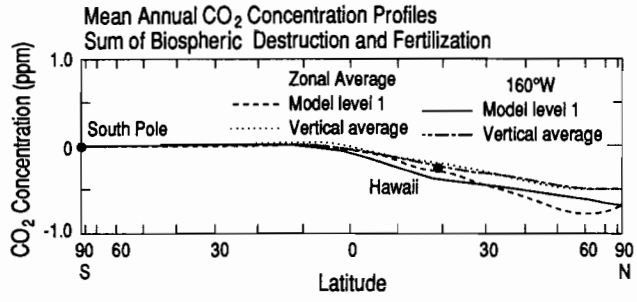

Fig. 14. North-south CO_2 concentration profiles for the sum of biospheric destruction and fertilization (shown separately in Figures 11 and 13).

where F_{ex} denotes the exchange flux in units of carbon mass per unit of time and area, and k_{ex} denotes an exchange coefficient, assumed in the standard case to be a constant, corresponding to an atmospheric residence time of CO_2 with respect to the oceans of 7.87 years with a magnitude of 2.1747×10^{-6} kgC m^{-2} day^{-1} ppm^{-1} [II.4.4, equation (4.26)]. The CO_2 partial pressure difference, ΔpCO_2, is defined as the difference in the partial pressure of CO_2 corresponding to equilibrium with inorganic carbon in the surface layer of the oceans, and that in the overlying air, i.e.,

$$\Delta pCO_2 = pCO_{2\,sea} - pCO_{2\,air} \tag{2.9}$$

In an attempt to represent gas exchange more realistically, we have alternatively computed k_{ex} for each grid location and month of the year assuming that it varies with wind speed and temperature according to the parameterization of Liss and Merlivat [1986] as implemented by Heimann and Monfray [1989]. All of their values were adjusted by a factor 1.7447 so that the annual, global average coefficient was the same as the constant value of k_{ex} used in our standard case. This alternative representation of k_{ex} as variable is used mainly in sensitivity tests discussed in later sections.

The exchange flux, F_{ex}, was decomposed into four model source components. One component, F_{TDE}, represents the seasonally varying exchange. Another, F_{UOS}, represents the global disequilibrium arising from industrial CO_2 and from biospheric destruction and fertilization. This perturbation flux is assumed to be nonseasonal and to be generated by a constant deficit in CO_2 partial pressure everywhere in the world oceans in disregard for any details of actual regional variability; its global average is forced to be compatible with the compartment model of Keeling et al. [this volume]. Two additional globally balanced, nonseasonal components represent large scale regional oceanic sources and sinks. After initially being specified via the bulk formulation for air-sea exchange with nominal magnitudes, they were globally adjusted

simultaneously to produce an optimal fit to atmospheric CO_2 observations. Very broadly they distinguish CO_2 transfers between tropical and extratropical waters, and between high latitude waters of the two hemispheres.

2.4.2 Seasonal exchange fluxes. The seasonally varying exchange of CO_2, dealt with in detail by Heimann et al. [this volume], contributes very little to the mean annual field, as shown in Figure 15. It will not be further discussed.

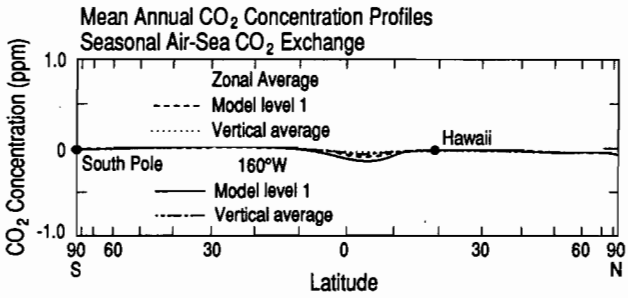

Fig. 15. North-south CO_2 concentration profiles, as in Figure 11, but for the model source component representing the seasonally varying exchange of CO_2 for the year 1980 between the atmosphere and the oceans. The component is distributed according to Heimann et al. [III.3.3, Figures 4 and 5].

2.4.3 Balanced oceanic exchanges of CO_2. Observational data establish the mean annual north-south variation in ΔpCO_2 near 150°W. between approximately 20°N. and 16°S. Less extensive data near the equator at other longitudes indicate roughly similar north-south profiles. From these ΔpCO_2 data Heimann and Keeling [I.4.4.2] constructed a source component, F_{EQU}, in which they assumed that the north-south pattern near 150°W. is repeated throughout the oceans between 15.65°S. and 15.65°N., but with variable intensity in the east-west direction. The flux in the equatorial region, which is a source to the atmosphere, was balanced in each hemisphere with an equal and opposite sink generated by a uniform deficit in CO_2 partial pressure poleward of 15.65° to achieve a zero net global flux. We call this coupled source and sink an "equatorial oceanic source component." Its flux distribution, integrated over each grid box, is shown by Heimann and Keeling [II.4.4.2, Figure 15], based on the assumption that the gas exchange coefficient has the constant standard value of 2.1747×10^{-6} kgC m^{-2} day^{-1} ppm^{-1}. Given this exchange rate, approximately 2×10^{12} kgC yr^{-1} as CO_2 is prescribed by the model to be released from tropical ocean water between the specified latitudes and to be reabsorbed poleward. The intensity of this source component, however, was afterwards adjusted with respect to the atmospheric CO_2 observations for each of the four historical periods by the global adjustment factors, v_{EQU} [see II.4.5, equation (4.33)], listed in the second column of Table 1.

Table 1 further lists for each of the four periods the zonal integral of F_{EQU} between 15.65°N. and 15.65°S. The four values show little variation from the unweighted average, which is 93 percent of the nominal value. The standard deviation (1 sigma) with respect to the nominal value is 14 percent. The expected statistical error arising from scatter in the original data, which can be derived

TABLE 1. Adjustment Factors (v_{EQU}) and Resulting Air-Sea Transfer Velocities and Fluxes for the Equatorial Oceanic Source Component

Historical Period	Adjustment Factor	Standard Error	Transfer Velocity (m day^{-1})	Flux* (10^{12} kgC yr^{-1})
nominal	1.0000		5.45	2.0288
1962	1.0922	0.0984	5.95	2.2159
1968	0.7452	0.0607	4.06	1.5119
1980	0.9758	0.0654	5.32	1.9797
1984	0.9018	0.1588	4.91	1.8296
Av.	0.9288		5.06	1.8843
Std. Deviation	0.145		0.79	0.29

*Evolved between 15.65°N. and 15.65°S. and reabsorbed poleward.

knowing the standard errors of the individual factors, listed in the third column, are typically smaller, however, and thus support the hypothesis that the flux varies somewhat from one historical period to the next. Changes of this flux between the individual observing periods could in principle be interpreted as caused by variations in the rate of upwelling of CO_2-enriched equatorial subsurface waters thus leading to variations in the degree of supersaturation of the equatorial mixed layer. We should, however, be mindful of uncertainties in the transport specifications of the model, and that this transport is assumed to be the same for the four historical periods. These shortcomings, as well as imprecision in the atmospheric CO_2 data, weaken any conclusions we may draw regarding the cause of the variability found for this component.

The north-south profile in the mean annual concentration field predicted by F_{EQU}, for the year 1980, is shown in Figure 16. At 160°W. near the equator, a prominent peak in concentration is predicted in the lower atmosphere. Its center is about 4° south of the equator. When vertically averaged the peak is smaller, less sharp, and centered nearer the equator. These differences reflect

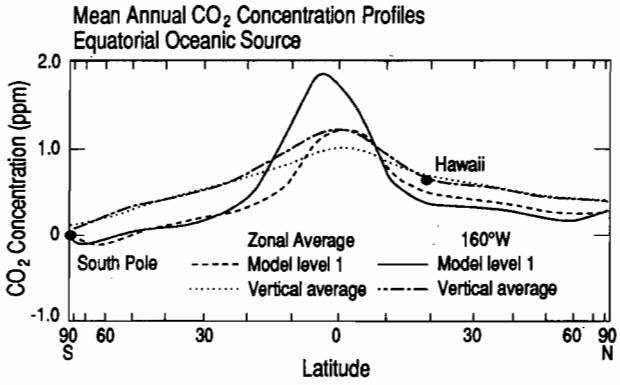

Fig. 16. North-south CO_2 concentration profiles, as in Figure 11, but for a model source component representing an equatorial oceanic source of 1.9797×10^{12} kgC yr^{-1} for the year 1980 between 15.65°N. and 15.65°S., in balance with an oceanic sink north of 15.65°N. and south of 15.65°S. See the distribution map in Heimann and Keeling [II.4.6, Figure 13].

the proximity of the lower air layers to the source, and the asymmetry of the source [II.4.6, Figure 15]. The peak near the equator is still less sharp and still closer to the equator when the concentration field is zonally averaged, either near the surface or as a vertical average, indicating how meridional circulation and turbulent mixing of the tropical atmosphere reshape the peak in regions remote from the major source region situated in the central and eastern tropical Pacific Ocean.

A further prescribed oceanic source component consists of an adjustable northern hemisphere sink coupled to a southern hemisphere source of equal but opposite total strength. This component, which we call the "North Atlantic sink component", F_{ATL}, was added to the model for reasons which will be discussed next.

The sum of the biospheric components, the oceanic components so far discussed, and the fossil fuel component to be discussed later, predict a north-south gradient of mean annual CO_2 concentration considerably larger than observed. Although deficiencies in the transport characteristics of the model, especially in the interhemispheric exchange intensity, as discussed in subsection 4.3.8, below, may account for part of the discrepancy, we wish to provide an additional oceanic component which allows the model to predict a smaller gradient than otherwise. Appealing to oceanic evidence that much of the deep water of the oceans in both hemispheres is formed in the North Atlantic Ocean by sinking surface water [see, for example, Pond and Pickard, 1983, p. 163–166], and that surface water of the North Atlantic is, on average, a net absorber of atmospheric CO_2 [Takahashi et al., 1983; Broecker and Takahashi, 1984, Figure 6], we postulate an additional source component, F_{ATL}, in which the entire surface of the Atlantic Ocean north of 23.48°N. exhibits a uniform deficit in CO_2 partial pressure, balanced by a uniform excess south of 39.13°S.

Since the locations of these presumed regions can be only vaguely reflected in the mean annual atmospheric CO_2 field deduced from our observational data, we chose zonal boundaries convenient to the grid arrangement of the transport model. Given that only very meager data for mean annual ΔpCO_2 exist over all seasons in the area of interest [Takahashi et al., 1985 and unpublished] we did not attempt to specify a spatially varying ΔpCO_2 field in the region of our hypothesized North Atlantic sink as we have in the case of the equatorial source component, F_{EQU}. As a rough guide we used a schematic map of mean annual ΔpCO_2 [Broecker et al., 1986, Figure 1] based on observations from GEOSECS and TTO and various other expeditions. This map indicates a negative ΔpCO_2 of 16 μatm between 10°N. and 40°N. in the Atlantic Ocean and a higher deficit of 33 μatm further north. Because we had already defined a component for the equatorial region on the basis of direct observations, and we wished to include a transition zone between positive and negative ΔpCO_2, we chose to define the region of negative ΔpCO_2 in the North Atlantic Ocean to begin at about 24°N., one grid length beyond the northern limit of our equatorial source component. As in the case of the equatorial component, we assume a constant gas exchange coefficient in the standard formulation of F_{ATL}.

At the time when we devised this component, unpublished data from several sources suggested to us that the mean annual $pCO_{2\,sea}$ in the North Pacific Ocean was close to or higher than equilibrium with atmospheric CO_2. We therefore chose to place the northern hemisphere sink entirely in the Atlantic Ocean. So that this sink would not require an extremely low average of $pCO_{2\,sea}$, we extended this sink as far south as 24°N. even though it appeared to us to be more realistic to restrict it to more northerly latitudes. We discuss the consequences of our chosen location of this sink in subsection 5.1, below.

In the southern hemisphere the map of Broecker et al. [1986] indicates mean annual $pCO_{2\,sea}$ to be near equilibrium with atmospheric CO_2 equatorward of 40°S. To avoid placing a source in this zone we chose a compensating region of positive ΔpCO_2 south of 40°S. This polar region is assumed to extend uniformly over all of the southern oceans, since there is no basis from existing chemical observations or from considerations of ocean circulation to confine it to a single ocean basin. The map of Keeling [1968] based on earlier observations is generally consistent with our choice of boundaries.

The intensity of the component, F_{ATL}, was adjusted with respect to the atmospheric CO_2 observations for each of the four historical periods by the global adjustment factors, v_{ATL} [see II.4.5, equation (33)], listed in Table 2. The average integrated flux between the two hemispheres is 0.96×10^{12} kgC yr^{-1} with a standard deviation

TABLE 2. CO_2 Transfers from the Southern to the Northern Hemisphere Prescribed for the North Atlantic Source Component

Historical Period	Flux (10^{12} kgC yr^{-1})	Standard Error (10^{12} kgC yr^{-1})
nominal	1.0000	
1962	0.9370	0.0584
1968	0.7987	0.0495
1980	1.1474	0.0708
1984	0.9486	0.0911
Av.	0.9579	
Std. Deviation	0.144	

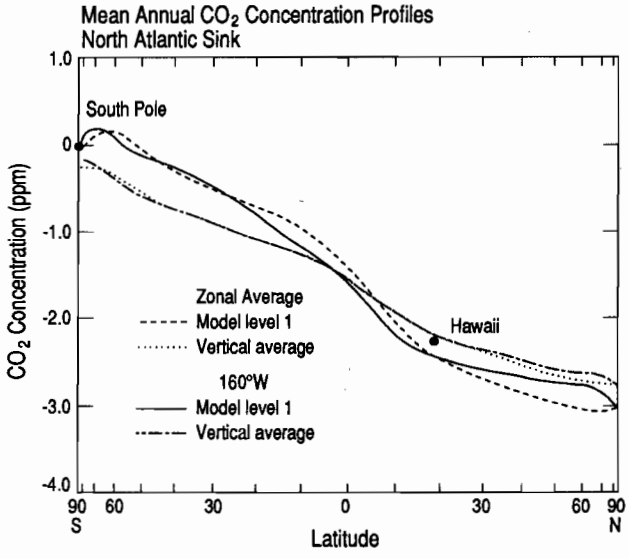

Fig. 17. North-south CO_2 concentration profiles, as in Figure 11, but for a model source component representing an oceanic sink of 1.1474×10^{12} kgC yr^{-1} for the year 1980 in the Atlantic Ocean north of 23.48°N., in balance with an oceanic source south of 39.13°S. The latter source extends over all longitudes.

of 0.14×10^{12} kgC yr^{-1}. This low relative standard error suggests a steady northern hemisphere sink for CO_2 from decade to decade, although, as in the case of the equatorial flux, F_{EQU}, the standard errors of the individual factors are smaller, suggesting real variability in the flux or in the transport of CO_2 produced by the flux. Component F_{ATL} promotes a large north-south gradient in atmospheric CO_2, shown for the year 1980 in Figure 17.

2.4.4 Perturbed oceanic exchanges of CO_2. The response of the oceans to the combined perturbations produced by the terrestrial biosphere and industrial CO_2 is modeled as a uniform oceanic sink component, F_{UOS}, having the same ΔpCO_2 at all locations. In the standard formulation, the gas exchange coefficient is assumed to be constant. The magnitude of the flux depends on the historical period of interest [II.4.6, Table 6]. In Figure 18 the north-south profile for this component is shown for the year 1980. The concentration of the mean field tends to diminish southward but with a pole-to-pole difference of only a few tenths ppm. This southward-diminishing gradient reflects the greater uptake in the southern hemisphere owing to a larger expanse of ocean, surface area being the only regionally varying factor that influences the model component. The concentration is lower in the lower atmosphere than on vertical average, as expected for a sink at the air-sea interface. The ΔpCO_2 needed to generate this flux is 8.36 μatm in 1980, assuming that the the gas exchange coefficient has the standard value of 2.1747×10^{-6} kgC m^{-2} day^{-1} ppm^{-1}.

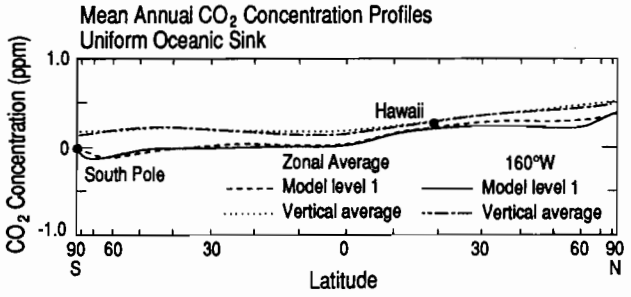

Fig. 18. North-south CO_2 concentration profiles, as in Figure 11, but for an oceanic sink produced by an areally uniform deficit in oceanic CO_2 partial pressure, $pCO_{2\,sea}$, of the magnitude required to produce an uptake of CO_2 of 2.2237×10^{12} kgC yr^{-1} as predicted by the compartment model of Keeling et al. [I.5] for the year 1980.

2.5 *Comparison of Biospheric and Oceanic Components*

The combined effect on the mean atmospheric CO_2 field of all of the biospheric source components is shown as a contour plot of C_{mean} at model level 1 in Figure 19 and as north-south profiles in Figure 20. The combined component field when vertically averaged (see Figure 20) is everywhere low in the northern hemisphere

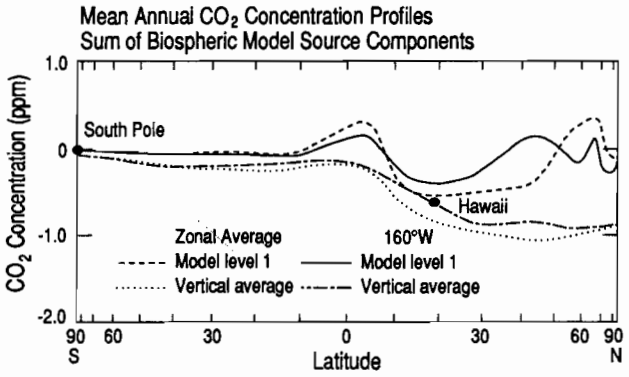

Fig. 20. North-south CO_2 concentration profiles, as in Figure 11, but for the sum of all terrestrial biospheric model source components for the year 1980.

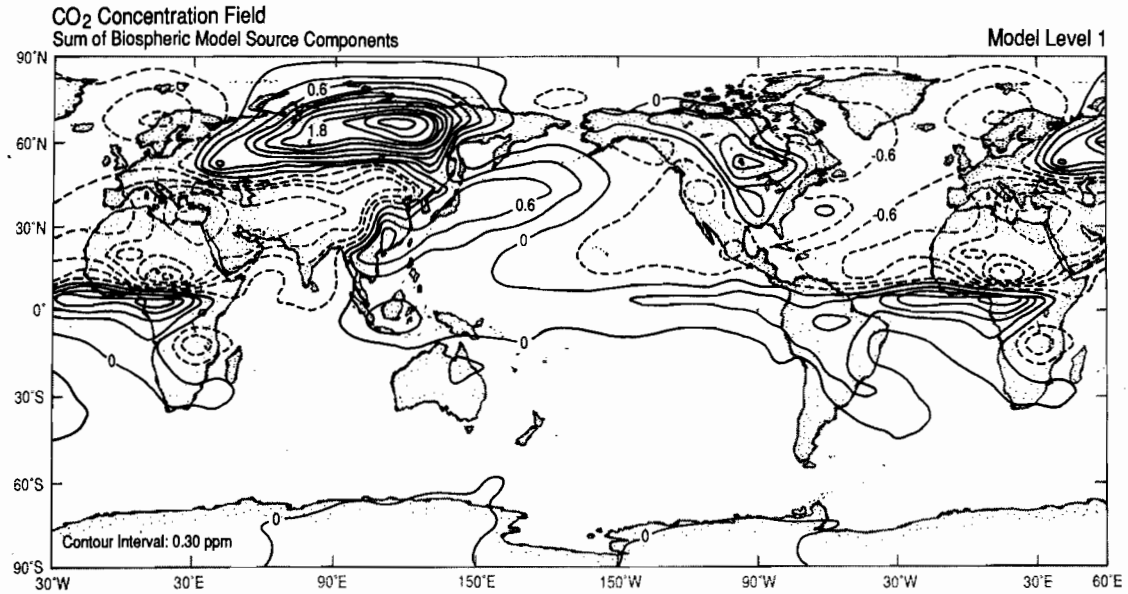

Fig. 19. Contour map of the mean annual CO_2 concentration field generated by the sum of all terrestrial biospheric model source components for the year 1980. Format is the same as for Figure 2.

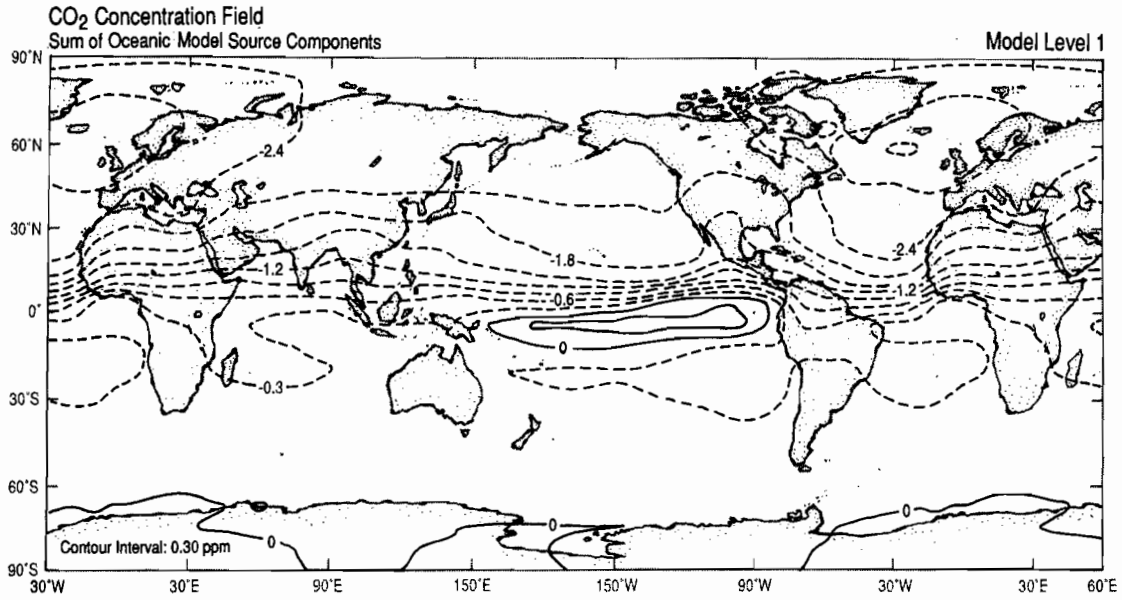

Fig. 21. Contour map of the mean annual CO_2 concentration field generated by the sum of all oceanic model source components for the year 1980. Format is the same as for Figure 2.

as a result of almost equal contributions to the field by the seasonal biosphere (Figure 8) and the perturbed biosphere (Figure 14). In contrast, the profiles at level 1 show low concentrations north of an equatorial peak, but higher concentrations further north owing to the seasonal biosphere. Altogether the extreme range in the plotted north-south profiles is approximately 1.4 ppm. Over land (Figure 19) the range is much larger, approximately 4.2 ppm.

Similar plots for the mean field of the combined oceanic components, referred to previously as $C_{OCD}(\mathbf{x},t)$ [II.5.4, equation (5.57)], are shown in Figures 21 and 22. The full range in concentration shown is 2.8 ppm in the profiles, slightly larger (3.2 ppm) in the contour map, at level 1. The predicted interhemispheric gradients are largely owing to the hypothesized North Atlantic sink, while the equatorial peak reflects the release of CO_2 by the tropical oceans. This peak is prominent near 160°W. at level 1 (see Figure 22), where it is about 3 times larger than an equatorial peak produced by the biospheric components. Thus altogether the oceanic components, as prescribed in the model, produce larger mean atmospheric gradients than do the biospheric components.

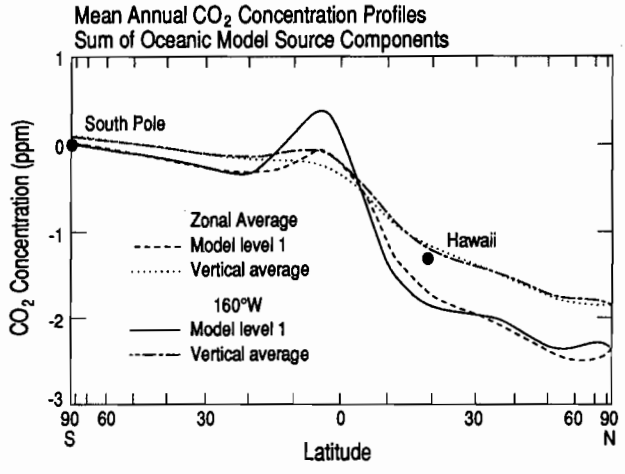

Fig. 22. North-south CO_2 concentration profiles, as in Figure 11, but for the sum of all oceanic model source components for the year 1980.

2.6 *The Industrial CO_2 Source*

This source component, whose global integral we derived from governmental statistical data on the production of fossil fuel and cement analyzed by Rotty [1987a], is by far the best established flux component contributing to the mean annual concentration field of atmospheric CO_2. Its annual mean spatial distribution, as established by Marland et al. [1985], is highly skewed with respect to latitude: 95 percent of the industrial CO_2 is released in the northern hemisphere, 60 percent in the mid-latitude zone between 16°N. and 47°N. (II.4.6, Figure 11].

This component varies with the seasons according to data supplied by Rotty [1987b] for the year 1980. For each of the other three historical periods the same amplitudes relative to the annual emissions were assigned to each grid box of the model [II.4.2].

The industrial CO_2 component produces larger north-south CO_2 concentration differences (Figure 23) than either the terrestrial biosphere or the oceans (cf. Figures 20 and 22). The vertical and zonal averages do not differ greatly from the profile at 160°W. at level 1. The component field at level 1 (Figure 24) shows highest values of C_{mean} over the eastern United States and Europe but is dominated by a north-south gradient, prominent in the profiles of Figure 23.

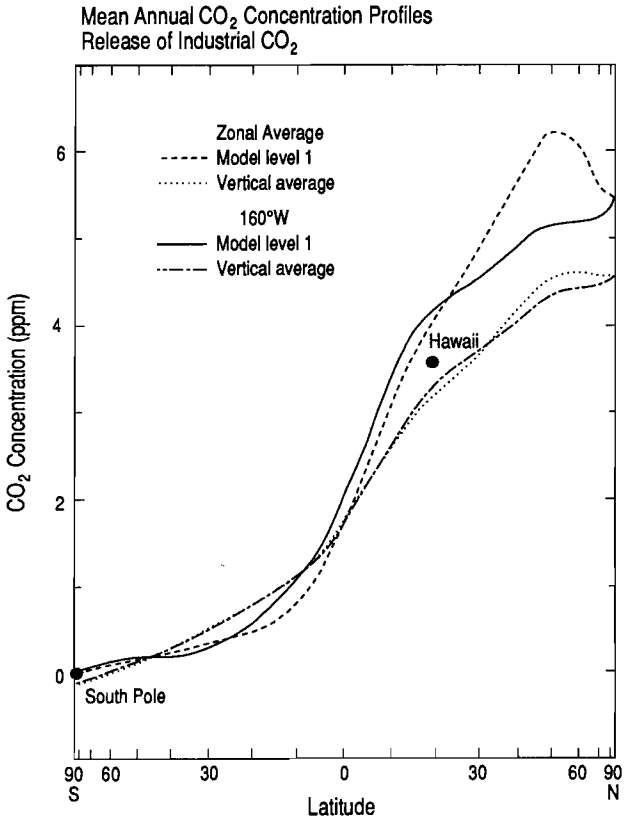

Fig. 23. North-south CO_2 concentration profiles, as in Figure 11, but for the release of industrial CO_2 (mainly from fossil fuel combustion) for the year 1980, distributed according to Heimann and Keeling [II.4.6, Figure 17].

2.7 *Isotopic Components*

The transfer of CO_2 between the atmosphere and the terrestrial biosphere causes a shift in the reduced $^{13}C/^{12}C$ isotopic ratio, δ, of atmospheric CO_2 of approximately 0.050‰ per ppm of CO_2 lost or gained, respectively, whereas the corresponding transfer for oceanic carbon produces a much smaller shift, or "scaling factor", of only about 0.0035‰ [I.3]. Thus, if account is taken of the influence of industrial CO_2, which is isotopically similar to CO_2 derived from the terrestrial biosphere [I.3], and if account is also taken of the temperature dependence of the equilibrium fractionation of air-sea exchange of CO_2, the carbon-13 Suess Effect (component ${}^*F_{SUE}$) and the combined oceanic components, ${}^*F_{OCD}$ [II.5.4], the remaining variation in δ of atmospheric CO_2 is owing to CO_2 exchanges involving the terrestrial biosphere. From the available measurements of both the concentration and isotopic ratio of atmospheric CO_2 it should be possible to distinguish the influence of the biospheric source components from those of the oceanic components.

This possibility was considered previously [III.5.4] with respect to seasonal variations in the source components. In preparation for a similar analysis of the annual mean δ of atmospheric CO_2 in section 4, below, we now discuss the component mean isotopic fields, $\delta_{i\ mean}$ (defined by equation 2.5) arising from the source components already discussed with respect to CO_2 concentration. We also discuss the additional components involving the Suess Effect and temperature-dependent isotopic air-sea exchange. The basic assumptions of the isotopic calculations are discussed by Heimann and Keeling [II.5] and are summarized by Heimann et al. [III.5.4].

The combined effect of all terrestrial biospheric source components on the composite field, δ_{mean}, is shown in north-south profiles in Figure 25. As can be seen by comparing these isotopic profiles with the corresponding profiles for concentration (Figure 20), the patterns are almost identical owing to the near constancy

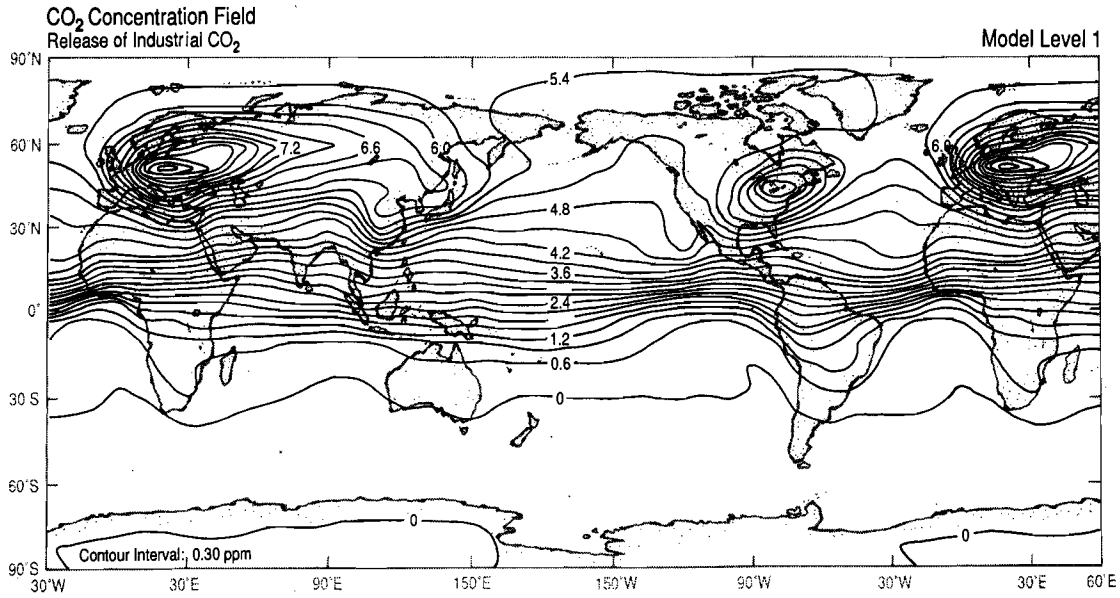

Fig. 24. Contour map of the mean annual CO_2 concentration field generated by the release of industrial CO_2 for the year 1980. Format is the same as for Figure 2.

of the scaling factors of the separate components. Similarly, the isotopic profiles arising from the sum of the previously discussed oceanic source components, shown in Figure 26, are almost identical to the corresponding concentration profiles (Figure 22), except that in this case the scaling factor, as noted above, is about a tenth as large. (The precise scaling factors of each component [see II.5.5, Table 8] differ very slightly with location.)

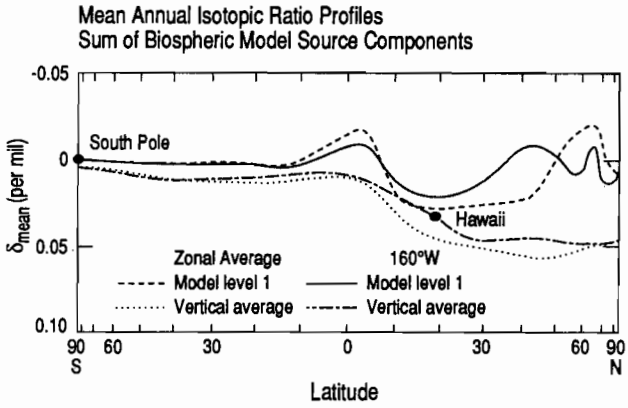

Fig. 25. North-south profiles of the mean annual field of the reduced isotopic ratio of atmospheric CO_2, δ_{mean}, in per mil, generated by the sum of all of the model source components arising from the terrestrial biosphere in the year 1980. The four difference curves depict the ratio at model layer 1 zonally averaged, vertically and zonally averaged, at model layer 1 at 160°W., and vertically averaged at 160°W. The components included in the sum are the same as in Figure 20 for CO_2 concentration. The vertical axis is the difference of δ_{mean} from the value generated for the South Pole at model level 1, inverted in order that the patterns appear similar to those for CO_2 concentration. Dots indicate the model generated isotopic ratios for Mauna Loa Observatory, Hawaii (19.53°N.), and the South Pole.

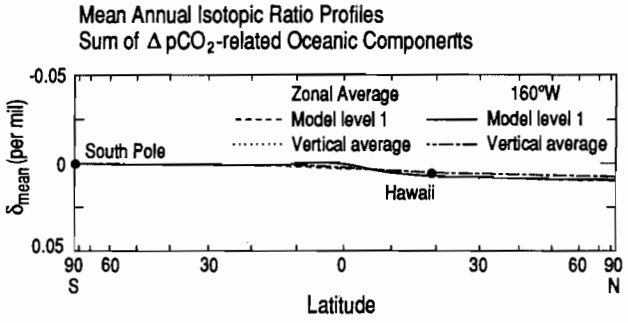

Fig. 26. North-south profiles of δ_{mean}, in per mil, as in Figure 25 but for oceanic model source components generated by the difference in CO_2 partial pressure between the atmosphere and the ocean surface in the year 1980. The components included in the sum are the same as in Figure 22.

The carbon-13 Suess Effect refers to the isotopic disequilibrium produced when CO_2, depleted in carbon-13, is added to the atmosphere by the combustion of fossil fuels. This depleted CO_2 afterwards redistributes between the reservoirs of the carbon cycle. As a result [see II.5, Table 11] the δ_{mean} of atmospheric CO_2 in 1980 was on average shifted by −1.2‰ from its preindustrial value, whereas that of inorganic carbon in surface ocean water was shifted by only −0.6‰. The consequent isotopic disequilibrium, owing to gas exchange at the air-sea interface, produces variations in δ_{mean} because of the nonuniform geographic distribution of land and oceans.

We have modeled the Suess Effect assuming that the isotopic disequilibrium is spatially uniform, because we lack an oceanic model capable of producing more precise simulations of the disequilibrium regionally. The neglected regional variations are expected to be small because the disequilibrium has developed slowly, thus allowing time for mixing to smooth out the effect of locally different rates of air-sea exchange and vertical oceanic mixing. As shown in Figure 27, the isotopic field of the component, ${}^*F_{SUE}$, is more positive in the southern hemisphere (greater effect) because of the larger ocean surface there. The north-south gradient, generally positive southward, reverses near the Antarctic continent (near 70° S.) such that δ_{mean} at the South Pole shows a reduced Suess Effect similar to that seen in the vertically averaged profiles.

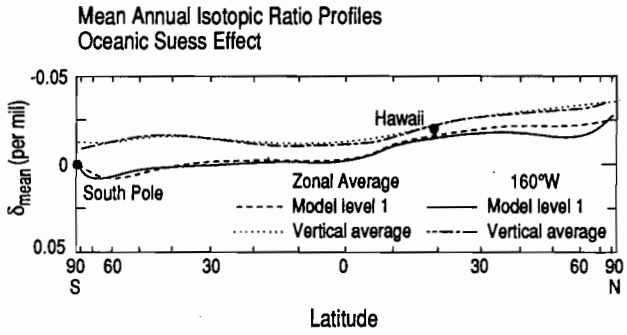

Fig. 27. North-south profiles of δ_{mean}, in per mil, as in Figure 25 but for the oceanic carbon-13 Suess effect in the year 1980.

We have modeled the equilibrium fractionation between CO_2 in the atmosphere and oceans by an additional component, ${}^*F_{TDF}$, that takes into account the spatially dependent monthly average temperature of the ocean as it influences the isotopic fractionation factor [II.5.4, equation (5.40)]. We have assumed that the mean annual isotopic ratio of dissolved inorganic carbon in the oceans is everywhere the same, with a value of 1.5512‰ for 1980 and 1.4964‰ for 1984 [I.5, Table 12]. Consistent with the model computation of the exchange of CO_2 gas, the gas exchange coefficient associated with the sum of ${}^{12}CO_2$ and ${}^{13}CO_2$ was set everywhere equal to the time-invariant, global average, standard value of 2.1747×10^6 kgC m^{-2} day^{-1} ppm^{-1} (see subsection 2.4, above). The zonally averaged north-south profile of δ_{mean} that would occur at local thermodynamic equilibrium, if only this component

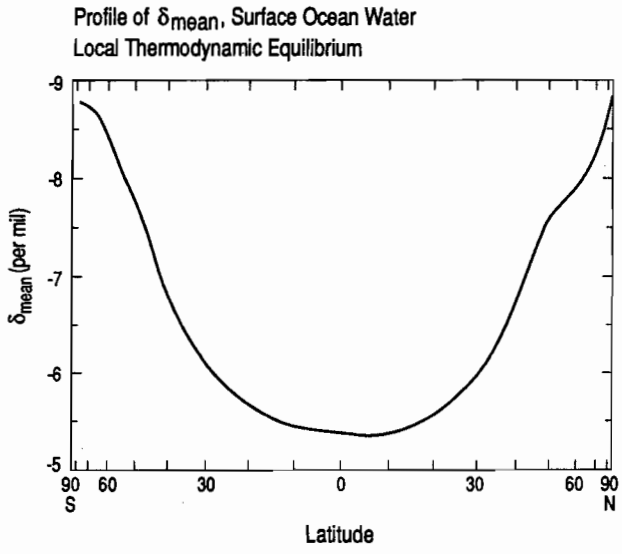

Fig. 28. North-south profile of δ_{mean}, in per mil, which would exist at local thermodynamic equilibrium with surface ocean water having everywhere δ equal to 2.2704‰, the preindustrial global average according to the compartment model of Keeling et al. [I.5, Table 11]. Values of δ_{mean} are computed from the zonally averaged mean annual temperature as specified in the three dimensional model using the fractionation factor relationship of Heimann and Keeling [I.5.4, equation (5.40)].

operated, is shown in Figure 28. Higher fractionation at high latitudes results in more negative δ values near the geographic poles.

The gradients in δ_{mean} predicted by the three-dimensional transport model as a result of this component are much less than for thermodynamic equilibrium owing to atmospheric mixing, as

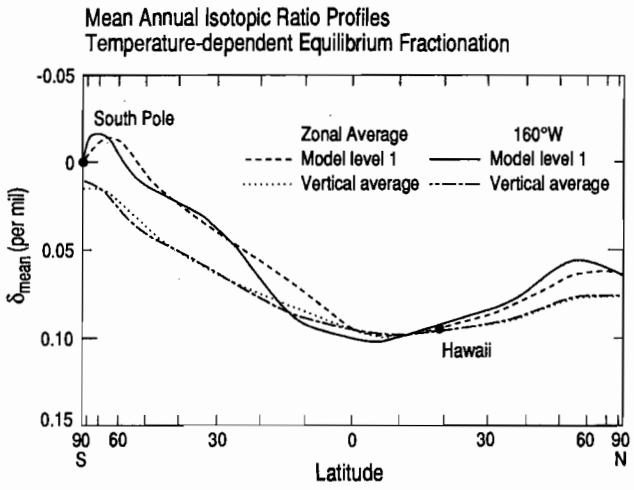

Fig. 30. North-south profiles of δ_{mean}, in per mil, as in Figure 25 but generated by the temperature-dependent equilibrium fractionation of CO_2 between the atmosphere and oceans, assuming a constant air-sea exchange coefficient.

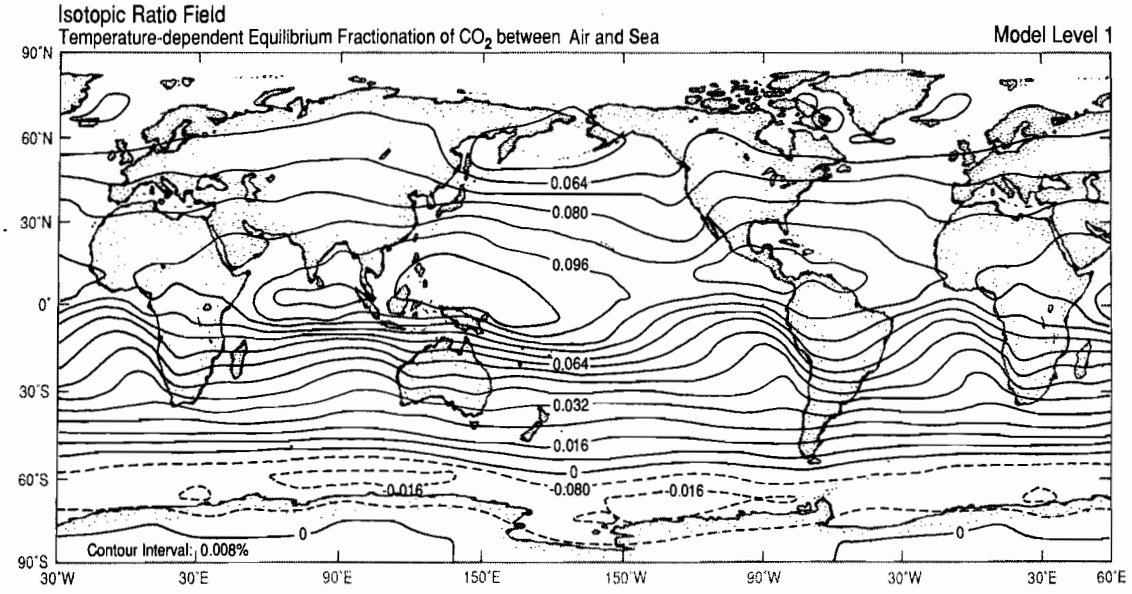

Fig. 29. Contour map of δ_{mean}, in per mil, generated by the temperature-dependent equilibrium fractionation of CO_2 between the atmosphere and the oceans at model level 1, assuming a constant air-sea exchange coefficient. Contour lines are labeled in ‰. Solid lines indicate positive or zero concentration differences from the South Pole. Dashed lines indicate negative differences.

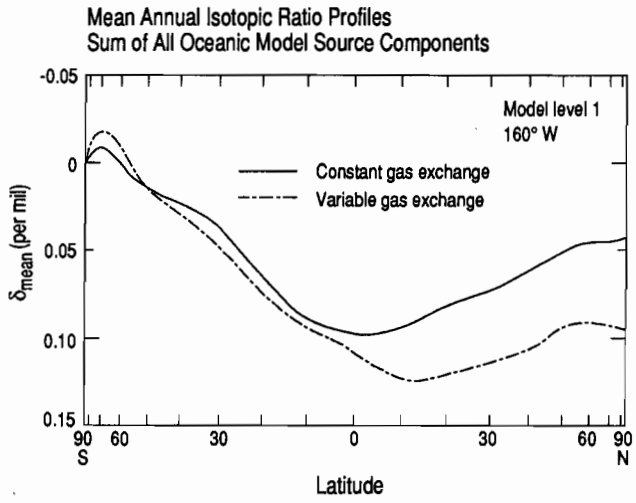

Fig. 31. North-south profiles of δ_{mean}, in per mil, at model level 1 (near the surface) at 160°W. for the sum of the oceanic components whose profiles are shown in Figures 26, 27, and 30. Also shown is the same profile except that the coefficient of gas exchange, k_{ex}, is assumed to vary with wind speed, as described in the text.

shown for the surface layer of the atmosphere (model level 1) in Figure 29. North-south profiles are crudely symmetric with respect to the equator (Figure 30), as expected given the hemispherically nearly symmetric mean annual temperature profile, but the latitudinal gradient is more pronounced in the southern hemisphere because of the greater extent of water than in the northern hemisphere, especially at high latitudes. As in the case of the Suess Effect, there is a reversal in the isotopic gradient of this component near the Antarctic Continent. The reversal is pronounced, because a strong differential in isotopic flux develops immediately north of the continent in the very cold water occurring there, while to the south there is no air-sea flux at all.

This isotopic component and, to some extent, the other oceanic components are sensitive to the rate of air-sea exchange of CO_2. Figure 31 shows a simulated north-south profile of δ_{mean} for the sum of all of the oceanic components for model level 1 near 160°W. from an additional model run in which the gas exchange rate is assumed to vary both seasonally and spatially in the manner described in subsection 2.4.1, above. For variable exchange, the interhemispheric difference in δ_{mean} is found to be approximately twice as large as that at constant exchange (shown as a dash-dot line) mainly reflecting a steeper north-south gradient in the tropics. Similar differences (not shown) are found in the fields when zonally and vertically averaged.

Fossil fuel contains carbon which is strongly fractionated isotopically with respect to the carbon of atmospheric CO_2. We have assumed that δ of this industrial CO_2, δ_{IND}, is everywhere equal to a global average estimate of –27.28‰ [see II.5.2], based on a study by Tans [1981]. This CO_2 source is predicted to contribute large north-south gradients in δ_{mean}, as shown in Figure 32.

2.8 *Composite CO_2 Source*

The mean annual field of CO_2 concentration predicted by the combination of all components is shown in north-south profiles in Figure 33. By comparing this figure with the plots for the individual components it is possible to establish the origin of the patterns

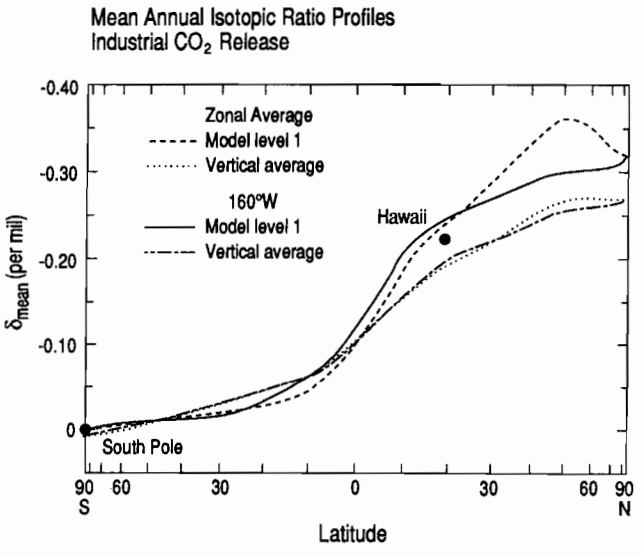

Fig. 32. North-south profiles of δ_{mean}, in per mil, as in Figure 25, but for the release of industrial CO_2. The profile is for the year 1980 as in Figure 23.

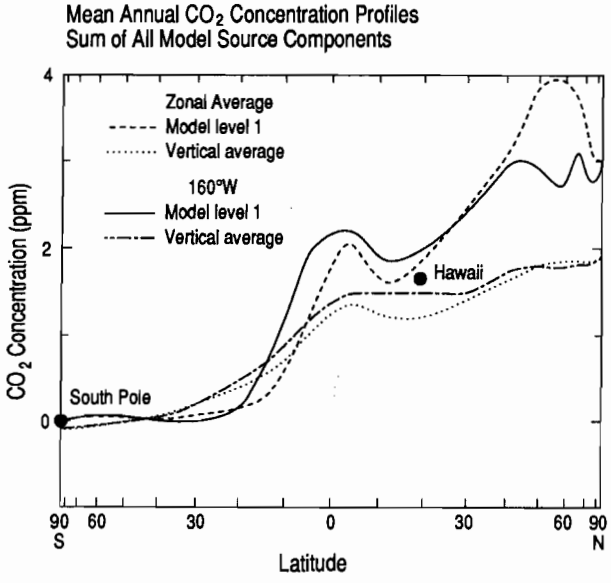

Fig. 33. North-south profiles of the mean annual CO_2 concentration field, in ppm (by volume), generated by the sum of all model source components for the year 1980. The four curves and the dots are as defined in Figures 8 and 9.

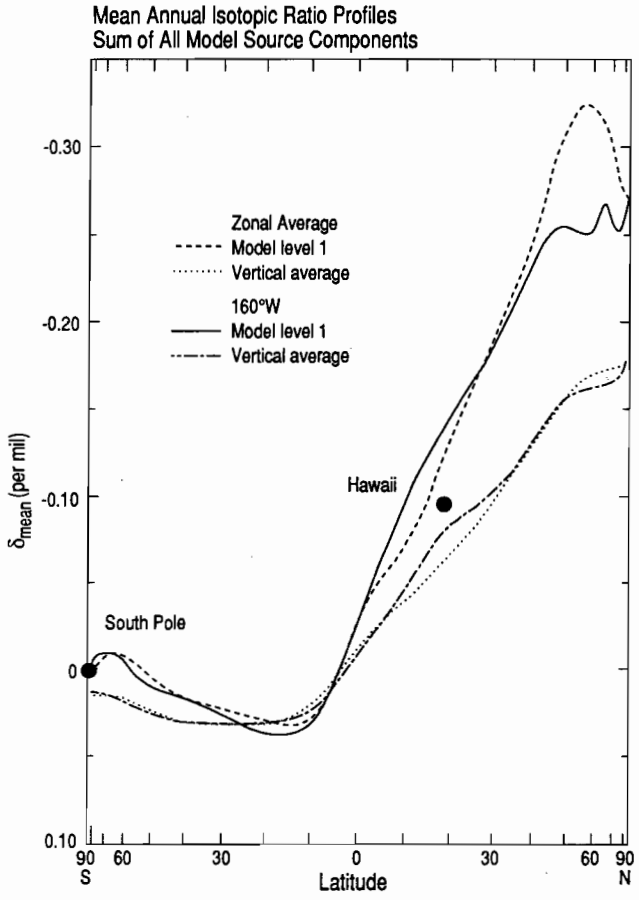

predicted by the model for the actual field of CO_2 concentrations. Figure 34 shows the corresponding profiles for δ_{mean}.

To gain an appreciation for the three-dimensional spatial variations in the mean annual concentration predicted by the model, we show in Figures 35 and 36 the field for concentration for 1980 at model level 1 (centered near 960 hPa) and model level 7 (near 200 hPa), respectively. In the lower atmosphere, represented by level 1, the influence of continental sources and sinks in the northern hemisphere is reflected by a region of high concentration projecting eastward into the Pacific and Atlantic Oceans in mid-latitudes. This feature shows up in the surface profile at 160°W. (Figure 33) as a small peak near 50°N. A region of low concentration near Hawaii, seen in the same profile in Figure 33, is shown by the contour map of level 1 to prevail in a limited region of the central Pacific. A similar feature appears in the Atlantic Ocean. Both features arise mainly from the seasonal biosphere (see Figure 2). At level 7 the influence of continental sources and sinks on the longitudinal patterns is reduced, but regions of high concentration are seen over regions of persistently rising air over northern Africa and Indonesia. The isotopic fields at level 1 and 7 shown in Figures 37 and 38, respectively, show similar but fewer features and, in particular, less longitudinal diversity.

Fig. 34. North-south profiles of δ_{mean}, in per mil, generated by the sum of all model source components for the year 1980, as in Figure 33, but with the addition of the Suess effect and temperature-dependent equilibrium fractionation assuming a constant air-sea exchange coefficient. The four curves and the dots are as defined in Figure 25.

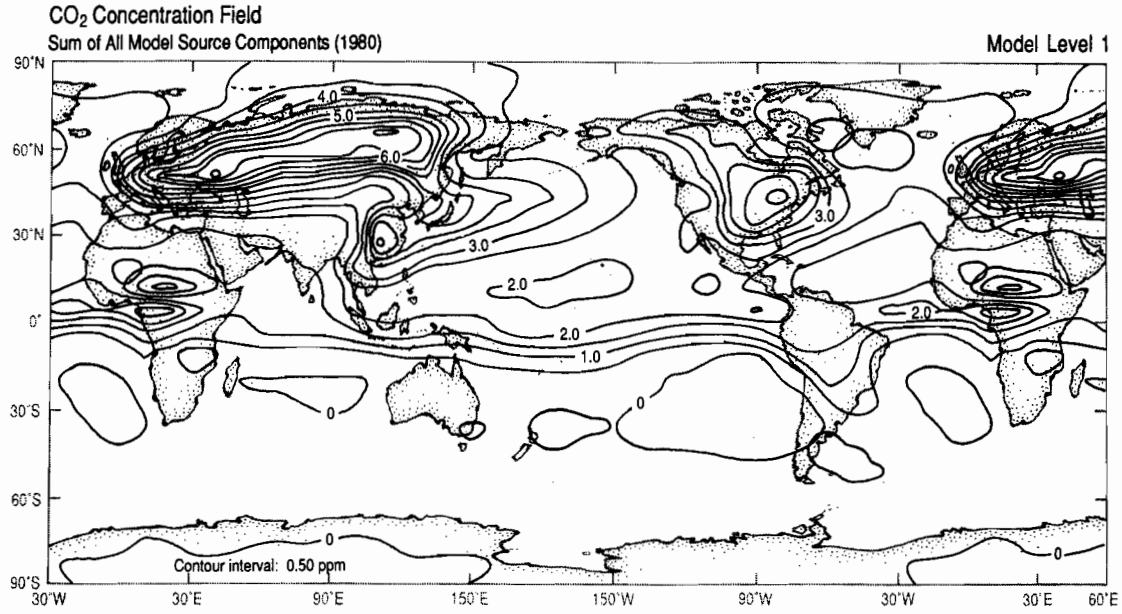

Fig. 35. Contour map of the mean annual CO_2 concentration field generated by the sum of all source components of the three dimensional model for the year 1980 at model level 1. Contour lines are labeled in ppm. Solid lines indicate positive or zero differences from the South Pole, dashed lines, negative differences, as in Figure 2.

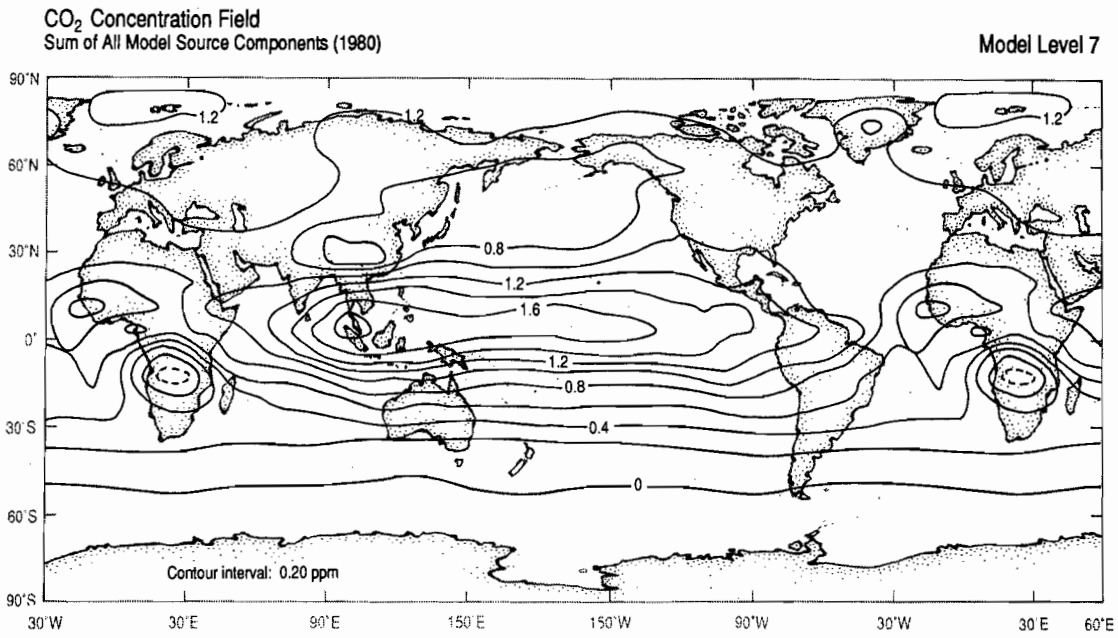

Fig. 36. Same as Figure 35 but at model level 7. Concentration differences, as in Figure 3, are with respect to the South Pole at model level 1.

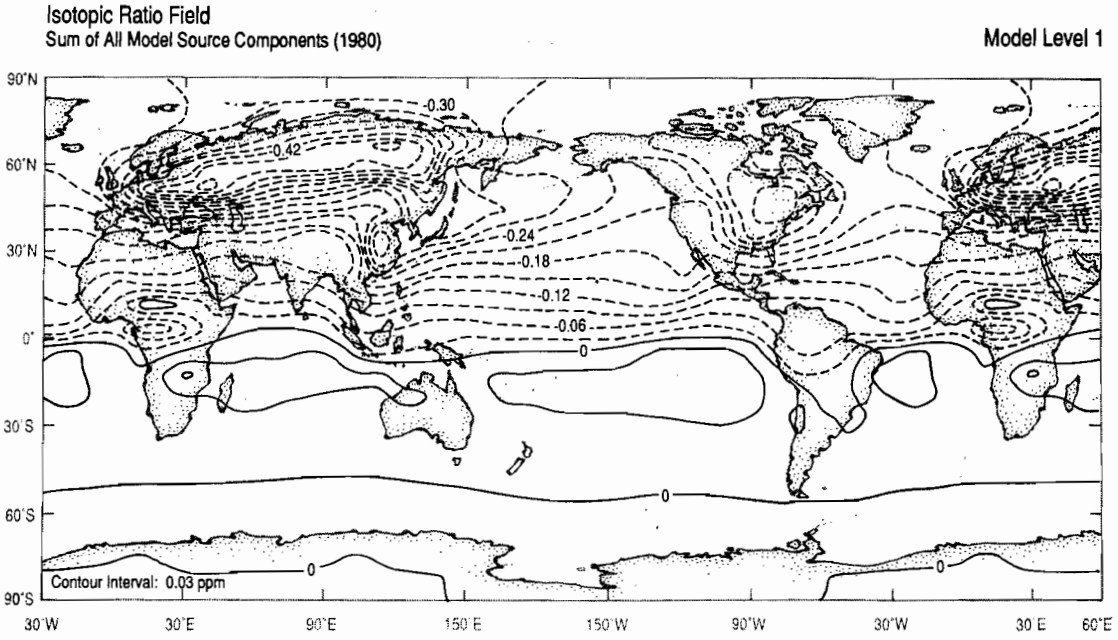

Fig. 37. Contour map of the mean annual reduced isotopic ratio of atmospheric CO_2, δ_{mean}, in per mil, generated by the sum of all source components of the three dimensional model for the year 1980 at model level 1. Contour lines are labeled in ‰. Solid and dashed lines are defined as in Figure 35.

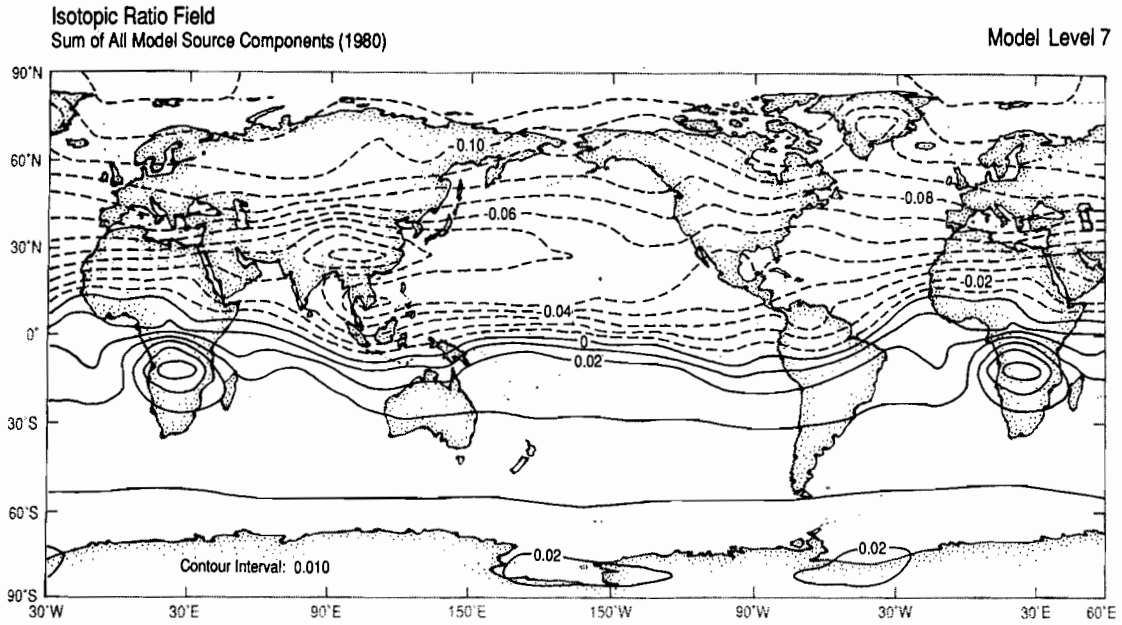

Fig. 38. Same as Figure 37 but at model level 7. Solid and dashed lines are defined, as in Figure 36, as differences from the South Pole at model level 1.

3. Observational Data

The atmospheric CO_2 data used in this study, and in the accompanying seasonal study of Heimann et al. [this volume], are described in detail by Keeling et al. [this volume]. In summary, these data were obtained in part from continuously recording gas analyzers, but mainly from samples collected in glass flasks. The samples from flasks were subsequently analyzed at the Scripps Institution of Oceanography for CO_2 concentration and at the University of Groningen for $^{13}C/^{12}C$ isotopic ratios. For the historical periods 1962, 1968, and 1980 measurements of air over the oceans substantially supplement measurements over land. For 1984 all data are from air sampled at land stations. Isotopic data are included for 1980 and 1984. Mean annual concentrations and isotopic ratios, together with estimates of their uncertainties, were established [I.2.3, Tables 1 to 4]. The geographical locations of the air samples are shown in Figures 39 through 42.

An iterative procedure was used to decompose concentration data at a given land station into seasonal and nonseasonal parts [I.2.2], the latter expressed by a spline function plus an exponential term [I.2.2, equation 2.2]. The degree of smoothing only slightly suppresses fluctuations on the scale of a few years, but in choosing periods to make model predictions we have selected times when variations associated with El Niño events are not prominent. Additional measurements obtained on ships were processed in an alternative manner owing to the shortness of the records but close spatial coverage [I, Appendix A]. Isotopic data were processed in a manner similar to the concentration data. As noted in subsection 2.1, above, we refer to these seasonally adjusted concentration and

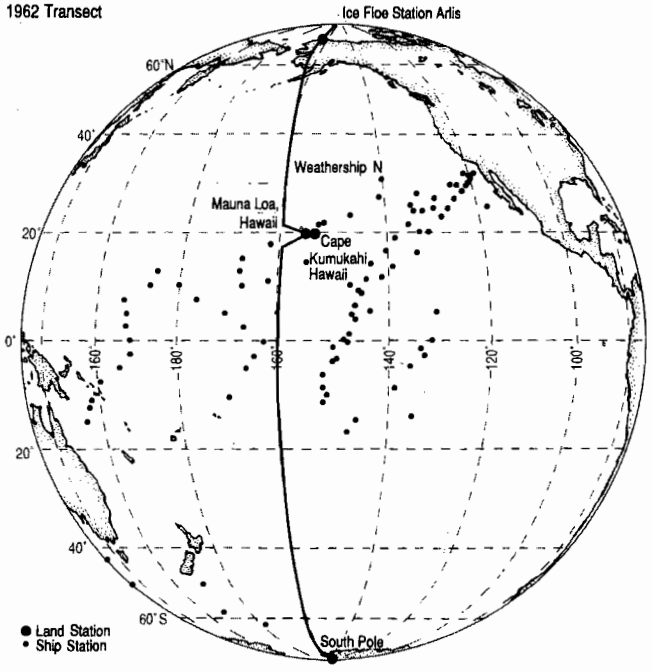

Fig. 39. Sampling locations and transect used for plotting model profiles for 1962. The sampling locations are shown for land station locations and for samples collected from ships. The transect is shown as a series of connecting line segments.

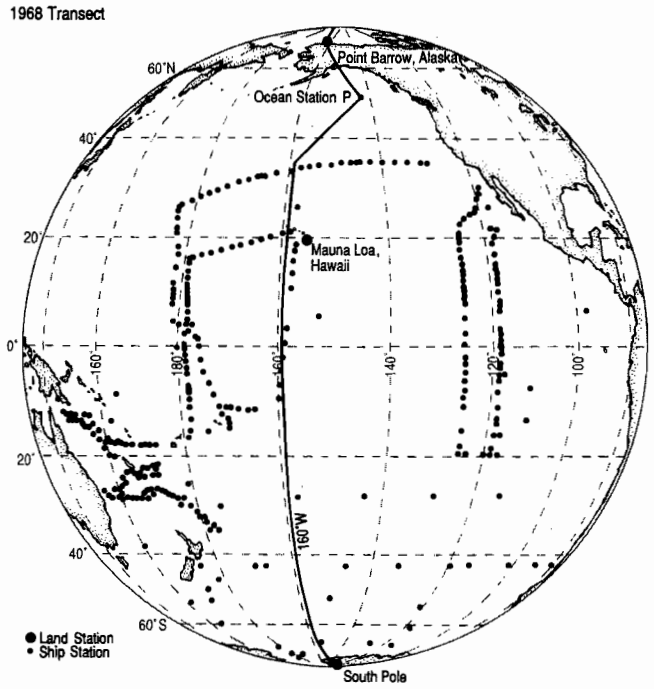

Fig. 40. Same as Figure 39 but for 1968.

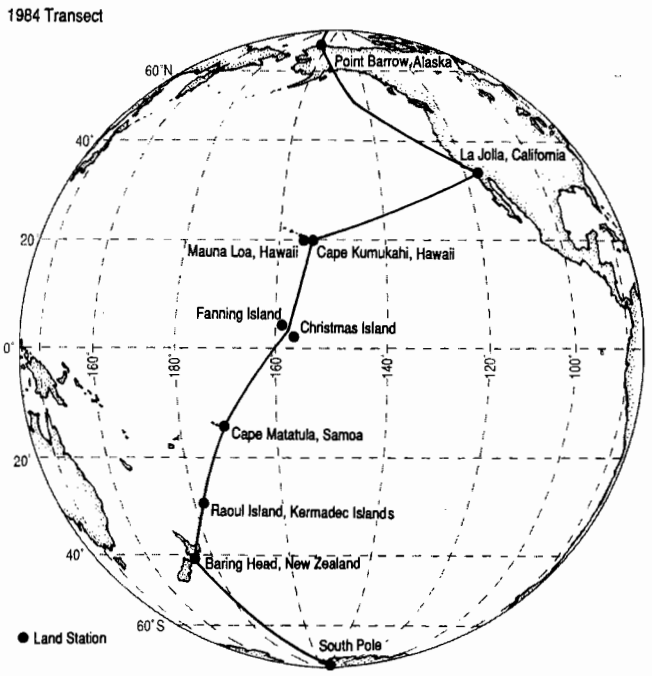

Fig. 42. Same as Figure 39 but for 1984.

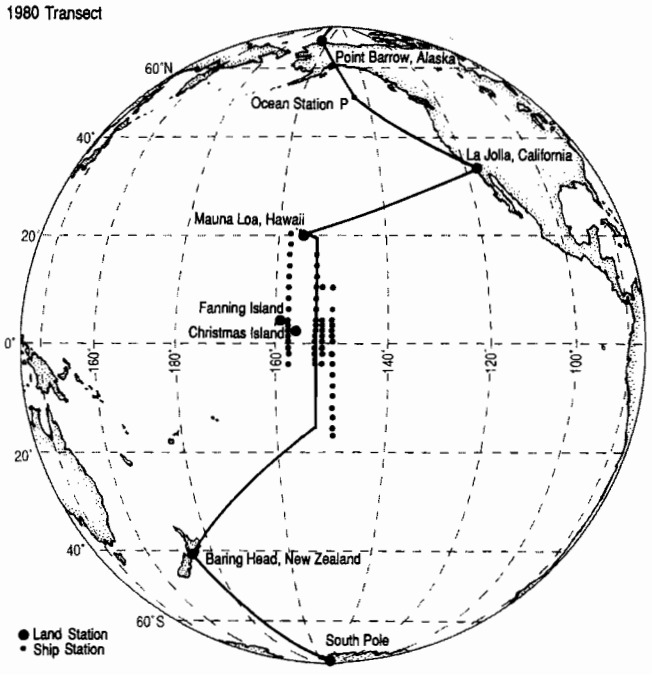

Fig. 41. Same as Figure 39 but for 1980. The transect from 19°N. to 16°S. remains at 153°W. along the middle line of stations of the FGGE Shuttle Expedition.

isotopic data as "observed C_{mean}" and "observed δ_{mean}," respectively. The corresponding model predictions are referred to simply as C_{mean} and δ_{mean} (see equations (2.6) and (2.7) of subsection 2.1, above).

In studying the seasonal cycle of CO_2 Heimann et al. [this volume] made use of additional CO_2 concentration data obtained from other sources. This was justified because systematic errors in calibration between different laboratories do not seriously affect the determination of phase and amplitude of an oscillatory signal. In the present study of mean annual data small calibrating errors may introduce serious biases, however, and we have therefore restricted our use of observational data to the results of the Scripps and Groningen laboratories.

The data coverage for the year 1980 is better in the tropics, but poorer at higher latitudes, than for 1984. Accordingly, for some purposes, we have merged the data for the two historical periods into single data sets, as listed in Table 3. To make negligible the influence of interannual changes, we made use of the three-dimensional model predictions of $C_{mean}(\mathbf{x})$ to adjust the 1984 data to apply to 1980, by determining for each location ($\mathbf{x}$) a weighted mean of the observed concentrations in 1980, $C_{obs\,1}(\mathbf{x})$ and in 1984, $C_{obs\,2}(\mathbf{x})$, after adjusting the latter by subtracting the interannual difference predicted by the model. Specifically, we computed:

$$\bar{C}(\mathbf{x}) = w_1(\mathbf{x})C_{obs\,1}(\mathbf{x}) + w_2(\mathbf{x})[C_{obs\,2}(\mathbf{x}) - (C_2(\mathbf{x}) - C_1(\mathbf{x}))] \qquad (3.1)$$

TABLE 3. Mean Annual CO_2 Concentration and Isotopic Ratio, δ_{mean}, as a Function of Latitude, 1980 and Model-adjusted 1984 Observations Combined for January 1, 1980

Latitude Interval of Shipboard Data or Name of Fixed Station	Mean Latitude (deg.)	Concentration (ppm)	Standard Error (ppm)	δ_{mean} (‰)	Standard Error (‰)
South Pole[a]	90.0S.	335.87	0.029	−7.544	0.007
Baring Head[a]	41.4S.	335.70	0.028	–	–
Raoul Is.[b]	29.2S.	335.85	0.088	−7.502	0.010
FGGE, 14-17 S.	15.6S.	336.59	0.039	−7.496	0.006
Cape Matatula[b]	14.2S.	336.82	0.105	−7.495	0.013
FGGE, 8-12 S.	9.6S.	337.01	0.035	−7.502	0.008
FGGE 2-6 S.	4.0S.	337.70	0.029	−7.509	0.009
FGGE, 1 N.-1 S.	0.0	337.93	0.023	−7.534	0.009
FGGE, 2-4 N.	3.0N.	337.89	0.026	−7.529	0.012
Fanning/Christmas[b]	3.0N.	337.89	0.085	−7.534	0.010
FGGE, 6-10 N.	8.0N.	337.71	0.031	−7.542	0.008
FGGE, 12-16 N.	13.8N.	337.84	0.033	−7.581	0.009
FGGE, 18-20 N.	19.0N.	337.89	0.074	−7.542	0.028
Cape Kumukahi	19.5N.	337.63	0.106	−7.594	0.011
La Jolla[a]	32.9N.	338.72	0.099	−7.702	0.014
Station P	50.0N.	338.21	0.123	–	–
Point Barrow[a]	71.3N.	338.67	0.137	−7.727	0.013

[a]Concentrations are weighted averages, $\bar{C}$ (**x**), for 1980 and 1984, defined according to equation (3.1). Isotopic data are similarly averaged.

[b]Concentrations for Fanning/Christmas, Cape Matatula, and Raoul Is. have been decreased by −0.011, +0.113 and +0.009 ppm, respectively, and the δ values by +0.0003, +0.0003, and −0.0012‰, respectively, differences predicted by the model for 1980 between the sample location and the transect location at the same latitude.

where C_1(**x**) and C_2(**x**) denote the model predictions of C_{mean}(**x**) for 1980 and 1984, respectively. Weights, w_i (i = 1, 2), are defined as functions of the standard errors of the means, σ_i(**x**), according to the formula of Bevington [1969, p. 74]:

$$w_i(\mathbf{x}) = \bar{\sigma}_i^{-2}(\mathbf{x}) / \bar{\sigma}^{-2}(\mathbf{x}) \tag{3.2}$$

where

$$\bar{\sigma}(\mathbf{x}) = (\sigma_1^{-2}(\mathbf{x}) + \sigma_2^{-2}(\mathbf{x}))^{-1/2} \tag{3.3}$$

We performed similar computations for the isotopic ratios. For standard errors, σ_i(**x**), we adopted previously established values [I.2.3, Tables 3 and 4].

4. Model Results

4.1 Comparison of Mean Fields with Data from Land Stations and Ships

In Figures 43 to 46 model predictions of CO_2 concentration, C_{mean}, are compared to smoothed, seasonally adjusted observational data, as discussed in section 3, above, for each historical period. The predicted profiles and their associated observations are plotted versus latitude along transects, shown in Figures 39 through 42, which approximately connect the observing stations. Linear interpolation was used to obtain predictions along the transects from data initially provided at the grid points of the model. The predictions are composites of the predictions of the individual source components of the model. In obtaining them, the strengths of the equatorial source and North Atlantic sink components, F_{EQU} and F_{ATL}, and the respiratory coefficient [II.4.3.4, equation (4.19)] were adjusted to obtain optimal fits to the data for each historical period, as discussed in section 2, above. The composite predictions for 1980, at the exact locations of the observations, are listed together with the associated individual component predictions in Table 4. Figures 47 and 48 compare the corresponding isotopic predictions of δ_{mean} to observations. These composite predictions, together with the contributions from the individual components, are listed in Table 5.

We also plot profiles in which we display the observational data for 1980 and 1984 merged. The 1984 data, before merging, were adjusted for the interannual changes in concentration and isotopic ratio, as described in section 3, above. These merged data, listed in Table 3, are useful when displaying the results of sensitivity tests, since they form more complete sets than are available for either historical period separately. The merged concentration data are shown in Figure 49. The optimal model prediction based on these merged data, also shown in the figure, is identical to those for 1980, owing to the method of adjustment. (In sensitivity tests presented in subsection 4.3 below, with one exception (see subsection 4.3.6), we do not readjust the merged 1984 data, however, because comparison of the plots is made easier by always displaying the same data points, and because the refinement is too small to

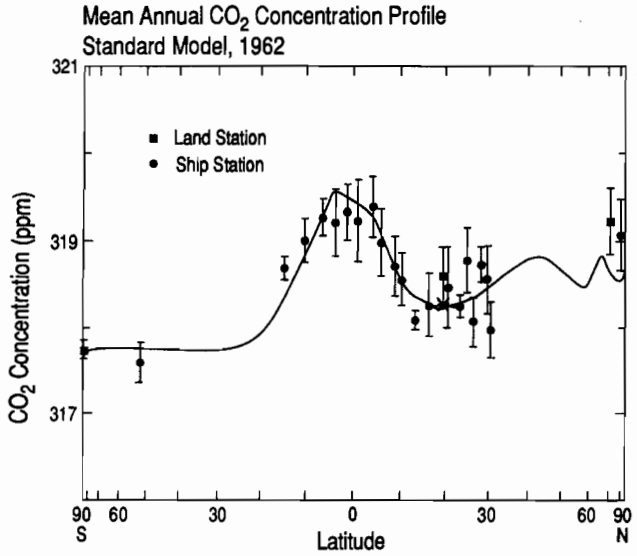

Fig. 43. Mean annual CO_2 concentration in ppm (by volume) as a function of latitude in 1962, near 160°W. Dots denote observations from samples collected over ocean water on ships, as listed by Keeling et al. [I.2.3, Table 1]. Solid squares denote samples collected over land at fixed stations, also so listed. Bars indicate ± 2 standard errors of the estimated concentrations for each location. The solid line indicates the profile as simulated by the three-dimensional model with standard parameters for model layer 1 along a transect that connects the land stations where observations were obtained. The transect passes only approximately through the area of ship observations which are distributed over a wide area of the Pacific Ocean, as shown in Figure 39. The concentration at Mauna Loa Observatory is indicated by a cross and was omitted from the fit of the model simulated profile, owing to the high elevation of the station.

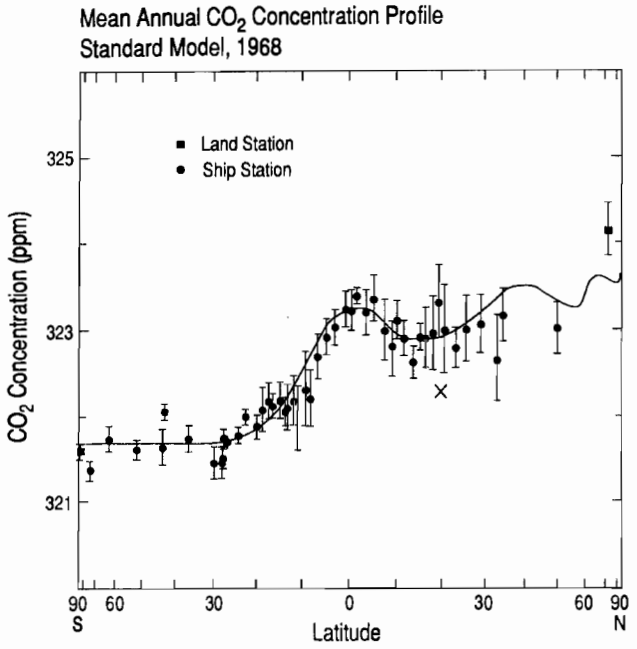

Fig. 44. Same as Figure 43, but for 1968, from observations as listed by Keeling et al. [I.2.3, Table 2]. The transect is shown in Figure 40.

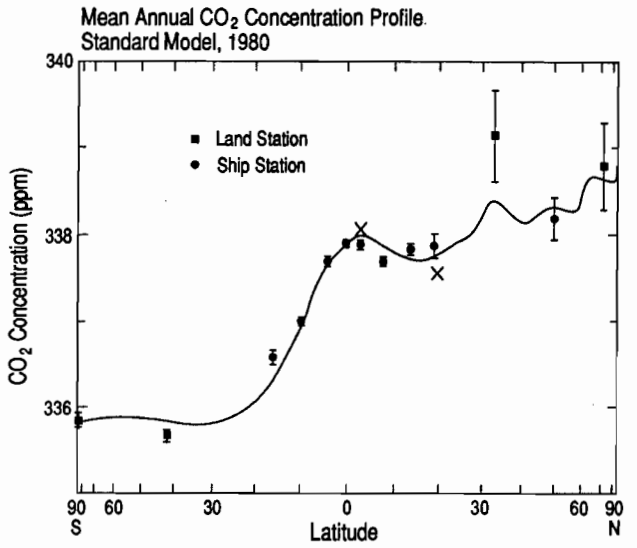

Fig. 45. Same as Figure 43, but for 1980, from observations as listed by Keeling et al. [I.2.3, Table 3]. The transect is shown in Figure 41. Crosses denote data for the Line Islands (Fanning and Christmas Islands combined) and for Mauna Loa Observatory (left and right, respectively). Both data were omitted from the fit of the model simulated profile. The datum for the Line Islands was omitted because of the availability of shipboard data in the vicinity. The Mauna Loa datum was omitted because of the high elevation of the station.

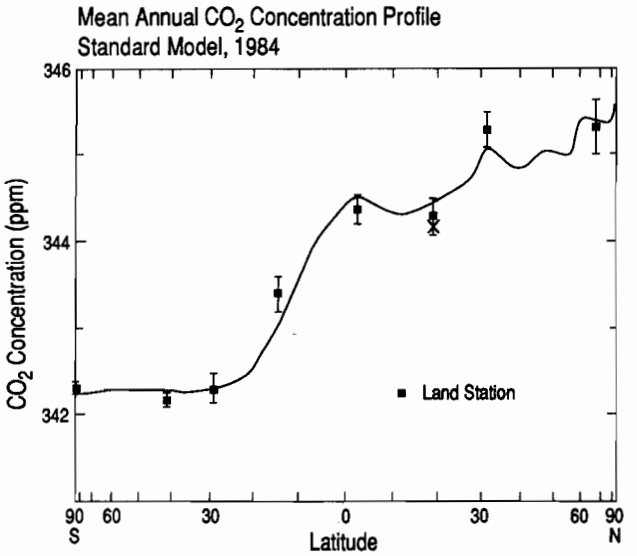

Fig. 46. Same as Figure 43, but for 1984, from observations as listed by Keeling et al. [I.2.3, Table 4]. The transect is shown in Figure 42. A cross denotes a datum for Mauna Loa Observatory, omitted from the fit of the model simulated profile.

TABLE 4. Predicted Mean Annual CO_2 Concentration (in ppm) together with Contributions of Individual Model Components at Observing Stations for 1980

Latitude Intervals of Shipboard Data or Name of Fixed Station	Lat. (deg.)	Long. (deg.)	Composite[a]		Individual Components[b]	
			C_{mean}	Difference	NPP + RES	DES
South Pole	90.00S.	--	335.83	0.0000	0.0000	0.0000
Baring Head	41.42S.	174.87E.	335.84	0.0165	–0.0464	0.0802
Raoul Is.	29.25S.	170.02W.	335.83	–0.0003	–0.0336	0.0967
FGGE, 14-17 S.	15.60S.	153.00W.	336.34	0.5132	–0.0503	0.1894
Cape Matatula	14.28S.	153.00W.	336.45	0.6231	–0.0505	0.2032
FGGE, 8-12 S.	9.60S.	153.00W.	336.94	1.1157	0.0045	0.2512
FGGE, 2- 6 S.	4.00S.	153.00W.	337.68	1.8543	0.1513	0.3075
FGGE, 1 N.-1 S.	0.00	153.00W.	337.87	2.0463	0.2727	0.3192
FGGE, 2- 4 N.	3.00N.	153.00W.	338.01	2.1848	0.3640	0.3275
Fanning/Christmas	3.00N.	153.00W.	338.01	2.1848	0.3640	0.3275
FGGE, 6-10 N.	8.00N.	153.00W.	337.88	2.0513	0.2218	0.2940
FGGE, 12-16 N.	13.80N.	153.00W.	337.7	1.9057	0.0425	0.2500
FGGE, 18-20 N.	19.00N.	153.00W.	337.77	1.9392	–0.0201	0.2219
Cape Kumukahi	19.53N.	154.68W.	337.77	1.9436	–0.0167	0.2200
Mauna Loa	19.53N.	155.58W.	337.47	1.6406	–0.3159	0.3010
La Jolla	32.87N.	117.25W.	338.42	2.5877	0.0076	0.2109
Station P	50.00N.	144.00W.	338.36	2.5301	0.3766	0.1562
Point Barrow	71.33N.	157.33W.	338.68	2.8493	0.5889	0.1137
Cape Kumukahi minus Mauna Loa	19.53N.	--	0.30	0.3030	0.2992	–0.0810

TABLE 4. -- continued

Latitude Interval of Shipboard Data or Name of Fixed Station	Individual Components					
	FER	TDE	EQU	ATL	UOS	IND
South Pole	0.0000	0.0000	0.0000	0.0000	0.0000	0.0000
Baring Head	–0.0992	0.0126	0.1088	–0.2663	–0.0117	0.2385
Raoul Is.	–0.1102	0.0256	0.1966	–0.4898	–0.0064	0.3207
FGGE, 14-17 S.	–0.2031	0.0192	0.7483	–0.9383	0.0112	0.7368
Cape Matatula	–0.2182	0.0162	0.8497	–0.9840	0.0140	0.7927
FGGE, 8-12 S.	–0.2777	–0.0127	1.2512	–1.1324	0.0115	1.0202
FGGE, 2- 6 S.	–0.3574	–0.0739	1.7923	–1.2909	–0.0093	1.3348
FGGE, 1 N.-1 S.	–0.4270	–0.1258	1.6427	–1.5232	0.0177	1.8702
FGGE, 2- 4 N.	–0.4795	–0.1650	1.5215	–1.6994	0.0386	2.2770
Fanning/Christmas	–0.4795	–0.1650	1.5215	–1.6994	0.0386	2.2770
FGGE, 6-10 N.	–0.5504	–0.1124	1.0221	–2.0235	0.1009	3.0988
FGGE, 12-16 N.	–0.6118	–0.0398	0.5373	–2.3207	0.1670	3.8813
FGGE, 18-20 N.	–0.6407	–0.0046	0.3744	–2.4500	0.2053	4.2530
Cape Kumukahi	–0.6413	–0.0037	0.3636	–2.4574	0.2097	4.2694
Mauna Loa	–0.5981	–0.0064	0.6483	–2.2466	0.2691	3.5891
La Jolla	–0.7365	–0.0361	0.3677	–2.5528	0.2739	5.0529
Station P	–0.7510	–0.0283	0.2013	–2.6936	0.2200	5.0490
Point Barrow	–0.8240	–0.0203	0.2489	–2.8435	0.3212	5.2644
Cape Kumukahi minus Mauna Loa	–0.0432	0.0027	–0.2847	–0.2108	–0.0594	0.6803

[a]The composite signal is specified both as the CO_2 concentration, C_{mean}, and as a concentration difference from the South Pole value. Concentrations for Fanning/Christmas, Cape Matatula, Raoul Is., and all FGGE locations are as determined along a 1980 transect at the station latitude. Mauna Loa is at model level 4; all other locations are at the surface (model level 1; see Table 2 of Heimann and Keeling [this volume]).

[b]Names of components: NPP, net primary productivity; RES, biospheric respiration; DES, biospheric destruction; FER, biospheric fertilization; TDE, temperature-dependent air-sea exchange; EQU, equatorial source; ATL, North Atlantic sink; UOS, uniform oceanic sink; and IND, industrial source. All biospheric components are terrestrial. A constant air-sea gas exchange coefficient is assumed for the oceanic components.

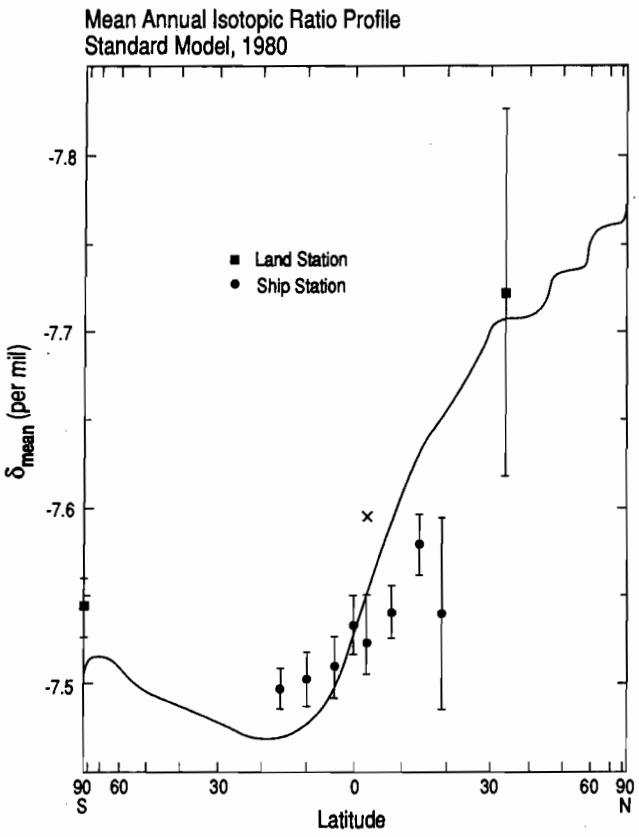

Fig. 47. Mean annual reduced isotopic ratio of atmospheric CO_2, δ_{mean}, in per mil, as a function of latitude in 1980, near 160°W. Dots denote measurements made on air samples collected on ships, as listed by Keeling et al. [I.2.3, Table 3]. Squares denote samples collected at land stations, also so listed. Bars indicate ± 2 standard errors of the estimated isotopic ratios at each location. The solid line indicates the simulated model profile for model layer 1 along the same transect as in Figure 45. A cross denotes a datum for the Line Islands as in Figure 45, omitted from the fit of the model simulated profile.

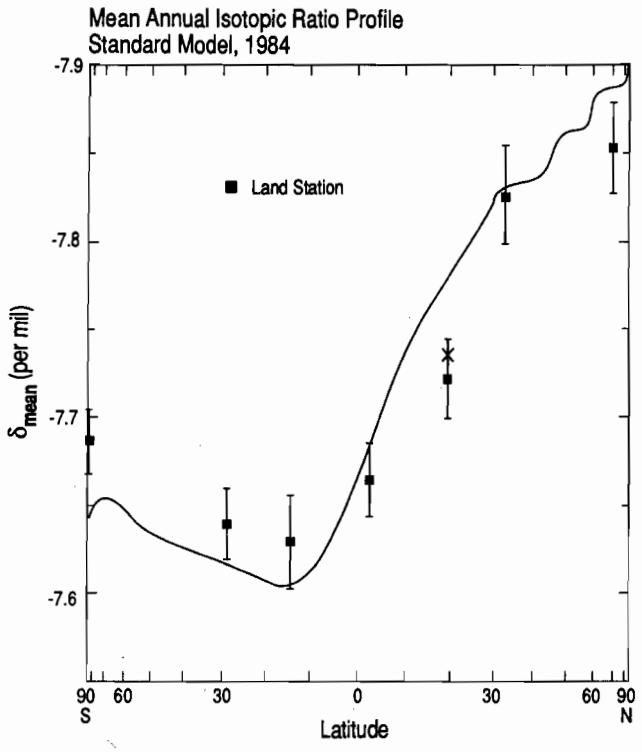

Fig. 48. Same as Figure 47 but for 1984 from observations as listed by Keeling et al. [I.2.3, Table 4]. The model profile is along the same transect as in Figure 46. A cross denotes a datum for Mauna Loa Observatory as in Figure 46, omitted from the fit of the model simulated profile.

be necessary. As a result, the fits in the sensitivity tests, being to the merged data, are slightly different than they would be to the 1980 data alone.)

In anticipation of a discussion in subsection 4.3.7, below, we further show, in Figure 50 (dash-dot line), the result of assuming a variable gas exchange coefficient for the oceanic components, as was done to produce the temperature-dependent fractionation field shown in Figure 31. By readjusting the three adjustable source components to obtain an optimal fit to the merged data, the profile is seen to be practically indistinguishable from that when assuming a constant coefficient, shown for comparison by a solid line. In contrast, as shown in Figure 51, the prediction of δ_{mean}, assuming a variable gas exchange coefficient, agrees considerably better with the merged 1980 and 1984 isotopic data than does the prediction assuming a constant coefficient.

As noted above, we have used direct observations of atmospheric CO_2 to adjust simultaneously the mean annual strengths of two poorly known oceanic source components in the model. Also, a respiratory coefficient controlling the seasonality of heterotrophic respiration in the terrestrial biosphere is adjusted with respect to the seasonal cycle exhibited by the observations. This adjustment, however, has only a very small effect on the mean annual fields discussed in this article. We have not adjusted the global strengths of any biospheric components, because they are to some degree established from independent data and because the mean annual north-south gradients in concentration which they generate are too similar to those of the oceanic components to permit additional unique fits to the data. Also, we have not adjusted any components to improve the model prediction of isotopic carbon, and we thus are able to use the observations of δ_{mean} as an independent check on the validity of the model prediction produced by our choice of adjustable components.

By adjusting the global strengths of the equatorial source and North Atlantic sink components we have achieved model predictions which agree moderately well with our mean annual concentration data. Shown in Table 6 are values of reduced chi square [Bevington, p. 188]

$$\chi^2_{red} = \frac{1}{l} \sum_{j=1}^{l} (d_j/\sigma_j)^2 \qquad (4.1)$$

TABLE 5. Predicted Mean Annual Isotopic Ratio (in per mil) together with Contributions of Individual Model Components at Observing Stations for 1980.

Latitude Interval of Shipboard Data or Name of Fixed Station	Lat. (deg.)	Long. (deg.)	Composite[a]		Individual Components[b]
			δ_{mean}	Difference	TDF
South Pole	90.00S.	--	–7.505	0.0000	0.0000
Baring Head	41.42S.	174.87E.	–7.490	0.0154	0.0245
Raoul Is.	29.25S.	170.02W.	–7.479	0.0257	0.0406
FGGE, 14-17 S.	15.60S.	153.00W.	–7.470	0.0354	0.0754
Cape Matatula	14.28S.	153.00W.	–7.470	0.0348	0.0783
FGGE, 8-12 S.	9.60S.	153.00W.	–7.478	0.0264	0.0860
FGGE, 2- 6 S.	4.00S.	153.00W.	–7.497	0.0077	0.0917
FGGE, 1 N.-1 S.	0.00	153.00W.	–7.529	–0.0243	0.0949
FGGE, 2- 4 N.	3.00N.	153.00W.	–7.554	–0.0487	0.0973
Fanning/Christmas	3.00N.	153.00W.	–7.554	–0.0487	0.0973
FGGE, 6-10 N.	8.00N.	153.00W.	–7.591	–0.0863	0.0966
FGGE, 12-16 N.	13.80N.	153.00W.	–7.628	–0.1227	0.0934
FGGE, 18-20 N.	19.00N.	153.00W.	–7.650	–0.1448	0.0886
Cape Kumukahi	19.53N.	154.68W.	–7.651	–0.1460	0.0886
Mauna Loa	19.53N.	155.58W.	–7.603	–0.0984	0.0934
La Jolla	32.87N.	117.25W.	–7.707	–0.2024	0.0777
Station P	50.00N.	144.00W.	–7.736	–0.2309	0.0600
Point Barrow	71.33N.	157.33W.	–7.762	–0.2567	0.0592
Cape Kumukahi minus Mauna Loa	19.53N.	--	–0.048	–0.0476	–0.0048

TABLE 5. -- continued

Latitude Interval of Shipboard Data or Name of Fixed Station	Individual Components				
	SUE	NPP + RES	DES	FER	TDE
South Pole	0.0000	0.0000	0.0000	0.0000	0.0000
Baring Head	0.0008	0.0025	–0.0042	0.0053	0.0000
Raoul Is.	0.0005	0.0018	–0.0051	0.0059	–0.0001
FGGE, 14-17 S.	–0.0008	0.0027	–0.0100	0.0109	–0.0001
Cape Matatula	–0.0010	0.0027	–0.0107	0.0117	–0.0001
FGGE, 8-12 S.	–0.0008	–0.0003	–0.0132	0.0148	0.0000
FGGE, 2- 6 S.	0.0007	–0.0081	–0.0161	0.0190	0.0003
FGGE, 1 N.-1 S.	–0.0013	–0.0147	–0.0167	0.0227	0.0004
FGGE, 2- 4 N.	–0.0028	–0.0196	–0.0172	0.0255	0.0006
Fanning/Christmas	–0.0028	–0.0196	–0.0172	0.0255	0.0006
FGGE, 6-10 N.	–0.0073	–0.0120	–0.0154	0.0293	0.0004
FGGE, 12-16 N.	–0.0121	–0.0024	–0.0131	0.0326	0.0001
FGGE, 18-20 N.	–0.0148	0.0010	–0.0116	0.0341	0.0000
Cape Kumukahi	–0.0151	0.0008	–0.0115	0.0342	0.0000
Mauna Loa	–0.0194	0.0169	–0.0158	0.0319	0.0000
La Jolla	–0.0197	–0.0005	–0.0110	0.0392	0.0001
Station P	–0.0158	–0.0202	–0.0082	0.0399	0.0001
Point Barrow	–0.0231	–0.0317	–0.0060	0.0438	0.0001
Cape Kumukahi minus Mauna Loa	0.0043	–0.0161	0.0043	0.0023	0.0000

TABLE 5. -- continued

Latitude Interval of Shipboard Data or Name of Fixed Station	Individual Components			
	EQU	ATL	UOS	IND
South Pole	0.0000	0.0000	0.0000	0.0000
Baring Head	–0.0004	0.0009	0.0000	–0.0140
Raoul Is.	–0.0007	0.0017	0.0000	–0.0189
FGGE, 14-17 S.	–0.0026	0.0033	0.0000	–0.0432

TABLE 5. -- continued

Latitude Interval of Shipboard Data or Name of Fixed Station	Individual Components			
	EQU	ATL	UOS	IND
Cape Matatula	–0.0030	0.0035	0.0000	–0.0465
FGGE, 8-12 S.	–0.0044	0.0040	0.0000	–0.0598
FGGE, 2- 6 S.	–0.0063	0.0045	0.0000	–0.0780
FGGE, 1 N.-1 S.	–0.0057	0.0053	–0.0001	–0.1093
FGGE, 2- 4 N.	–0.0053	0.0059	–0.0001	–0.1330
Fanning/Christmas	–0.0053	0.0059	–0.0001	–0.1330
FGGE, 6-10 N.	–0.0036	0.0071	–0.0004	–0.1811
FGGE, 12-16 N.	–0.0019	0.0081	–0.0006	–0.2269
FGGE, 18-20 N.	–0.0013	0.0086	–0.0007	–0.2486
Cape Kumukahi	–0.0013	0.0086	–0.0007	–0.2495
Mauna Loa	–0.0023	0.0079	–0.0009	–0.2100
La Jolla	–0.0013	0.0089	–0.0010	–0.2948
Station P	–0.0007	0.0094	–0.0008	–0.2946
Point Barrow	–0.0009	0.0099	–0.0011	–0.3069
Cape Kumukahi minus Mauna Loa	0.0010	0.0007	0.0002	–0.0395

[a]Specified both as the isotopic ratio, δ_{mean}, and as a difference from the South Pole value. Isotopic ratios for Fanning/Christmas, Cape Matatula, Raoul Is., and all FGGE locations are as determined along the 1980 transect at the station latitude. Mauna Loa is at model level 4; all other locations are at the surface (model level 1; see Table 2 of Heimann and Keeling, this volume).

[b]For names of components, see Table 4. Additional components are: TDF, temperature-dependent fractionation between air and seawater, and SUE, the departure from global isotopic equilibrium brought about by perturbations to the carbon cycle, principally industrial CO_2 (Suess Effect). A constant air-sea gas exchange coefficient is assumed for the oceanic components.

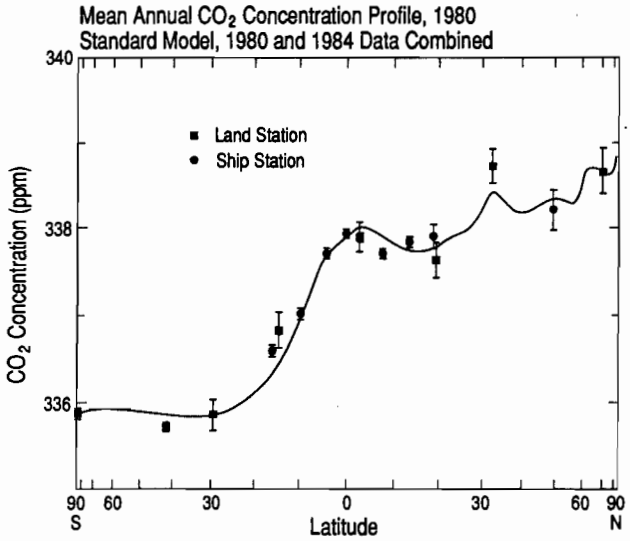

Fig. 49. Mean annual CO_2 concentration in ppm (by volume) as a function of latitude near 160°W. based on observations of 1980 and 1984 combined. The 1984 data are adjusted to apply to 1980 as described in the text. The solid line indicates the profile as simulated for 1980 at model level 1 as in Figure 45. Symbols are the same as in Figures 45 and 46, except that the only data shown are those included in the model fit.

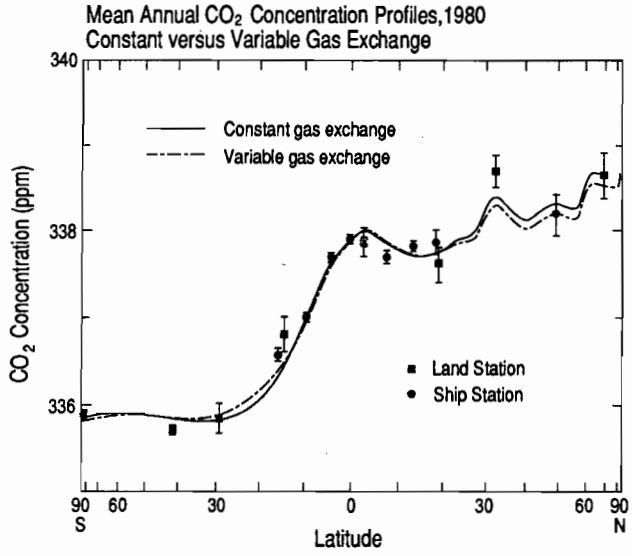

Fig. 50. Mean annual CO_2 concentration in ppm (by volume) in 1980 as in Figure 49, compared with a profile in which the coefficient of gas exchange, k_{ex}, is assumed to vary with wind speed, as described in the text. The standard profile assuming a constant exchange coefficient (Figure 49) is shown as a solid curve, the profile for variable k_{ex} by a dash-dot curve.

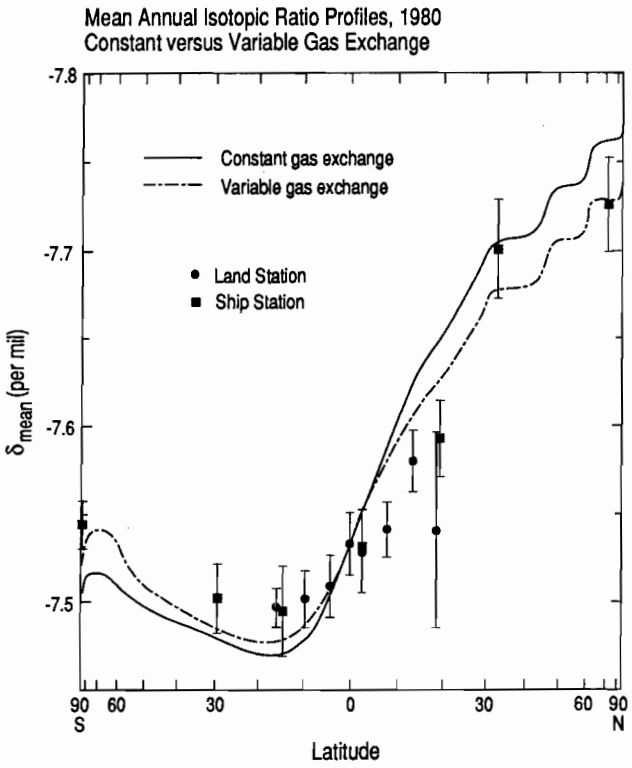

Fig. 51. Mean annual δ_{mean}, in per mil, in 1980 computed for both constant and variable coefficient of gas exchange, k_{ex}, and plotted as in Figure 50.

where d_j denotes the departure at observing station j from the observed C_{mean} or δ_{mean}, σ_j denotes the standard error of the observed values at that station (cf. equation 3.5) and l denotes the number of data points compared. The values of χ^2_{red} for concentration range from 4.9 to 14.7.

The high χ^2_{red} value of 14.7 for 1980 is mainly a consequence of the small standard errors of the shipboard concentration data from the FGGE Shuttle Expedition [I.2.3, Table 3], which in turn reflect an exceptionally good two-dimensional fit of the original measurements with respect to time and latitude. Even if the sources and sinks could be more realistically prescribed, the three-dimensional model, having a coarser grid, is unable to replicate this surface based, as it is, on data with a spacing of 1–2 degrees. The shipboard data for 1962 and 1968 [I.2.3, Tables 2 and 3] are also closely spaced but, having considerably larger standard errors, produce lower values of χ^2_{red} for the model fits. The data for 1984, lacking shipboard observations, are spaced more widely than the model grid. Thus the simulated surface is readily fit to these observations via the two adjustable oceanic parameters.

The goodness of these fits to observed C_{mean}, to a considerable degree, is controlled by our use of two nearly orthogonal components that strongly influence predictions of the north-south concentration gradients: especially mean differences between the two hemispheres and between the equatorial zone and polar regions. These two oceanic components are, indeed, similar to the first and second Legendre polynomial used by Bolin and Keeling [1963] for a similar latitudinal fit to the data for the 1962 historical period, shown for the present study in Figure 43. Legendre polynomials, however, furnish no details regarding the longitudinal distribution of sources and sinks. In contrast the patterns of the three-dimensional model component fields, based on *a priori* assignments of relative regional and of global source strengths, are spatially somewhat more realistic, and with better oceanic data could be made still more realistic. On the other hand, as indicated below, these two components are not entirely orthogonal, making interpretation of their strengths more complicated than otherwise.

The large differences in observed interhemispheric gradient in C_{mean} from one historical period to the next, between 1962 and 1980, are achieved in the model predictions almost exclusively by changes in the strength of the industrial CO_2 component. This fact is made clear by the relatively small differences in source strengths found for the two adjustable oceanic components. The deduced strengths of the equatorial source for the four historical periods vary with a standard deviation of only 0.29×10^{12} kgC yr^{-1} (Table 1); the North Atlantic sink with a still smaller standard deviation of 0.14×10^{12} kgC yr^{-1} (Table 2). In contrast, the annual strength of the industrial component increases by 2.5×10^{12} kgC yr^{-1} from 1962 to 1984 (see I.5, Table 12).

The model (see Figure 49) predicts a peak in C_{mean} near the equator and a trough near 20°N. Neither of these predicted features is sensitive to the adjustments made to the equatorial source or North Atlantic sink components. The good prediction of the latitude of the equatorial peak is evidence that our choice of data to represent the oceanic CO_2 partial pressure, $pCO_{2\,sea}$, in the tropics is realistic. The good prediction of the minimum near 20°N. depends partly on the chosen north-south profile of $pCO_{2\,sea}$, but also depends on the validity of the model prediction of a dip in concentration associated with the terrestrial biosphere, shown by the upper curve of Figure 9. This dip we attribute in part to the influence of the Hadley cell circulation on the fields generated by NPP and respiration discussed in subsection 2.3, above. This circulation also influences the shape of the concentration field generated by the equatorial source component. It is clearly not related to industrial CO_2 emissions which produce a monotonically decreasing CO_2 concentration field from north to south (see Figure 23). We are led to conclude that the model has produced a series of predictions (Figures 43 through 46) which reflect a degree of realism, not solely dependent on our making adjustments to the strength of selected oceanic components.

Isotopic profiles of δ_{mean} are available only for the most recent historical periods, 1980 and 1984. The model predictions (Figures 47 and 48) are independently adjusted only to the extent that the mean position of the profile is determined by a weighted least squares fit to the observations [cf. II.5.4, text after equation (5.53)]. The resulting agreement of model predictions with observations is less successful than for CO_2 concentration. For 1980 the small standard errors of the isotopic data from the FGGE Shuttle Expedition forces the profile curve in the tropics to pass near these data, resulting in relatively poor agreement at the South Pole. With respect to La Jolla, California (33°N.), the only other station outside of the tropics having isotopic observations that year, the quality of the data is exceptionally poor as a result of unusually sparse sampling in 1979 and 1980. No meaningful comparison of model prediction and data is possible.

TABLE 6. Reduced chi square, χ^2_{red}, for Three-dimensional Model Predictions of the Mean Annual Atmospheric CO_2 Concentration, C_{mean}, and Reduced Isotopic Ratio, δ_{mean}.

	C_{mean}			δ_{mean}		
Historical Period	No. of Data	Degrees of Freedom	χ^2_{red}	No. of Data	Degrees of Freedom	χ^2_{red}
1962	24	21	5.1	–	–	–
1968	50	47	4.9	–	–	–
1980	13	10	14.7	10	9	13.9
1984	8	5	6.4	7	6	11.7
1980–1984*	17	14	12.3	15	14	13.7

*Combined data, as explained in text

Irrespective of the data for La Jolla and the South Pole, the predicted gradient within the tropics is significantly steeper than the observations indicate, so that overall the fits are poor (χ^2_{red} of 13.9 in 1980, 11.7 in 1984, see Table 6). For 1984 the precision and density of the tropical data are lower, and the prediction is in slightly better overall agreement with the observations, but again the predicted gradient in the tropics appears to be too steep.

For 1984 the predicted δ_{mean} again agrees poorly with the observations for the South Pole, but it also agrees poorly with observations at an additional station, Point Barrow, Alaska (71°N.), which provides isotopic data beginning in 1983 [see I.4.3, Table 6]. The predicted pole-to-pole difference in δ_{mean} is too large because the prediction for the South Pole is too positive and for Point Barrow too negative.

We gain insight into the construction of the model predictions of the gradient in δ_{mean} in the tropics by intercomparing the model predictions of the individual components that are mainly responsible for this isotopic gradient. By far the most important of these is the industrial CO_2 component which generates a north-south gradient far steeper than that of the observations (solid curve in Figure 32). The profile for the sum of the biospheric components (solid curve in Figure 25) offsets this steep gradient in the northern tropics, while temperature-dependent fractionation (solid curve in Figure 30) offsets it in the southern tropics. These offsets, however, are not sufficient to produce good agreement with the observations. Possible causes of the lack of satisfactory agreement are discussed in subsection 4.3, below.

4.2 *Assessment of Errors in the CO_2 Source Formulations*

4.2.1 Introduction. The reliability of our model predictions cannot, in a practical sense, be defined simply by an analysis of identifiable errors. The phenomena which the model addresses are too complex for us to be able to specify all of the systematic errors which may influence the predictions. We will, however, discuss errors that can be readily identified. These are mainly imprecisions of a statistical nature and estimated upper and lower limits. They apply especially to the isotopic formulations. We will express these errors at approximately the 90 percent confidence level (1.6 times the standard error), if we have any basis for doing so. Then, in the next subsection, we will test the uniqueness of the model predictions by means of sensitivity analyses.

4.2.2 Errors in the simulation of the terrestrial biosphere. The seasonal cycles of net primary productivity (NPP) and of respiration are predicted by the model quite realistically [III.5.2]. We therefore do not expect the mean annual fields associated with these predictions to be in serious error. The predictions arising from biospheric destruction and fertilization, in contrast, depend directly on global magnitudes that are highly uncertain. For fertilization, even the existence of this flux is in doubt. We have not attempted to assign errors to these perturbation fluxes, but, rather have examined the consequences of possible unknown errors by conducting sensitivity tests, described in subsection 4.3, below.

The $^{13}C/^{12}C$ isotopic ratio of plant carbon has a direct influence on the prediction of all of the isotopic fields associated with the terrestrial biosphere. The ratio in the model is assumed to be spatially constant during any given historical period [I.5, Table 8], and is derived from an estimate of approximately –25‰ for the global average δ value of carbon in living matter on land. The observed seasonal cycle of atmospheric CO_2 indicates a range in the δ of CO_2 released by plants from –23 to –28‰ [I.5, Table 5], neglecting the influence of oceanic CO_2 on the observed cycle. Since the global average δ of atmospheric CO_2 in recent times was approximately –7.5‰ [I.5, Table 11] the isotopic difference is approximately 18‰. The relative uncertainty in the predicted δ field of atmospheric CO_2 associated with errors in estimating this difference is thus in the neighborhood of 10 percent. We lack data to estimate additional errors arising from spatial and seasonal variability in the $^{13}C/^{12}C$ ratio of plant CO_2 exchanged with the atmosphere.

4.2.3 Errors in the simulation of oceanic fluxes. Here we are mainly concerned with spatial variations in the annual mean fluxes, since the seasonal cycle of oceanic CO_2 has only a minor influence on the mean annual fields of atmospheric CO_2 (see Figure 15). The CO_2 partial pressure in surface sea water, $pCO_{2\,sea}$, and the rate of gas exchange both contribute directly to a computation of the net flux of CO_2 across the air-sea interface. Neither factor is well known. As in the case of biospheric perturbations, we examine the consequences of systematic errors by conducting sensitivity tests, discussed in subsection 4.3, below.

The isotopic fields of atmospheric CO_2 are only very slightly influenced by bulk gas exchange driven by variations in CO_2 partial pressure between the atmosphere and the oceans, because of the small degree of kinetic fraction involved [I.3, equation (3.4)]. Errors in the associated fractionation factors introduce negligible errors in the model predictions. This is not the case, however, with respect to the equilibrium fractionation between oceanic and atmospheric CO_2, a process as defined in the three-dimensional model to be independent of gradients in $pCO_{2\,sea}$ at the air-sea boundary [II.5.4, equation 5.42]. This purely isotopic exchange is strongly temperature-dependent, and produces greater variations in δ_{mean} than are generated by the terrestrial biosphere (cf. Figures 25 and 30). Indeed, in the southern hemisphere the variations from this exchange far exceed those produced by the biosphere.

The associated fractionation factor for equilibrium exchange has been determined in laboratory experiments [Mook et al., 1974]. The standard error in the estimated mean factor, 0.75‰, does not contribute to the model predictions, because in our modeling we consider only differences in δ_{mean} from the prediction for the South Pole. Even the standard error in the temperature coefficient, which

is about 2 percent of that coefficient [Mook et al., 1974, p. 174], produces only minor errors in the predicted δ_{mean} field. This statistical error was established with respect to the exchange of CO_2 gas with dissolved bicarbonate ion. Neglect of the slightly smaller fractionation contributed by dissolved carbonate, which comprises about 10 percent of the exchangeable dissolved inorganic carbon in sea water, causes an overestimate of the extent of fractionation between dissolved inorganic carbon and gaseous CO_2 by 1.4 percent at 0°C. and 1.2 percent at 30°C. [Mook, 1986, p. 213], thus overestimating the extreme range predicted for δ_{mean} (0.15‰) by 0.002‰, also a negligible error. Errors in estimating sea-surface temperature also contribute negligibly, owing to the wide range in temperature which produces the δ_{mean} field.

More serious errors in the prediction of δ_{mean} arise because of uncertainties in the coefficient of gas exchange. As shown in Figure 51, if we assume that gas exchange varies with wind speed, keeping the global average exchange rate the same as when we assume the rate to be constant (cf. Figure 31), we obtain a considerably altered profile of δ_{mean}. Predicted pole-to-pole differences are approximately 0.05‰ less than if a constant exchange rate is assumed, i.e., about 15 percent of the extreme range predicted for δ_{mean} assuming a constant exchange. Data on gas exchange at the sea surface do not exist to verify the dependency on wind speed that we assumed; the errors in predicting δ_{mean} could be as great as the differences in prediction between the constant and variable cases.

To arrive at some kind of quantitative estimate, however crude, we have assumed that the two estimates, based on constant and variable exchange, are equally likely in their prediction of the difference in δ_{mean} between Point Barrow, Alaska, and the South Pole. This assumption results in an estimate of the error at the 90 percent confidence level of 54 percent (1.65 times the relative standard deviation of the two estimates of the difference in δ_{mean} between the stations; see, for example, Parratt [1961, p. 173]). An additional error results because the average rate of gas exchange employed in both predictions of the difference between stations is known only to a precision of about 20 percent at the 90 percent confidence level [Bolin, 1981, p. 12]. The combined error from both uncertainties is then 58 percent, assuming that the errors are uncorrelated and that the relative variances, to first order, are therefore additive [see, for example, Parratt, 1961, p. 116].

4.2.4 Errors associated with emissions of CO_2 from fossil fuel combustion. Errors in reporting fuel production are mainly systematic with no firm basis for establishing uncertainties. Marland and Rotty [1984], after a detailed analysis, concluded that the uncertainty in the global production at the 90 percent confidence level lies between 6 percent and 10 percent [loc cit., p. 256]. They did not attempt to assess the regional distribution of these errors. Since the consumption of fossil fuel is mainly concentrated in a few industrial regions between 30°N. at 60°N., regional errors probably have little effect on the model predictions. Thus we expect that uncertainty in emissions can be characterized by a global constant error not greater than 10 percent.

The influence of industrial CO_2 on the δ_{mean} field is uncertain owing to imprecise knowledge of both the amount and isotopic composition of the fuels emitted to the atmosphere. Firstly, with respect to the isotopic ratio of various fossil fuels, Tans [1981] found that extensive data for coal, lignite and petroleum were so consistent that the means should not be in error by more than "several tenths per mil". Natural gas, however, exhibits such a wide range in δ (from −20‰ to −75‰) that Tans estimated an uncertainty in the global mean of "several per mil". Natural gas contributes approximately 17 percent of the carbon emitted as CO_2 by fuel combustion according to data of Rotty [1987a] (0.873×10^{12} kgC from natural gas in 1980 including flared gas, compared to total emissions of 5.13×10^{12} kgC). If the uncertainty in the δ of natural gas is 10 times that of the other fuels, approximately as implied by Tans, the overall uncertainty in δ of fossil fuel is 25 percent of the uncertainty for natural gas. Using this rough guess, the overall uncertainty in δ of fossil fuel at the 90 percent confidence level could approach 2‰. The CO_2 produced by cement manufacture is too small for the error in the associated δ to contribute significantly to the error in δ of industrial CO_2. Given that the global average δ of atmospheric CO_2 in 1980 was approximately −7.5‰ [I.5, Table 11] while the δ of industrial CO_2 was −27‰ [Tans, 1981], the difference was approximately 20‰ in 1980. Thus an uncertainty of 2‰ in the δ of fossil fuel (and hence in industrial CO_2) introduces a relative uncertainty in the predicted δ field of atmospheric CO_2 of 10 percent.

Secondly, uncertainty in fossil fuel emission data contribute errors to the predictions of δ_{mean}. If we adopt the estimate of Marland and Rotty [1984, p. 256] of 10 percent for this uncertainty (in which the errors for each fuel type are not assumed to be independent), and we combine this estimate with the above estimate of 10 percent for the isotopic ratio, the overall uncertainty for δ of industrial CO_2 at the 90 percent confidence level is 14 percent, assuming that the two errors are uncorrelated and that the relative variances are therefore additive (cf. subsection 4.2.3 above).

4.2.5 Errors arising from neglecting variations in the atmospheric concentration field in the computation of air-sea exchange. In the three-dimensional model [II.4.4, see text after equation (4.26)], we have neglected spatial variations in atmospheric CO_2 in defining the air-sea exchange of CO_2. This neglect produces an underestimate of the uptake of CO_2 by the oceans in the northern hemisphere, and an overestimate in the southern hemisphere, because the CO_2 concentration today is typically 2 ppm higher in the northern hemisphere than in the southern (see, for example, Figure 45). Most of the error in the model is compensated for by the North Atlantic sink component, which also produces a north-south CO_2 gradient roughly similar to that of atmospheric CO_2. Evidently the strength of this oceanic component is predicted to be too large. But since the gradient in oceanic CO_2 partial pressure, $pCO_{2\,sea}$, associated with this component between high latitudes in both hemispheres [II.4.4.2, Figure 10] is on average the order of 20 times larger than the corresponding gradient in atmospheric CO_2 concentration, the overestimate in determining the strength of the North Atlantic sink arising from this particular model approximation is only a few percent. Other sources of errors in the determination of the North Atlantic sink component are discussed in subsection 5.1, below.

4.3 Model Sensitivity Tests

4.3.1 Introduction. One of our primary objectives in simulating the mean annual distribution of CO_2 in the atmosphere is to identify the regional exchanges of CO_2 involving the terrestrial

biosphere and the oceans. As shown above in subsection 4.1, we have found a set of three-dimensional model source components that produce simulations in quite close agreement with direct observations of CO_2 concentration and in fair agreement with the $^{13}C/^{12}C$ ratio. Our choice of components is by no means unique, however; we have not proved that they depict actual sources and sinks realistically. The error analysis of the previous subsection is inadequate to judge the realism of the model simulations, because of the complexity of the data which contribute to the model and the unknown degree of validity of some of the simplifying model assumptions. We have therefore carried out a set of tests to explore the sensitivity of the model results to our specification of its source components and transport parameters.

In particular we risk mistaking terrestrial sources and sinks for oceanic, and vice versa. Isotopic observations aid in reducing this risk, but do not eliminate it. The biospheric contribution to the north-south profile of δ_{mean} (Figure 25) is overshadowed by the contributions from temperature-dependent fractionation at the air-sea boundary (Figure 30) and industrial CO_2 emissions (Figure 32). Thus errors in simulating either of these latter processes seriously interfere with deducing the residual isotopic signal produced by the terrestrial biosphere.

Simulations of all of the model source components are influenced by shortcomings in the model's portrayal of atmospheric transport. Predictions of the mean annual fields, C_{mean} and δ_{mean}, are particularly sensitive to errors in the parameterization of vertical convection, of exchange of CO_2 at the air-sea interface, and of exchange of air between the northern and southern hemispheres.

We will first examine how well we can distinguish oceanic and terrestrial sources and sinks, and afterwards discuss errors arising from the specifications of vertical convection, gas exchange, and interhemispheric exchange in the model. We will also investigate errors arising from the neglect of short-term interannual variations. Table 7 summarizes the various assumed changes in source components which we employ in this sensitivity analysis. The standard case, used as a basis for comparison, is as described in section 2, above.

TABLE 7. Sensitivity Tests Performed with the Three-Dimensional Model

	Component Flux in 1980 (in 10^{12} kgC yr^{-1})						Respiratory Coefficient	Reduced Chi Square[a]	
Sensitivity Test	F_{IND}	F_{DES}	F_{FER}	F_{EQU}	F_{ATL}	F_{UOS}	ν_{RES}	C_{mean}	δ_{mean}
Sign:	+	+	−	±	±	−	−		
Standard case (std)	5.3	1.8	2.1	2.0	1.1	2.2	0.69	12.3	13.7
North Atlantic sink eliminated[b]	std	std	std	std	0	std	0.69	399.0	15.4
North Atlantic sink replaced by biospheric sink	std	12.4	12.7	0.6	0	std	0.69	24.9	10.8
Equatorial source replaced by biospheric source	std	27.8	std	0	3.5	28.2	0.69	42.2	106.4
Biospheric fertilization eliminated	std	std	0	2.1	1.6	4.3	0.69	14.9	23.2
Also biospheric destruction increased	std	4.7	0	1.9	1.8	7.2	0.69	15.6	28.6
Vertical convection reduced by 50%	std	std	std	1.4	1.1	std	0.77	21.8	19.2
With variable exchange[c]	std	std	std	1.5	1.3	std	0.64	12.8	6.8
With horizontal diffusion[d]	std	std	std	2.1	1.0	std	0.65	8.5	6.3
With variable exchange and horizontal diffusion[c]	std	std	std	1.6	1.1	std	0.61	9.9	3.4
High scenario (doubled fertilization and offsetting destruction)[e]	std	3.9	4.2	1.4	0.9	std	0.61	11.5	3.7
Low scenario (fertilization and destruction eliminated)[e]	std	0	0	1.8	1.4	2.5	0.60	9.5	4.8
Destruction scenario (fertilization eliminated, destruction increased)[e]	std	4.7	0	1.1	2.3	7.2	0.57	13.0	9.6
Double deconvolution	std	2.8	std	1.9	1.2	2.4	0.69	12.8	14.8

[a]Obtained by comparing model predictions to observational data of 1980–1984 combined. 17 observations (14 degrees of freedom) for C_{mean} and 15 observations (14 degrees of freedom) for δ_{mean}.

[b]With refit of constant only; 16 degrees of freedom for C_{mean} and 14 degrees of freedom for δ_{mean}.

[c]In which $<\bar{\alpha}_{eq}>$ is 0.990983 and δ_{OCD} is –9.181423‰ (see II.5.4).

[d]Such that the interhemispheric exchange time decreases from 1.37 to 1.09 yr.

[e]With variable exchange and horizontal diffusion.

4.3.2 Evidence for a North Atlantic sink. The simulated meridional profile of atmospheric CO_2 closely fits the observed profile when the model includes a CO_2 sink in the North Atlantic Ocean of approximately 1×10^{12} kgC yr^{-1}, in addition to the sinks simulated for this ocean by the equatorial component, F_{EQU}, and the uniform sink component, F_{UOS}. This oceanic flux, although not especially large, produces a large meridional gradient in C_{mean}, because of its northern location coupling with a source far to the south. If this flux is removed from the model, and no other adjustments are made, the predicted profile of C_{mean} (Figure 52, with data of 1980 and 1984 merged) is far steeper than the observations indicate that it should be (χ^2_{red} of 399, see Table 7), but the isotopic profile, which is insensitive to bulk oceanic CO_2 exchange, remains virtually as in the standard case (solid line of Figure 51). Clearly, to account for the observed meridional gradient in CO_2 concentration with the present model, it is necessary to postulate a sink in the north. If the sink is not oceanic, as assumed in the standard case just discussed, it must be biospheric.

No terrestrial biospheric source component can be realistically distributed with respect to latitude in a manner similar to our assumed North Atlantic oceanic sink component, because no continental land masses exist in the high southern latitudes where this component prescribes an oceanic source. A similar north-south concentration gradient is simulated, however, by summing equal contributions of biospheric destruction and fertilization, because the sink produced by fertilization in the model tends to lie to the north of the source produced by destruction. Therefore as a sensitivity test, we have substituted a combination of increased destruction and fertilization for the North Atlantic sink component. With this substitution, a best fit to the observed concentrations of combined 1980 and 1984 data requires that both destruction and fertilization be increased by 10.6×10^{12} kgC yr^{-1}. The predicted profiles of C_{mean} and δ_{mean} (Figures 53 and 54) are both poor fits to the observations, the former largely because the 1980 shipboard data of the FGGE Shuttle Expedition largely control the fit to concentration and force the source adjustments to be too extreme at high latitudes. The predicted isotopic difference between Point Barrow, Alaska and the South Pole is only 0.08‰, in contrast to the observed difference of 0.18‰ (see Table 3). If the fit to concentration is made only to the 1984 data (profile shown as a dash-dot line in Figure 53), biospheric destruction and fertilization increase by only 6.8×10^{12} kgC yr^{-1} and the prediction of C_{mean} is generally reasonable (χ^2_{red} of 10.3). The δ_{mean} profile (dash-dot line in Figure 54) is still poor, however; the predicted isotopic gradient north of 20°N. is far too small. Thus the isotopic data indicate that it is unrealistic to postulate a biospheric sink in place of the North Atlantic sink.

Errors in the model and in the measured δ_{mean} may exaggerate the poorness of these predictions, but it would require extreme errors to accept an unidentified biospheric source/sink couple to

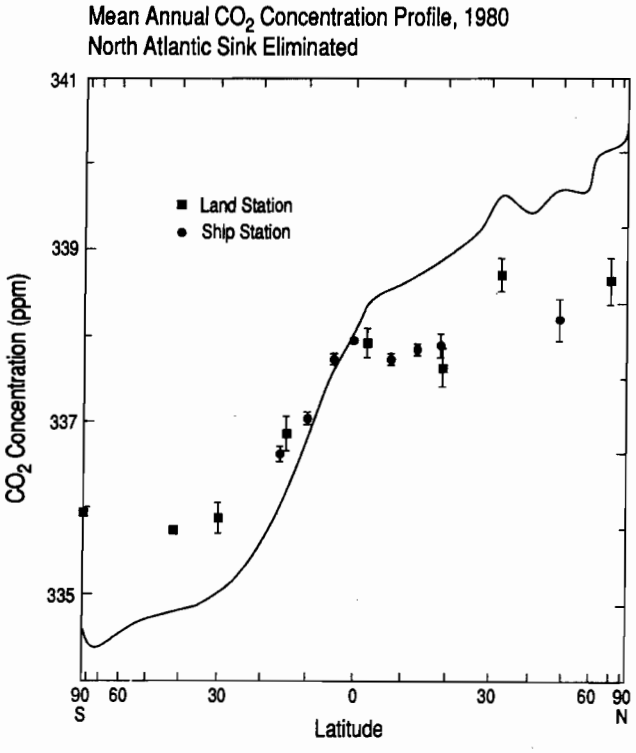

Fig. 52. Mean annual CO_2 concentration, in ppm, in 1980, based on combined 1980 and 1984 observations as in Figure 49, except that the model source component representing a North Atlantic sink, F_{ATL}, has been omitted.

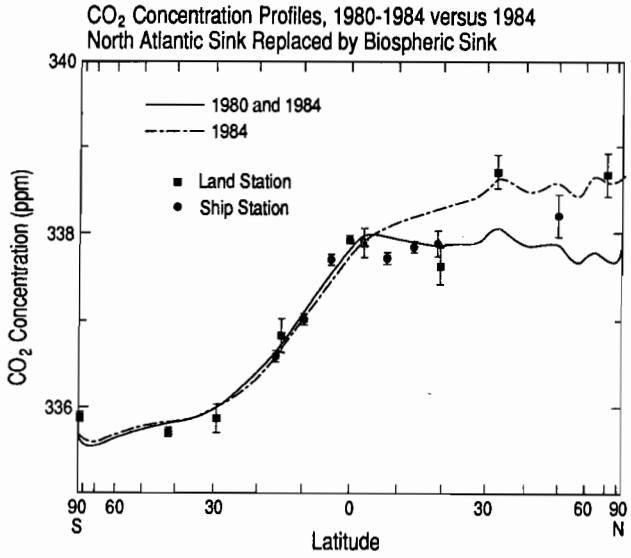

Fig. 53. Same as Figure 52, except that in compensation for the removal of the Atlantic component, the model source components for biospheric destruction and fertilization, F_{FER} and F_{DES}, have each been increased globally in absolute magnitude by 10.573×10^{12} kgC yr^{-1} from the standard case (Figures 11 and 13, respectively). Also the equatorial component, F_{EQU}, was reduced from the standard case (Figure 16) by 1.3752×10^{12} kgC y^{-1} (to 0.6045×10^{12} kgC yr^{-1}). These adjustments were made to achieve an optimal fit to the observations for 1980 and 1984 combined, as shown on the plot. The dash-dot curve shows, for comparison, the fit to observations for 1984 only.

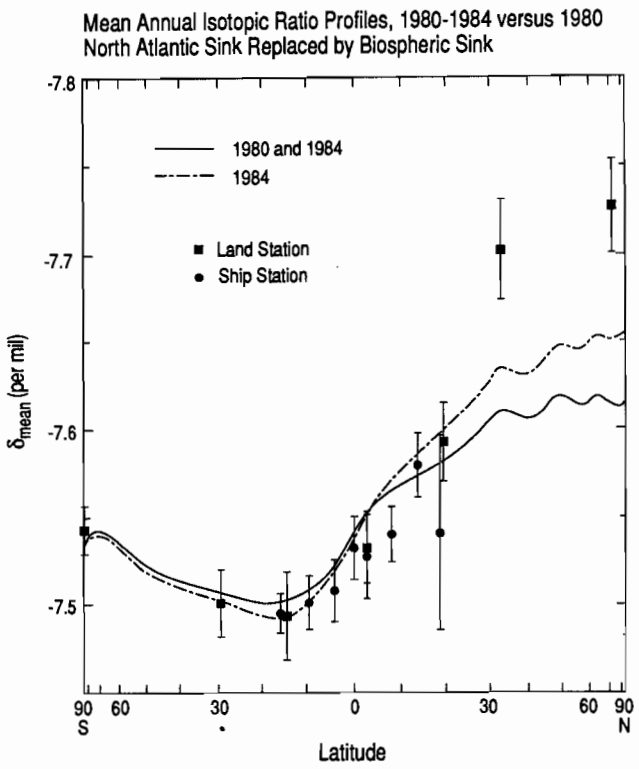

Fig. 54. δ_{mean}, in per mil, corresponding to the concentration profile of Figure 53.

replace completely our hypothetical oceanic component. We conclude that an oceanic sink similar to the North Atlantic sink is required to achieve agreement with atmospheric CO_2 observations. The latitudinal placement of this oceanic component is, however, only crudely defined by the observations; it could, for example, be partially located in the North Pacific Ocean. Also, a combination of biospheric and oceanic sinks cannot be ruled out, given the uncertainties in the isotopic observations and in the modeling of CO_2 transport and air-sea exchange.

It might be argued as unreasonable to augment both biospheric destruction and fertilization by as much as 10×10^{12} kgC yr^{-1}. On the other hand the two components in this alternate formulation overlap to a large extent; the prescribed local *net* flux at most grid points is not altogether unrealistic. Thus we do not claim that the augmented components are demonstrably unrealistic *a priori*, but rather that the isotopic predictions that they produce in combination are inconsistent with our observations.

4.3.3 Evidence for an equatorial oceanic component. Measurements of the CO_2 partial pressure in surface sea water, $pCO_{2\,sea}$, discussed in subsection 2.4.3, above, are direct evidence that an oceanic source of CO_2 exists in the tropical oceans. It is nevertheless of interest to inquire how the model profiles would be altered if this source were replaced in the model with a terrestrial biospheric source. Since this oceanic source produces a nearly symmetric profile of C_{mean} about the equator (solid line in Figure 16), we cannot realistically replace it with a biospheric source in which the fertilization component contributes significantly, since the resulting concentration field is strongly asymmetric in the tropics. The profile of biospheric destruction (solid line in Figure 11) is similar to that produced by the equatorial source. For a sensitivity test we have therefore replaced the equatorial oceanic source by a source-sink couple consisting of an increased biospheric destruction source and a correspondingly increased uniform oceanic sink.

The inclusion of this oceanic sink is in violation of the compartment model of Keeling et al. [I.5], but is qualitatively consistent with the assertions of ecologists, such as Woodwell et al. [1978, 1983], who have claimed greater biospheric destruction than we have assumed in our model without any offset by fertilization, i.e., the oceans are a larger sink for CO_2 than appears otherwise to be the case. The added destruction needed to produce an optimal fit in this case, however, is ridiculously large, 26.0×10^{12} kgC yr^{-1}, and the predicted concentration profile (χ^2_{red} of 42), shown in Figure 55, exhibits peculiar peaks and troughs not supported by the observations. The isotopic profile (Figure 56, χ^2_{red} of 106) is still less plausible. We conclude that an oceanic source in the equatorial region is supported by our atmospheric CO_2 measurements as interpreted by the standard case of the three-dimensional model.

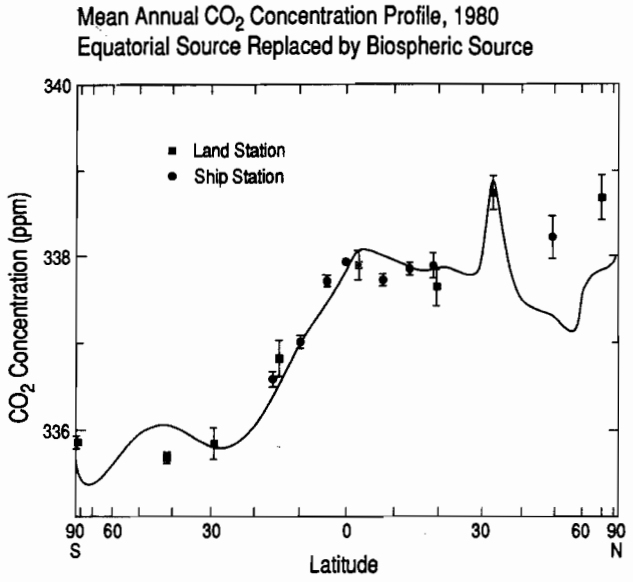

Fig. 55. Mean annual CO_2 concentration, in ppm, in 1980, as in Figure 49, except that the equatorial model source component F_{EQU}, has been omitted. In compensation the model source components for biospheric destruction and uniform oceanic sink, F_{DES} and F_{UOS}, were both increased in absolute magnitude by 25.9864×10^{12} kgC yr^{-1} from the standard case (Figures 11 and 18, respectively). Also the North Atlantic sink component, F_{ATL}, was increased by 2.3646×10^{12} kgC yr^{-1} (to 3.5120×10^{12} kgC yr^{-1}) from the standard case (Figure 17). These adjustments were made to achieve an optimal fit to the observations for 1980 and 1984 combined, as shown on the plot.

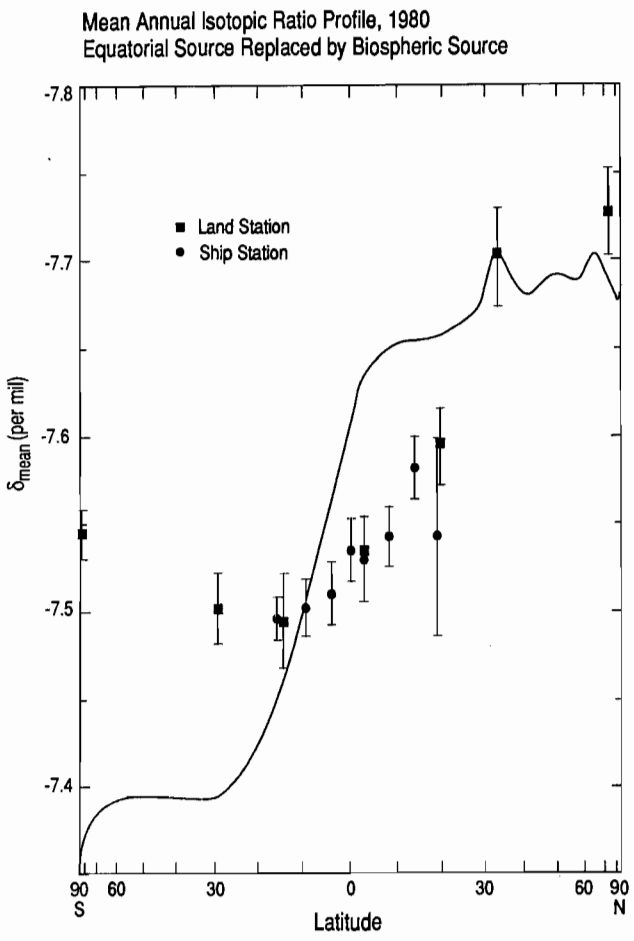

Fig. 56. δ_{mean}, in per mil, corresponding to the concentration profile of Figure 55.

4.3.4 Evidence for biospheric fertilization. Little direct evidence exists that plants growing in nature are stimulated by elevated ambient CO_2. Many ecologists doubt that fertilization in nature occurs, although it has been often observed in controlled experiments [see, for example, Strain and Cure, 1985]. We have nevertheless assumed that fertilization operates in nature in order to achieve a global balance of CO_2 sources and sinks consistent with current wisdom regarding the response of the oceans to the observed build-up in atmospheric CO_2 [see I.5 and I.6]. The postulated flux of CO_2 in 1980 owing to fertilization, 2.1×10^{12} kgC yr^{-1}, produces a nearly uniform decrease in C_{mean} from the South Pole to the North Pole (see Figure 13) and a similar decrease in δ_{mean}. The predicted difference in δ_{mean} between Point Barrow, Alaska, and the South Pole is 0.04‰. If this fertilization component is omitted in the model and an equal amount of CO_2 as a uniform oceanic sink is added to restore a global balance, and if the other oceanic components and the respiratory coefficient are readjusted to obtain an optimal fit to the observed CO_2 concentration, we obtain the profiles shown as solid lines in Figures 57 and 58.

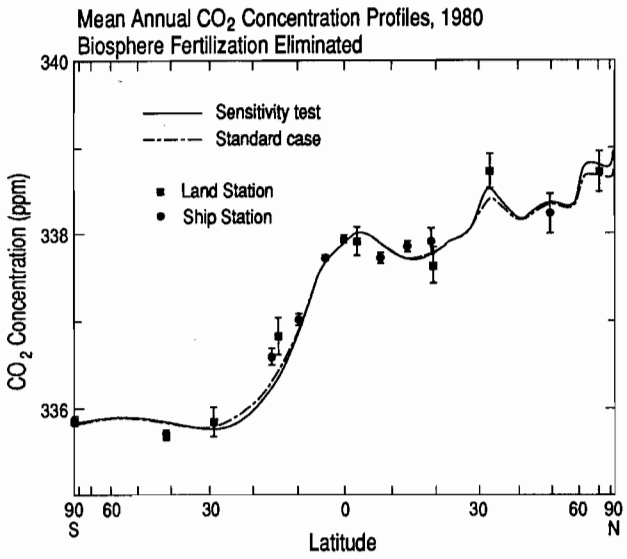

Fig. 57. Mean annual CO_2 concentration, in ppm, in 1980 as in Figure 49, except that the model source component for biospheric fertilization, F_{FER}, is omitted. In compensation the uniform oceanic sink component, F_{UOS}, has been increased by 2.1037×10^{12} kgC yr^{-1} (to 4.3274×10^{12} kgC yr^{-1}). To effect an optimal fit to the observations for 1980 and 1984 combined, shown in the plot, the oceanic components, F_{EQU} and F_{ATL}, were adjusted to 2.0961×10^{12} kgC yr^{-1} and 1.5600×10^{12} kgC yr^{-1}, respectively. The dash-dot curve shows the model simulation for the standard case, for comparison.

The predicted concentration profile is slightly poorer than for the standard case shown as a dash-dot line (χ^2_{red} of 14.9 instead of 12.3); the predicted isotopic profile is somewhat more degraded (23.2 instead of 13.7). The predicted isotopic difference between Point Barrow and the South Pole, which in the standard case was already too great, increases by 0.04‰. Nevertheless, given the uncertainties in our present model and observational data, this discrepancy is too small to demonstrate conclusively that fertilization occurs. We reconsider this topic in subsection 5.2 below, after having assessed errors in the transport model.

4.3.5 Evidence for increased biospheric destruction. The upper limit of biospheric destruction according to Houghton et al. [1983] is 4.7×10^{12} kgC yr^{-1}. In a later study Houghton et al. [1987] reduce the upper limit to 2.5×10^{12} kgC yr^{-1}. Both estimates assume that destruction is unaccompanied by fertilization. If we repeat the previous sensitivity test with destruction increased to the larger figure of 4.7×10^{12} kgC yr^{-1}, and if we further adjust the oceanic source/sink components and the respiratory coefficient to obtain a global balance and an optimal fit to observations, we obtain profiles which are virtually indistinguishable from those with the standard amount of destruction of 1.79×10^{12} kgC yr^{-1} (χ^2_{red} for C_{mean} increases from 14.9 to 15.6, for δ_{mean} from 23.2 to 28.6). This result is expected, because the destruction component produces only weak meridional gradients. We conclude that the present observations interpreted by the model, defined by its standard case, do not confirm the strength, or even the existence, of

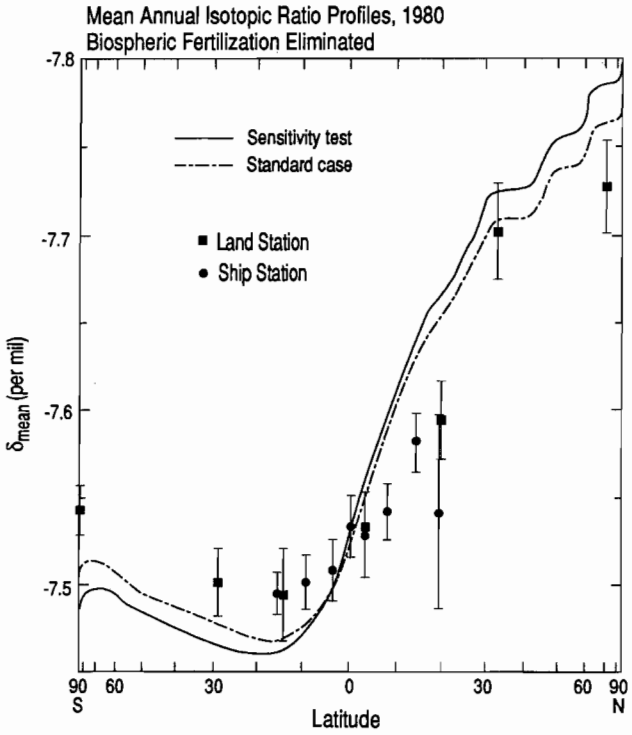

Fig. 58. δ_{mean}, in per mil, corresponding to the concentration profile of Figure 57.

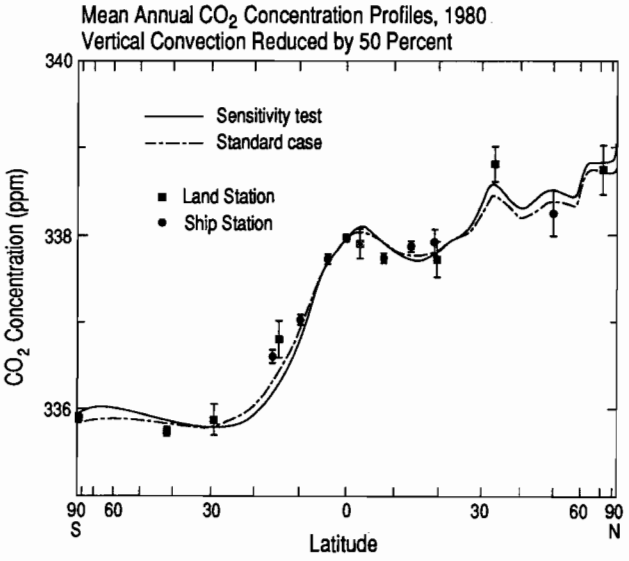

Fig. 59. Mean annual concentration, in ppm, in 1980 as in Figure 49, except that the vertical convection of the model has been reduced globally by 50 percent as indicated in the text. To effect an optimal fit to the observations for 1980 and 1984 combined, shown in the plot, the oceanic components F_{EQU} and F_{ATL} were adjusted to 1.3919×10^{12} kgC yr^{-1} and to 1.1310×10^{12} kgC yr^{-1}, respectively. The dash-dot curve shows the model simulation for the standard case, for comparison.

biospheric destruction, except to rule out fluxes much higher than recent estimates indicate, such as the flux that produces the profiles of Figures 55 and 56.

4.3.6 Influence of vertical convection on the estimates of the oceanic fluxes. We carried out computations with the convective matrices of the model reduced to half of the strength of the standard case (a reduction in the original specification of the convective parameter, ζ, from 0.50 to 0.25 [II.2, equation 2.3]). In Figures 59 and 60 the predicted profiles of both concentration and isotopic ratio for 1980 are shown, including the merged data of 1984. As an exception to our normal presentation of the merged data, the data for 1984 were adjusted to 1980 via equation (3.1), by employing model predictions based on the reduced convective matrices. Thus, as in the standard case, the fit of the components to the merged data is exactly the same as for 1980 alone.

The predicted north-south profile for the mean concentration field, C_{mean} (solid line in Figure 59), is changed only slightly when the vertical convection is reduced 50 percent, the maximum change being less than 0.2 ppm (χ^2_{red} rising, however, from 12.3 to 21.8). The isotopic field, δ_{mean} (solid line in Figure 60), is altered more noticeably (χ^2_{red} rising from 13.7 to 19.2). The changes in concentration are small because the profile with reduced convection was

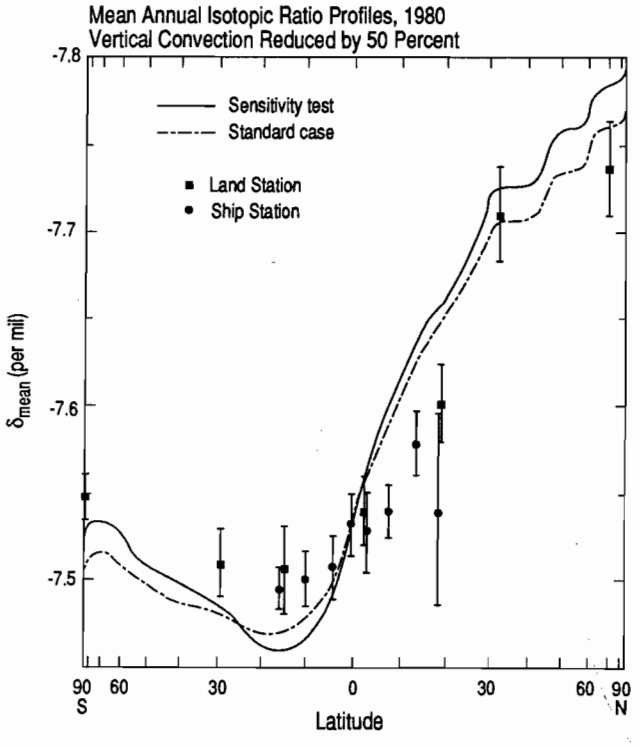

Fig. 60. δ_{mean}, in per mil, corresponding to the concentration profiles of Figure 59.

obtained, as in the case of standard convection, by adjusting the equatorial source and the North Atlantic sink, adjustments which, for most of the above-described sensitivity tests, have been adequate to achieve good fits for C_{mean}. More noticeable changes occur in the isotopic profile, because this profile is insensitive to the adjustable oceanic components and reflects only changes in components which were not adjusted.

Reduced convection affects the isotopic gradients more in the tropics than between high latitudes of the two hemispheres. Indeed, the tropical patterns of all of the individual components are to some degree enhanced isotopically at lower convection. For example, between the stations of the FGGE Shuttle Expedition near 15°N. and 16°S. (see Figure 60) the gradient in δ_{mean} is increased above the standard case by 12 percent at reduced convection in contrast to 4 percent between Point Barrow, Alaska, (71°N.) and the South Pole.

As expected for a model parameter controlling vertical mixing, its influence on predictions is greatest with respect to vertical gradients of CO_2. Particularly sensitive is the equatorial source component, which can be falsely estimated if these gradients are incorrectly simulated. The strength of this component at reduced convection for the optimal fit to the concentration data of 1980 is 30 percent smaller than in the standard case (adjustment factor, v_{EQU}, reduced from 0.99 to 0.69). This large reduction occurs because the available atmospheric CO_2 observations in the tropics were made on board ships close to the sea surface source of CO_2. To maintain the observed CO_2 concentration field immediately above that surface with lowered vertical mixing, this source must be significantly lessened.

The North Atlantic sink, in contrast, is remote from the locations of CO_2 observations which are in or near the Pacific Ocean basin. Lowering vertical convection by 50 percent reduces this component, after adjustment, by only 1 percent. In the high southern latitudes, where the component is counter-balanced by a CO_2 source, the influence of vigorous winds overshadows vertical convection in determining the CO_2 field.

Observations at Mauna Loa and Cape Kumukahi, Hawaii, provide a check on the model predictions of vertical gradients, since these two sites differ in altitude by 3500 m. The observed concentration difference over six years of record [I.4.3, Table 6] is 0.27 ppm (Kumukahi higher) with a standard error of the mean of 0.15 ppm. This difference is more closely predicted by the standard case (0.30 ppm, see Table 4), than with reduced convection (0.60 ppm). The observed difference in δ_{mean}, 0.031‰, with a standard error of the mean of 0.011‰, is predicted by the standard case less well than for concentration (0.048‰, see Table 5) but still worse (0.067‰) at reduced convection.

We conclude that uncertainties in the parameterization of vertical convection only weakly influence the predictions of mean annual fields of atmospheric CO_2 and its isotopic ratio at the surface, provided that the equatorial source component is adjustable. Close examination of the predictions, however, suggests that the lower vertical convection tends to degrade the predictions. The values of χ^2_{red} are higher for both C_{mean} and δ_{mean} with reduced convection. In three instances involving the tropics, the predictions appear to be less reasonable with lower convection. The predicted profile of δ_{mean}, already too steep for the standard case, is made worse with reduced convection. The gradients in both C_{mean} and δ_{mean} between Cape Kumukahi and Mauna Loa Observatory in Hawaii are exaggerated. Also, predictions of the seasonal cycle in the tropics are less reasonable [III.5.3].

4.3.7 Influence of gas exchange on the estimates of the oceanic fluxes.

The mechanism of gas exchange across gas-liquid boundaries is not sufficiently well known to specify precisely how the exchange of CO_2 at the sea surface varies as a function of physical parameters. To avoid possibly overestimating the affect of variations of these parameters on the oceanic fluxes of our model, we have chosen to assume, as a standard case, that the rate of gas exchange is constant in time and space. Admittedly, this assumption is an oversimplification. Direct experiments in wind-wave facilities leave little doubt that gas exchange increases with wind speed and varies with temperature [see, for example, Liss and Merlivat, 1986].

We have carried out additional model simulations in which the gas exchange coefficient, k_{ex}, varies as indicated by recent laboratory experiments (see subsection 4.2.1, above). As in the sensitivity tests already discussed, the strengths of the equatorial and North Atlantic components, F_{EQU} and F_{ATL}, and of the respiratory coefficient (defined by equation (4.1.9) of [II.4.3.4]) were readjusted to achieve an optimal fit to the merged 1980 and 1984 concentration data of Table 3. As shown in Figure 50, the simulated profile of the concentration, C_{mean}, assuming variable k_{ex}, is only very slightly different from the standard case, the χ^2_{red} of the fit changing insignificantly (from 12.3 to 12.8). The adjusted strengths of the oceanic components changes appreciably, however. The equatorial component is lowered by 25 percent and the North Atlantic component is increased by 12 percent.

These changes reflect a redistribution of CO_2 fluxes because of higher exchange rates in polar regions, decisively so in the southern hemisphere. The shape of the peak in atmospheric CO_2 generated by the equatorial component near the equator at the lowest model level near 160°W. (seen as the solid line in Figure 16 for the standard case) is virtually unchanged, but the concentration field relative to that peak descends more steeply poleward, especially in the southern hemisphere. To preserve approximately the same amplitude of the peak, as required by the observations, the equatorial flux is less than when constant k_{ex} is assumed.

The greater asymmetry in the concentration field of F_{EQU} requires a readjustment of the North Atlantic sink component, F_{ATL}, because this component in the new fit must compensate for the stronger southern polar sink of the equatorial component. It does so by increasing in strength and thus providing a stronger southern hemisphere source. The composite sink generated by the sum of all oceanic components in the North Atlantic Ocean increases only 4 percent, however.

The isotopic field, δ_{mean}, simulated by the model with variable k_{ex} for the sum of the oceanic components depends strongly on where the regions of high and low exchange are located, even though the field is insensitive to gradients in CO_2 partial pressure (see Figure 26) and is thus virtually unaffected by changes in strength of the equatorial and North Atlantic components. This dependency arises because the strengths of the two isotopic source components, ${}^*F_{SUE}$ and ${}^*F_{TDF}$, which involve solely isotopic disequilibria, are not constrained regionally or globally in the model; they depend directly on k_{ex}. Because higher rates of exchange prevail in the polar regions relative to low latitudes, the predicted field of δ_{mean} for the sum of the oceanic components shows larger gra-

dients (see Figure 31). Also, because higher rates generally prevail in the southern hemisphere, the gradient in δ_{mean} reverses sign between the equator and 10°N. The composite prediction of δ_{mean}, including the biospheric and industrial components (see dash-dot line in Figure 51), is substantially improved relative to the standard case (χ^2_{red} from 13.7 to 6.8), suggesting that this alternative representation of gas exchange does not overestimate the dependency of gas exchange on wind speed and temperature.

4.3.8 Influence of interhemispheric exchange on the estimates of the oceanic fluxes. Another critical feature of the transport model is the interhemispheric exchange time, which strongly influences the predicted meridional gradients in concentration and isotopic composition. The ability of the model to predict meridional gradients was tested by means of a simulation of the large scale dispersal of the radioactive noble gas krypton-85 (^{85}Kr) [II.3.1]. Agreement is only fair between the model predictions and observation of this passive tracer with respect to north-south profiles at sea level over the Atlantic Ocean; the model appears to overestimate the interhemispheric concentration gradient by 10 to 20 percent. According to the model simulation, the annually averaged interhemispheric exchange time for ^{85}Kr is 1.3 years. This value depends to some degree on the assumed strength of the vertical convection: if the convective parameter, ζ, is lowered from the standard value of 0.5 to 0.25 [II.2, equation (2.3)], the interhemispheric exchange time is reduced to 1.2 years.

These estimates are larger than a value of 1.1 years for the interhemispheric exchange time reported in a recent modeling study of ^{85}Kr by Jacob et al. [1987]. The difference between the result of this study [loc. cit., 1987, p. 6620] and our calculation may be related, in part, to interannual changes in the interhemispheric transport which we cannot estimate, because the model winds which we have used were observed only during the specific period of the Global Weather Experiment of 1978–1979. We also note, however, that our model, as formulated up to this point in our discussion, does not include any explicit horizontal diffusion terms; horizontal transport is specified solely by advective motions which are resolved on the rather coarse model grid. This contrasts with the study of Jacob et al. [1987], who include in their model a horizontal diffusion term representing horizontal subgridscale transport associated with large vertical convective processes. Thus we expect that our model does not significantly overestimate the interhemispheric exchange, but it may underestimate it.

In order to explore the sensitivity of the model to this particular feature we have made additional model runs in which we have introduced subgridscale horizontal diffusion into the model, coupled to vertical convection in the same way as described by Prather et al. [1987] and Jacob et al. [1987]. According to these authors, deep convective vertical motions may be associated with large convective complexes which result in significant horizontal redistributions of tracer between adjacent grid boxes of the model. The strength of this horizontal diffusive transport process is characterized by means of a length scale, D. By setting D equal to 100 km, we find that the interhemispheric exchange time of industrial CO_2 in the model [see II.3.1, equation (3.4)] is reduced by 20 percent, from 1.37 to 1.09 years.

With the interhemispheric exchange time thus decreased, the predicted north-south profile of C_{mean} for 1980, including the merged data of 1984, is as shown by the solid line in Figure 61. The strengths of the equatorial and North Atlantic components,

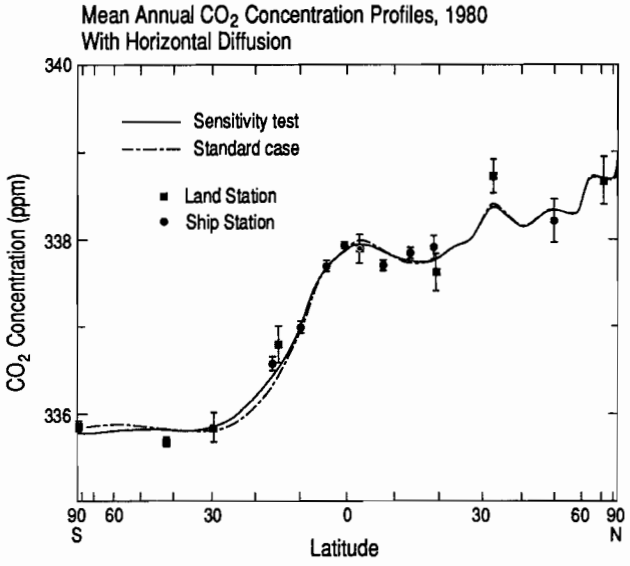

Fig. 61. Mean annual concentration, in ppm, in 1980 as in Figure 49, except that the interhemispheric exchange time of the three-dimensional transport of the model has been decreased 20 percent by including explicit subgridscale horizontal diffusion as described in the text. To achieve an optimal fit to the observations for 1980 and 1984 combined, shown in the plot, the oceanic components F_{EQU} and F_{ATL} were adjusted to 2.0973 x 10^{12} kgC yr^{-1} and to 1.0042 × 10^{12} kgC yr^{-1}, respectively. The dash-dot curve shows the model simulation for the standard case for comparison.

F_{EQU} and F_{ATL}, and the respiratory coefficient, as in the previous sensitivity test (subsection 4.3.7), have been again readjusted to achieve an optimal fit to the observations. The profile is improved from the standard case, shown as a dash-dot line (χ^2_{red} value reduced from 12.3 to 8.5). The equatorial component is increased slightly (by 6 percent) from the standard case (see Table 7). The North Atlantic sink component is altered more, being reduced by 12 percent. The composite sink generated by the sum of all oceanic components in the North Atlantic Ocean is decreased by 8 percent.

This latter reduction occurs because the primary contributor to the meridional profile is industrial CO_2. In the standard case this industrial source produces a concentration difference of 5.5 ppm pole-to-pole in 1980. When the interhemispheric exchange is decreased by introducing horizontal diffusion, this predicted difference is decreased to 4.7 ppm. The North Atlantic component, which in the standard case produces an opposing pole-to-pole difference of 3.0 ppm, if held at the same strength, would produce a corresponding lesser difference of 2.7 ppm. When, however, this component is decreased by 12 percent to maintain an optimal fit of the model profile to the observations, the difference is further reduced to 2.3 ppm.

The predicted profile of δ_{mean} at reduced interhemispheric exchange is altered only infinitesimally by the adjustment of the oceanic components, F_{EQU} and F_{ATL}, and therefore is reduced everywhere with little change in pattern from that of the standard case (see Figure 62). The fit is improved markedly from the stan-

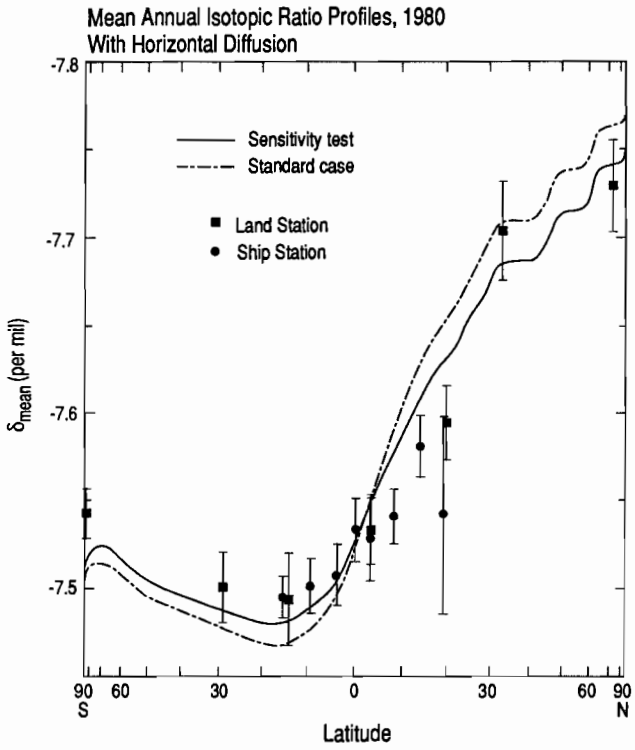

Fig. 62. δ_{mean}, in per mil, corresponding to the concentration profiles of Figure 61.

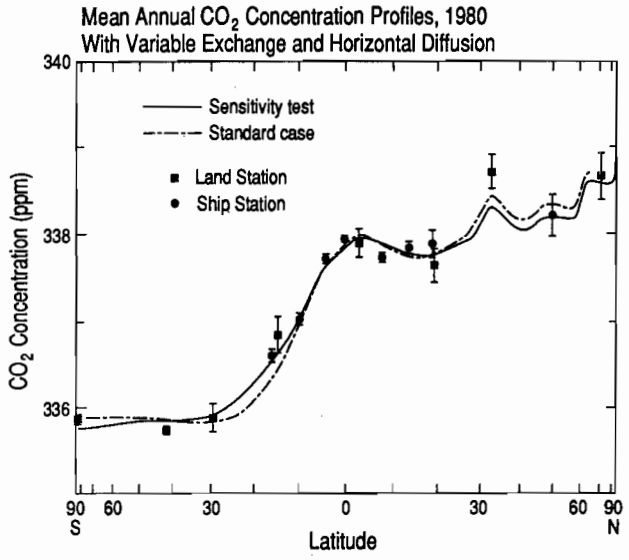

Fig. 63. Same as Figure 61, except that, in addition, the coefficient of gas exchange, k_{ex}, is assumed to vary with wind speed, as in Figure 31 and as described in the text. To achieve an optimal fit to the observations for 1980 and 1984 combined, the oceanic components F_{EQU} and F_{ATL} were adjusted to 1.5809×10^{12} kgC yr^{-1} and to 1.1428×10^{12} kgC yr^{-1}, respectively. The dash-dot curve shows the model simulation for the standard case, for comparison.

dard case, however (χ^2_{red} reduced from 13.7 to 6.3), because this reduced gradient is almost everywhere in better agreement with observations.

If, in addition to horizontal diffusion, a variable gas exchange coefficient is assumed, as was the case in producing the prediction in Figure 51, the fit for CO_2 concentration (see Figure 63) is virtually unchanged after again readjusting the strengths of F_{EQU}, F_{ATL}, and the respiratory coefficient. The fit to the isotopic data (solid line in Figure 64), however, is considerably improved beyond the improvement achieved by introducing horizontal diffusion alone, and remarkably improved over the standard case, shown as a dash-dot line. The χ^2_{red} value is reduced from 6.8 to 3.4 (from 12.3 for the standard case). The addition of explicit horizontal diffusion and variable air-sea gas exchange produces roughly additive changes in the strength of the equatorial source component (which is lowered by 20 percent), and almost exactly additive changes in the composite sink in the North Atlantic Ocean (lowered by 4 percent).

An outcome of this sensitivity analysis is that our previous conclusion still holds that an oceanic sink in the northern hemisphere is required for the model to produce a satisfactory simulation of the atmospheric CO_2 field. A reduction in the interhemispheric

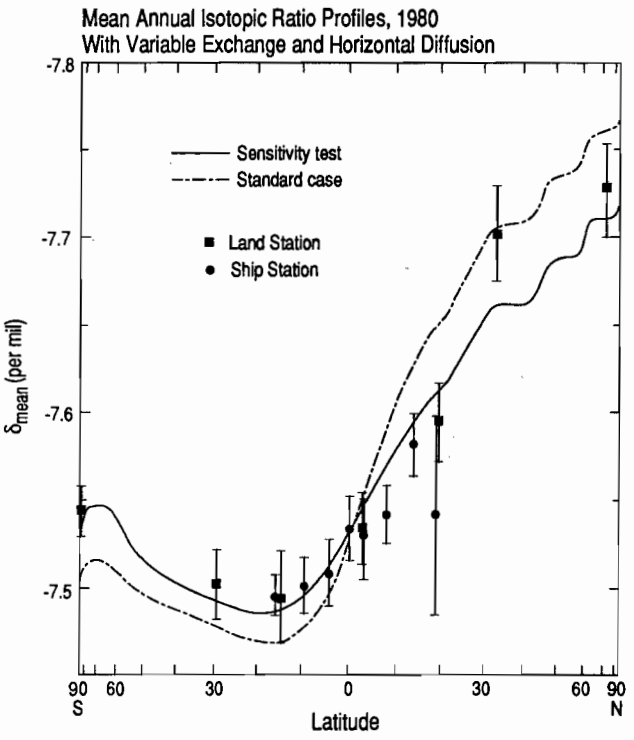

Fig. 64. δ_{mean}, in per mil, corresponding to the concentration profiles of Figure 63.

TABLE 8. Predicted Mean Annual CO_2 Concentration (in ppm) together with Contributions of Individual Model Components at Observing Stations for 1980 (Assuming Variable Air-Sea Gas Exchange and Explicit Horizontal Diffusion)

Latitude Intervals of Shipboard Data or Name of Fixed Station	Lat. (deg.)	Long. (deg.)	Composite[a]		Individual Components[b]	
			C_{mean}	Difference	NPP + RES	DES
South Pole	90.00S.	–	335.73	0.0000	0.0000	0.0000
Baring Head	41.42S.	174.87E.	335.82	0.0865	–0.0501	0.0771
Raoul Is.	29.25S.	170.02W.	335.90	0.1688	–0.0426	0.0936
FGGE, 14-17 S.	15.60S.	153.00W.	336.51	0.785	–0.0440	0.1767
Cape Matatula	14.28S.	153.00W.	336.62	0.8866	–0.0416	0.1883
FGGE, 8-12 S.	9.60S.	153.00W.	337.04	1.3149	0.0097	0.2268
FGGE, 2- 6 S.	4.00S.	153.00W.	337.66	1.9283	0.1329	0.2696
FGGE, 1 N.-1 S.	0.00	153.00W.	337.85	2.1165	0.2228	0.2802
FGGE, 2- 4 N.	3.00N.	153.00W.	337.98	2.2535	0.2902	0.2879
Fanning/Christmas	3.00N.	153.00W.	337.98	2.2535	0.2902	0.2879
FGGE, 6-10 N.	8.00N.	153.00W.	337.88	2.1532	0.2242	0.2667
FGGE, 12-16 N.	13.80N.	153.00W.	337.75	2.0229	0.1213	0.2347
FGGE, 18-20 N.	19.00N.	153.00W.	337.75	2.0184	0.0602	0.2081
Cape Kumukahi	19.53N.	154.68W.	337.75	2.0212	0.0637	0.2064
Mauna Loa	19.53N.	155.58W.	337.41	1.6852	–0.2785	0.2767
La Jolla	32.87N.	117.25W.	338.29	2.5608	0.0435	0.1966
Station P	50.00N.	144.00W.	338.19	2.4630	0.4362	0.1454
Point Barrow	71.33N.	157.33W.	338.57	2.8388	0.6747	0.1048
Cape Kumukahi minus Mauna Loa	19.53N.	–	0.34	0.3360	0.3422	–0.0703

TABLE 8. -- continued

Latitude Interval of Shipboard Data or Name of Fixed Station	Individual Components					
	FER	TDE	EQU	ATL	UOS	IND
South Pole	0.0000	0.0000	0.0000	0.0000	0.0000	0.0000
Baring Head	–0.0962	–0.0252	0.1322	–0.2584	0.0734	0.2335
Raoul Is.	–0.1079	–0.0304	0.2507	–0.4717	0.1529	0.3242
FGGE, 14-17 S.	–0.1936	–0.0873	0.7626	–0.8866	0.3385	0.7190
Cape Matatula	–0.2066	–0.0929	0.8417	–0.9276	0.3563	0.7690
FGGE, 8-12 S.	–0.2561	–0.1218	1.1472	–1.0607	0.4000	0.9698
FGGE, 2- 6 S.	–0.3202	–0.1690	1.5492	–1.2025	0.4244	1.2439
FGGE, 1 N.-1 S	–0.3755	–0.2120	1.4672	–1.3828	0.4607	1.6560
FGGE, 2- 4 N.	–0.4172	–0.2444	1.3994	–1.5193	0.4882	1.9687
Fanning/Christmas	–0.4172	–0.2444	1.3994	–1.5193	0.4882	1.9687
FGGE, 6-10 N.	–0.4721	–0.2480	1.0319	–1.7579	0.5410	2.5674
FGGE, 12-16 N.	–0.5212	–0.2376	0.6559	–1.9890	0.5938	3.1649
FGGE, 18-20 N.	–0.5480	–0.2259	0.5033	–2.1191	0.6249	3.5149
Cape Kumukahi	–0.5484	–0.2253	0.4930	–2.1258	0.6287	3.5288
Mauna Loa	–0.5078	–0.1939	0.6906	–1.9196	0.6927	2.9251
La Jolla	–0.6452	–0.2664	0.4619	–2.2373	0.6778	4.3299
Station P	–0.6558	–0.2646	0.2992	–2.3821	0.5883	4.2965
Point Barrow	–0.7295	–0.2374	0.3498	–2.5380	0.7012	4.5132
Cape Kumukahi minus Mauna Loa	–0.0406	–0.0314	–0.1976	–0.2062	–0.0640	0.6037

[a]The composite signal is specified as in Table 4.

[b]For names of the components, see Table 4.

exchange time of 20 percent only slightly reduces the inferred strength of this sink.

As an aid to further study of the present model, as modified by including variable gas exchange and explicit horizontal diffusion, we list in Tables 8 and 9, respectively, the composite and associated individual component predictions of C_{mean} and δ_{mean}. Similar predictions are listed for the standard case in Tables 4 and 5 (see subsection 4.1, above).

4.3.9 Influence of gas exchange and subgridscale horizontal diffusion on the estimates of biospheric fluxes.

The improvement just described in predicting δ_{mean}, with a model having a variable gas exchange coefficient and explicit subgridscale horizontal diffusion, justifies a reexamination of the sensitivity of the model to assumptions regarding biospheric perturbations associated with the source components of destruction and fertilization. These components, in the standard formulation of the three-dimensional tracer model (standard model), produce only weak isotopic signals, as noted above in subsections 4.3.4 and 4.3.5. Their presence or absence causes relatively insignificant changes in the goodness of fit to the isotopic observations, because the fit using the standard model is poor (χ^2_{red} of 13.7). When, however, the standard model is modified to include both variable gas exchange and horizontal diffusion, the predicted isotopic field, δ_{mean}, agrees far better with the observations (χ^2_{red} of 3.4). This improved agreement suggests that the modified model more realistically simulates tracer transport than the standard model. If so, the strengths of these biospheric perturbations may be prescribed by the modified model more closely than indicated in our earlier discussion.

From a global compartment model study utilizing direct atmospheric CO_2 measurements and data from ice core samples, Keeling et al. [I.6.6] have argued that the trend in atmospheric CO_2 concentration in the twentieth century is better explained than otherwise by assuming that some degree of biospheric fertilization has occurred. Firstly, the net flux appears generally to have been smaller than expected in the twentieth century, assuming that it solely reflects destruction. For part of the century, indeed, the terrestrial biosphere appears to have been a sink for atmospheric CO_2 rather than a source. Secondly, the computed net flux of CO_2 from the biosphere to the atmosphere does not appear to have increased during a period when destruction almost surely was increasing. Within the past two decades, however, a sharp reversal of trend appears to have occurred, so that the biosphere is again a net source. This reversal is too sharp to be attributed to accelerating destruction alone, even assuming that the calculation of the net flux is biased and indicates too little uptake of CO_2 by the oceans. The sharpness of the reversal can be explained, however, as if it is a result of differential increases in opposing fluxes of fertilization and destruction.

To illustrate this possibility, Keeling et al. [loc. cit.] postulated a "high scenario" in which the global flux owing to fertilization is made large enough that the opposing flux of destructive increases monotonically from the beginning of this century to the present. The global strength of this fertilization flux is approximately twice that of the standard scenario in which fertilization is 2.1×10^{12} kgC yr^{-1}. Destruction is raised from 1.8×10^{12} kgC yr^{-1} to 3.9×10^{12} kgC yr^{-1}.

In Figures 65 and 66 we compare the predicted north-south profiles of concentration and isotopic ratio for this high scenario with the standard scenario. We also show two additional scenarios to be discussed below. All four scenarios employ the modified tracer model that includes variable gas exchange and subgridscale

TABLE 9. Predicted Mean Annual Isotopic Ratio (in per mil) together with Contributions of Individual Model Components at Observing Stations for 1980 (Assuming Variable Air-Sea Gas Exchange and Explicit Horizontal Diffusion)

Latitude Interval of Shipboard Data or Name of Fixed Station	Lat. (deg.)	Long. (deg.)	Composite[a]		Individual Components[b]
			δ_{mean}	Difference	TDF
South Pole	90.00S.	–	–7.524	0.0000	0.0000
Baring Head	41.42S.	174.87E.	–7.502	0.0220	0.0328
Raoul Is.	29.25S.	170.02W.	–7.489	0.0347	0.0527
FGGE, 14-17 S.	15.60S.	153.00W.	–7.484	0.0402	0.0854
Cape Matatula	14.28S.	153.00W.	–7.484	0.0392	0.0879
FGGE, 8-12 S.	9.60S.	153.00W.	–7.493	0.0311	0.0953
FGGE, 2- 6 S.	4.00S.	153.00W.	–7.509	0.0146	0.1017
FGGE, 1 N.-1 S.	0.00	153.00W.	–7.530	–0.0060	0.1069
FGGE, 2- 4 N.	3.00N.	153.00W.	–7.545	–0.0215	0.1108
Fanning/Christmas	3.00N.	153.00W.	–7.545	–0.0215	0.1108
FGGE, 6-10 N.	8.00N.	153.00W.	–7.568	–0.0441	0.1139
FGGE, 12–16 N.	13.80N.	153.00W.	–7.590	–0.0667	0.1147
FGGE, 18–20 N.	19.00N.	153.00W.	–7.607	–0.0828	0.1123
Cape Kumukahi	19.53N.	154.68W.	–7.608	–0.0837	0.1124
Mauna Loa	19.53N.	155.58W.	–7.566	–0.0424	0.1096
La Jolla	32.87N.	117.25W.	–7.659	–0.1348	0.1011
Station P	50.00N.	144.00W.	–7.685	–0.1611	0.0872
Point Barrow	71.33N.	157.33W.	–7.707	–0.1835	0.0860
Cape Kumukahi minus Mauna Loa	19.53N.	–	–0.041	–0.0413	0.0028

TABLE 9. -- continued

Latitude Interval of Shipboard Data or Name of Fixed Station	Individual Components				
	SUE	NPP + RES	DES	FER	TDE
South Pole	0.0000	0.0000	0.0000	0.0000	0.0000
Baring Head	–0.0013	0.0027	–0.0041	0.0052	0.0001
Raoul Is.	–0.0026	0.0023	–0.0049	0.0058	0.0001
FGGE, 14-17 S.	–0.0058	0.0024	–0.0093	0.0103	0.0004
Cape Matatula	–0.0061	0.0022	–0.0099	0.0110	0.0005
FGGE, 8-12 S.	–0.0068	–0.0005	–0.0119	0.0137	0.0006
FGGE, 2- 6 S.	–0.0072	–0.0071	–0.0141	0.0171	0.0008
FGGE, 1 N.-1 S.	–0.0078	–0.0120	–0.0147	0.0200	0.0010
FGGE, 2- 4 N.	–0.0083	–0.0156	–0.0151	0.0222	0.0012
Fanning/Christmas	–0.0083	–0.0156	–0.0151	0.0222	0.0012
FGGE, 6-10 N.	–0.0092	–0.0121	–0.0140	0.0251	0.0012
FGGE, 12-16 N.	–0.0101	–0.0066	–0.0123	0.0278	0.0012
FGGE, 18-20 N.	–0.0106	–0.0033	–0.0109	0.0292	0.0011
Cape Kumukahi	–0.0107	–0.0035	–0.0108	0.0292	0.0011
Mauna Loa	–0.0118	0.0149	–0.0145	0.0271	0.0009
La Jolla	–0.0115	–0.0024	–0.0103	0.0343	0.0013
Station P	–0.0100	–0.0233	–0.0076	0.0349	0.0013
Point Barrow	–0.0119	–0.0362	–0.0055	0.0388	0.0012
Cape Kumukahi minus Mauna Loa	0.0011	–0.0184	0.0037	0.0021	0.0002

TABLE 9. -- continued

Latitude Interval of Shipboard Data or Name of Fixed Station	Individual Components			
	EQU	ATL	UOS	IND
South Pole	0.0000	0.0000	0.0000	0.0000
Baring Head	–0.0006	0.0013	–0.0004	–0.0137
Raoul Is.	–0.0012	0.0023	–0.0007	–0.0190
FGGE, 14-17 S.	–0.0037	0.0043	–0.0017	–0.0422
Cape Matatula	–0.0041	0.0045	–0.0017	–0.0451
FGGE, 8-12 S.	–0.0056	0.0052	–0.0020	–0.0568
FGGE, 2- 6 S.	–0.0075	0.0059	–0.0021	–0.0727
FGGE, 1 N.-1 S.	–0.0071	0.0067	–0.0022	–0.0967
FGGE, 2- 4 N.	–0.0068	0.0074	–0.0024	–0.1150
Fanning/Christmas	–0.0068	0.0074	–0.0024	–0.1150
FGGE, 6-10 N.	–0.0050	0.0085	–0.0026	–0.1500
FGGE, 12-16 N.	–0.0032	0.0097	–0.0029	–0.1849
FGGE, 18-20 N.	–0.0024	0.0103	–0.0030	–0.2054
Cape Kumukahi	–0.0024	0.0103	–0.0031	–0.2062
Mauna Loa	–0.0034	0.0093	–0.0034	–0.1711
La Jolla	–0.0022	0.0109	–0.0033	–0.2526
Station P	–0.0015	0.0116	–0.0029	–0.2507
Point Barrow	–0.0017	0.0123	–0.0034	–0.2631
Cape Kumukahi minus Mauna Loa	0.0010	0.0010	0.0003	–0.0351

[a]The composite signal is specified as in Table 5.

[b]For names of the components, see Table 5.

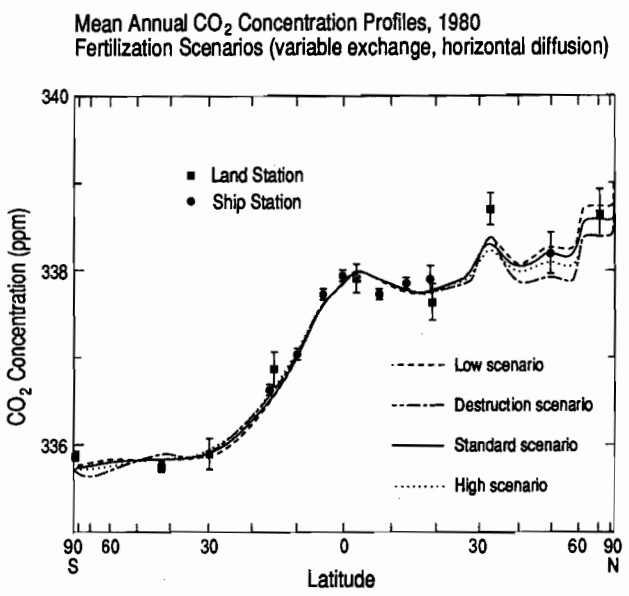

Fig. 65. Mean annual CO_2 concentration, in ppm, in 1980 as in Figure 49, except that the coefficient of gas exchange is assumed to vary with wind speed and the interhemispheric exchange time has been decreased by 20 percent. Three of the curves represent, respectively, scenarios described in the text as "high" scenario (2 × standard fertilization), "low" scenario (no fertilization, no destruction) and "destruction" scenario (no fertilization, high destruction). For each of these scenarios biospheric fertilization and destruction have been altered from the standard scenario (1 × standard fertilization), also shown. For all scenarios the components F_{EQU} and F_{ATL}, and the respiratory coefficient were adjusted as indicated in Table 7 to produce an optimal fit to the observations for 1980 and 1984 combined.

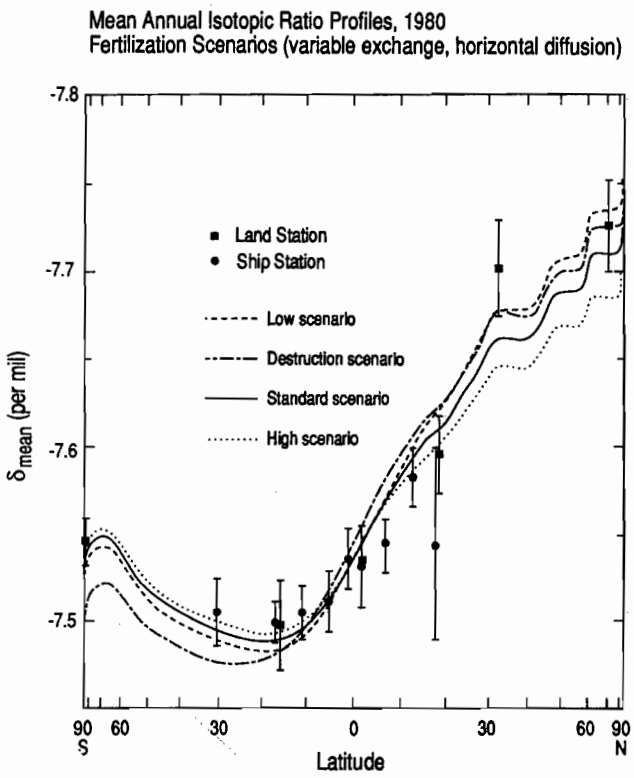

Fig. 66. δ_{mean}, in per mil, corresponding to the concentration profiles of Figure 65.

horizontal diffusion. In each scenario, the three adjustable source components of the model have been readjusted to obtain optimal fits to the observations of CO_2 concentration. For the high scenario, as indicated in Table 7, both the equatorial source and the North Atlantic sink components decrease in strength relative to the standard scenario. These decreases in oceanic fluxes occur because additional destruction partially substitutes for the equatorial oceanic source, and additional fertilization partially substitutes for the North Atlantic sink (cf. figures 11 and 13, respectively). The composite sink generated by the sum of all oceanic components in the North Atlantic Ocean decreases substantially compared to the standard scenario; it is 20 percent less than for the standard model, 16 percent less than for the modified model. The values of χ^2_{red} rise for both concentration (from 9.9 to 11.5) and isotopic ratio (from 3.4 to 3.7) relative to the standard scenario, but the increases are modest. The increases do not prove that this high scenario is demonstrably incorrect.

Also shown in Figures 65 and 66 are the results of a "low scenario" in which fertilization is assumed to be absent altogether. Because fertilization slightly exceeds standard destruction in the standard scenario, a small increase in oceanic CO_2 uptake is postulated in this low scenario to preserve the same net flux of CO_2 into the atmosphere as before. This added oceanic sink, modeled by the oceanic component, F_{UOS}, has little impact on the predicted concentration profile because of the weak gradients that it generates (see Figure 18). The adjustable oceanic components, as expected, change in strength in the opposite sense from those of the high scenario. The χ^2_{red} for C_{mean} decreases slightly (from 9.9 to 9.5), but the χ^2_{red} for δ_{mean} increases significantly (from 3.4 to 4.8). This latter increase exceeds that found for the high scenario (to 3.7), suggesting that a rate of fertilization greater than in the standard scenario is more likely than a lesser rate.

As a final example, Figures 65 and 66 show a profile in which the upper limit of destruction according to Houghton et al. [1987] is adopted (4.7 10^{12} kgC yr^{-1}) without any offsetting fertilization, as in a sensitivity test discussed in subsection 4.3.5, above. The fit to the data of this "destruction" scenario is definitely poorer than the other three shown in Figures 65 and 66. The χ^2_{red} for δ_{mean}, 9.6, is substantially greater than for the standard scenario (3.4).

Of the four scenarios just discussed, the high one provides the best fit to the isotopic observations throughout the tropical Pacific region where the FGGE Shuttle expedition provides closely spaced data. The fit is less satisfactory at high latitudes, however. An incorrect specification of the biospheric fluxes could explain the poor agreement in the northern hemisphere, but at the South Pole,

situated far from terrestrial vegetation, poor agreement more likely reflects a poor simulation of oceanic CO_2 fluxes arising from some remaining defect in the physical formulation of the three-dimensional tracer model.

A possible, perhaps likely, cause for this poor agreement at high latitudes in both hemispheres is the crude formulation of vertical convection in the tracer model. Although it seems unlikely from the analysis of subsection 4.3.6 that the vertical convection in the standard model formulation is too high in the lower latitudes, it may be too high in the polar regions. As indicated by the profiles in Figure 60, a 50 percent reduction of vertical convection from the standard model produces shifts in δ_{mean} in the polar regions of both hemispheres that are approximately of the magnitude required to produce agreement with observations there. In any case, a further investigation of the model parameterization of subgridscale vertical convection should be carried out before ascribing the poor simulation of δ_{mean} in the polar regions for the high scenario to some additional unidentified biospheric component of the carbon cycle.

In conclusion, according to predictions of the three-dimensional model formulated with variable gas exchange and subgridscale horizontal diffusion, a fertilization flux between 2 and 4×10^{10} kgC yr^{-1} agrees approximately with the isotopic observations. If a lesser fertilization flux is postulated, or any additional flux from biospheric destruction when not offset by additional fertilization, the agreement is poorer.

4.3.10 Influence of short-term interannual variations on model predictions.

The source components of the model that simulate perturbations in the carbon cycle are derived from the output of a compartment model of the global carbon cycle [I.5] in which the perturbing influences of fossil fuel combustion and human impacts on the terrestrial biosphere are portrayed by slowly varying functions of time, and in which the responses of the oceans and the biosphere to these forced disturbances are prescribed by constant parameters, thereby introducing no short time scale variations of their own. Consequently, these source components do not reflect interannual variations on time scales of less than a decade, even though the record of atmospheric CO_2 indicates that significant short-term interannual variations occur, for example in association with El Niño events.

In an alternative use of the compartment model, Keeling et al. [I.6] have investigated the effects caused by the suppression of short-term interannual variations in the direct compartment model computations by carrying out an inverse, "double deconvolution" computation in which the exchanges of CO_2 between carbon reservoirs are forced to reflect the variations seen in atmospheric CO_2 concentration and isotopic ratio, as expressed directly by the functions C_{mean} and δ_{mean} (see subsection 2.1, above). As their analysis shows [I.6.7, Table 15], for an interval of two years centered on January 1, 1980, the average increase of atmospheric CO_2 was 3.6×10^{12} kgC yr^{-1} rather than 2.8×10^{12} kgC yr^{-1} prescribed in the original compartment model computations. Although the net uptake of CO_2 by the oceans was only slightly different (an increase of 6 percent) for the double deconvolution computation, the terrestrial biosphere released 0.99×10^{12} kgC yr^{-1} more CO_2 to the air than in the direct model, assuming the same biospheric fertilization rate.

The effects of assuming the fluxes of CO_2 called for by double deconvolution in place of those by the standard case are indicated in Table 7. The adjustable components are changed only slightly, as are the values of χ^2_{red}, both for concentration and isotopic ratio. The changes are small because only weak atmospheric CO_2 gradients are generated by the three-dimensional model components whose strengths are altered by adopting the results of the double deconvolution computations. Thus, the results of the three-dimensional model are not sensitive to our neglect to consider short-term interannual phenomena, within the framework of the assumptions of that model.

The three-dimensional model, however, has been structured to portray only the seasonal and mean annual fields of atmospheric CO_2 [see II.4.1]; it cannot account for interannual fluctuations of the carbon cycle which are interactive with the atmospheric circulation. Left to future investigations is to construct a three-dimensional model that can properly account for the short-term interannual variations seen in the double deconvolution analysis.

5. Discussion

5.1. *Interpretation of Inferred Oceanic CO_2 Fluxes*

The inferred strengths of the oceanic source components of the three-dimensional model, as described in the previous section, are of interest with respect to the air-sea gas exchange rates which they imply. These components are specified as functions of the CO_2 partial pressure difference between the atmosphere and the oceans by means of the bulk formula for air-sea exchange given by equation (2.8), above. The partial pressure fields for the individual components, after adjustment to produce the model prediction for the year 1980, sum to the composite field shown in Figure 67. In the zone between 15.65°N. and 15.65°S. a relatively detailed pattern of partial pressure is prescribed on the basis of direct observations, modified by a constant adjustment factor. Elsewhere the field is only broadly defined, for whole ocean basins or zones, because of a lack of adequate data to specify more exact mean annual patterns. We will now interpret the fluxes generated in the model by this partial pressure field in terms of the air-sea exchange rates which are implied by the available measurements of CO_2 partial pressure.

At any location, $\mathbf{x}$, in this equatorial region the net CO_2 flux, $F_{net}(\mathbf{x})$, emanating from the oceans is given by the sum

$$F_{net}(\mathbf{x}) = F_{EQU}(\mathbf{x}) + F_{UOS}(\mathbf{x}) \tag{5.1}$$

where $F_{EQU}(\mathbf{x})$ and $F_{UOS}(\mathbf{x})$ denote the equatorial and uniform oceanic sink component fluxes, respectively, as described in subsection 2.4.3, above. For the year 1980 the model simulates a flux, F_{net}, of 1.277×10^{12} kgC yr^{-1} between 15.65°N. and 15.65°S. (see Table 10) with contributions from F_{EQU} and F_{UOS} of 1.980×10^{12} kgC yr^{-1} and -0.702×10^{12} kgC yr^{-1}, respectively.

Formally, the integral of F_{net}, over the area, A_{EQU}, of the equatorial ocean from 15.65°N. to 15.65°S., is specified in the model as

$$\int_{A_{EQU}} F_{net} dA = k_{ex} \int_{A_{EQU}} (v_{EQU} \Delta pCO_{2EQU} + \Delta pCO_{2UOS}) dA \tag{5.1}$$

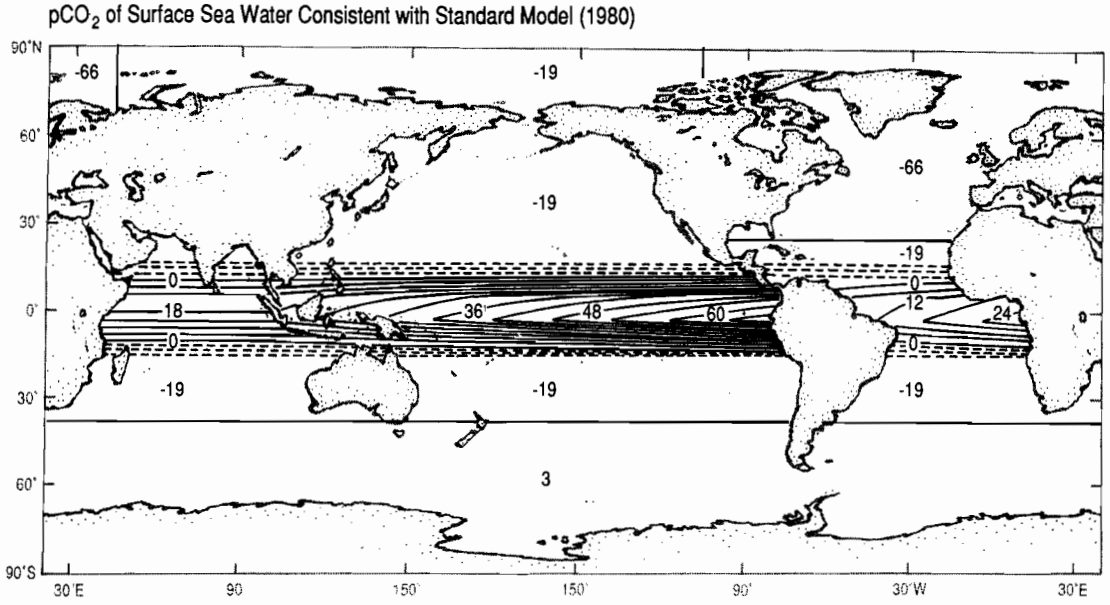

Fig. 67. Stationary distribution of CO_2 partial pressure in surface sea water in units of ppm (approximately equal to microatmospheres) generated by the sum of all oceanic source components, adjusted to be consistent with the prediction of the standard model for the year 1980. Contour interval is 6 ppm.

where k_{ex} denotes the nominal exchange coefficient used in the original specification of the model source components. This coefficient is assumed to be a constant with the value of 2.1747×10^{-6} kgC m^{-2} day^{-1} ppm^{-1} (see equation (2.8)). The factor v_{EQU} denotes an adjustment factor which determines the strength of the equatorial source component; it was previously determined from the fit of the model concentration profile to the observations of the CO_2 partial pressure, $pCO_{2\,sea}$ (see Table 1, above, and [II.4.5, equation 4.33]). The quantities ΔpCO_{2EQU} and ΔpCO_{2UOS} denote differences in CO_2 partial pressure between air and sea ascribed to the equatorial source and the uniform ocean sink component, respectively.

Alternatively we may interpret this net flux as the product of the actual, yet unknown equatorial air-sea exchange coefficient, k_{equ}, assumed to be constant throughout the equatorial ocean area, and the actual observed sea-air difference in CO_2 partial pressure in 1980, $\Delta pCO_{2\,obs}$

$$\int_{A_{EQU}} F_{net}\,dA = k_{equ} \int_{A_{EQU}} \Delta pCO_{2\,obs}\,dA \tag{5.2}$$

Equating the right sides of equations (5.1) and (5.2) we obtain for k_{equ} the expression

$$k_{equ} = \frac{k_{ex}(v_{EQU}\overline{\Delta pCO}_{2EQU} + \overline{\Delta pCO}_{2UOS})}{\overline{\Delta pCO}_{2\,obs}} \tag{5.3}$$

Here, the overbars denote averages taken over the entire equatorial ocean area, A_{EQU}. By our assuming that k_{equ} is a constant in deriving equation (5.3) we have neglected the possible covariance between k_{equ} and $\Delta pCO_{2\,obs}$.

In order to evaluate equation (5.3) numerically, we equate $\overline{\Delta pCO}_{2\,obs}$ to $\overline{\Delta pCO}_{2EQU}$, since observations of the air-sea difference, ΔpCO_2, were used in the first place to define the pattern of the equatorial source component [II.4.4.2.]. These observations as mapped [II.4.2.2, Figure 10] lead to an average ΔpCO_{2EQU} of 24.16 ppm. With a value of −8.36 ppm for ΔpCO_{2UOS} [II.4.4.3.] and with v_{EQU} set equal to 0.9758 (see Table 1), we find

$$k_{equ} = 0.6298 \cdot k_{ex} = 1.3696 \times 10^{-6}\ \text{kgC m}^{-2}\ \text{day}^{-1}\ \text{ppm}^{-1} \tag{5.4}$$

This value is 63 percent of the nominal value of 2.1747×10^{-6} kgC m^{-2} day^{-1} ppm^{-1} which was chosen in accordance with the carbon compartment model [II.4.4, equation (4.26)], and was established to be consistent with the distribution of radiocarbon in the oceans.

The value of k_{equ} found above, of course, is dependent on the characteristics of the three-dimensional transport model and in particular on the model's representation of vertical convection and of the boundary layer over the tropical ocean. If the above calculation is performed, with the convective parameter, ζ, reduced to 0.25 (see subsection 4.3.6), an adjustment factor, v_{EQU}, of 0.6861 results for 1980. The estimated equatorial air-sea exchange coefficient is then only 34 percent of the nominal value, or 54 percent of the value for the standard case in which ζ is 0.50.

The model's lack of an explicit atmospheric boundary layer may also have contributed to an overestimate in k_{equ}. However, since the equatorial flux was determined by adjusting the model predictions to atmospheric data obtained over the open ocean, the layer is

TABLE 10. Mean Annual Flux Associated With Each Source Component and Integrated Over Each of 6 Zonal Compartments for Each Historical Period. Fluxes Are Expressed in Units of 10^{12} kgC yr^{-1}. Positive and Negative Values Represent Fluxes Into and Out Of the Atmosphere, Respectively.

Model Component	90.00 – 39.13 S.	39.13 – 15.65 S.	15.65 S. – 0.00	0.00 – 15.65 N.	15.65 – 39.13 N.	39.13 – 90.00 N.	Totals
Jan. 1, 1962							
Net primary productivity (NPP)	–0.242	–6.766	–11.003	–9.119	–9.352	–13.014	–49.495
Respiration (RES)	0.242	6.766	11.003	9.119	9.352	13.014	49.495
Biospheric destruction (DES)	0.001	0.147	0.642	0.507	0.352	0.044	1.693
Biospheric fertilization (FER)	–0.007	–0.195	–0.317	–0.263	–0.269	–0.375	–1.425
Equatorial source (EQU)	–0.618	–0.706	1.324	0.891	–0.560	–0.331	0.000
North Atlantic sink (ATL)	0.937	0.000	0.000	0.000	–0.430	–0.507	0.000
Uniform oceanic sink (UOS)	–0.268	–0.306	–0.220	–0.218	–0.235	–0.139	–1.385
Industrial source (IND)	0.005	0.098	0.027	0.064	0.931	1.530	2.656
Jan. 1, 1968							
Net primary productivity (NPP)	–0.252	–7.056	–11.475	–9.511	–9.753	–13.573	–51.620
Respiration (RES)	0.252	7.056	11.475	9.511	9.753	13.573	51.620
Biospheric destruction (DES)	0.001	0.150	0.656	0.518	0.360	0.045	1.729
Biospheric fertilization (FER)	–0.008	–0.219	–0.356	–0.295	–0.303	–0.421	–1.602
Equatorial source (EQU)	–0.422	–0.482	0.904	0.608	–0.382	–0.226	0.000
North Atlantic sink (ATL)	0.799	0.000	0.000	0.000	–0.366	–0.432	0.000
Uniform oceanic sink (UOS)	–0.313	–0.358	–0.256	–0.255	–0.274	–0.162	–1.618
Industrial source (IND)	0.006	0.130	0.035	0.085	1.230	2.021	3.507
Jan. 1, 1980							
Net primary productivity (NPP)	–0.273	–7.645	–12.432	–10.304	–10.567	–14.705	–55.927
Respiration (RES)	0.273	7.645	12.432	10.304	10.567	14.705	55.927
Biospheric destruction (DES)	0.001	0.156	0.679	0.536	0.373	0.047	1.791
Biospheric fertilization (FER)	–0.010	–0.288	–0.468	–0.388	–0.397	–0.553	–2.104
Equatorial source (EQU)	–0.552	–0.631	1.183	0.796	–0.501	–0.296	0.000
North Atlantic sink (ATL)	1.147	0.000	0.000	0.000	–0.526	–0.621	0.000
Uniform oceanic sink (UOS)	–0.430	–0.491	–0.352	–0.350	–0.377	–0.223	–2.224
Industrial source (IND)	0.010	0.196	0.053	0.128	1.859	3.053	5.300
May 15, 1984							
Net primary productivity (NPP)	–0.281	–7.859	–12.780	–10.593	–10.863	–15.117	–57.493
Respiration (RES)	0.281	7.859	12.780	10.593	10.863	15.117	57.493
Biospheric destruction (DES)	0.001	0.157	0.686	0.541	0.376	0.047	1.809
Biospheric fertilization (FER)	–0.011	–0.310	–0.504	–0.418	–0.429	–0.597	–2.269
Equatorial source (EQU)	–0.510	–0.583	1.094	0.736	–0.463	–0.273	0.000
North Atlantic sink (ATL)	0.949	0.000	0.000	0.000	–0.435	–0.514	0.000
Uniform oceanic sink (UOS)	–0.444	–0.508	–0.364	–0.361	–0.390	–0.230	–2.297
Industrial source (IND)	0.010	0.192	0.052	0.126	1.821	2.991	5.192

probably modeled well enough to prevent a serious overestimate of the CO_2 flux on this account. Steep vertical gradients in CO_2 in the lower tropical atmosphere which could contradict the model calculations for the lowest model layer are unlikely, given the rarity of sharp marine air temperature inversions in the tropics. Thus we do not expect that errors in the boundary layer formulation can contribute to a serious overestimation of k_{equ}.

There exists evidence, independent of our model calculations, that the gas exchange coefficient is smaller in the equatorial region than the global average, because of lighter wind speeds. From a global map of the annual average coefficient constructed by Heimann and Monfray [1989], we calculate a spatial average over the equatorial latitude band from 15.65°S. to 15.65°N., that is 53 percent of the global average calculated from the same map. Thus our finding k_{equ} to be substantially less than the nominal exchange rate compatible with radiocarbon data, tends to confirm the spatial structure of the exchange coefficient determined by these authors. In terms of absolute magnitude, however, our estimate of k_{equ} for the standard convective case (equation (5.4)) is substantially larger than the corresponding equatorial average from the maps of Heimann and Monfray [1989]. This discrepancy is not restricted to the equatorial region. The global rate found by these authors is, indeed, a factor 1.74 weaker than our nominal global exchange rate. Thus our finding of a slower exchange rate in the equatorial region is consistent with their field for air-sea exchange only in a relative sense.

The large North Atlantic sink, inferred from the model fit to the mean annual concentration profile, also merits further discussion.

For the year 1980 we deduce a net sink of 1.628×10^{12} kgC yr^{-1} by summation of the fluxes from the three components, F_{UOS}, F_{EQU}, and F_{ATL} integrated over the Atlantic Ocean north of 23.48°N. If the nominal global average exchange coefficient, k_{ex}, is valid for the North Atlantic Ocean, this flux is maintained by an average ΔpCO_2 of –66 ppm. The evaluation of this gradient is not sensitive to uncertainties in the model's formulation of gas exchange or subgridscale diffusion. If a variable gas exchange coefficient is assumed (see subsection 4.3.7, above), ΔpCO_2 is lowered to –61 ppm. If, in addition, horizontal diffusion is assumed (see subsection 4.3.8, above), it is lowered to –62 ppm. Changing vertical convection has even a smaller effect on evaluating this gradient (see subsection 4.3.6, above). An air-sea disequilibrium as large as –66 ppm is not substantiated by the few available measurements of $pCO_{2\,sea}$ which lead to estimates of the mean annual average $pCO_{2\,sea}$ approximately half as large [Takahashi et al., 1985; Broecker et al., 1986; Peng et al., 1987].

From the maps constructed by Heimann and Monfray [1989], we calculate a mean annual exchange coefficient over the region of the North Atlantic sink component which is very close to the global average. This finding, at first sight surprising, results from the fact that the strong wind speeds in winter are offset on annual average by rather low winds in summer. Thus we have no strong evidence that our assumed value of k_{ex} is seriously in error when computing the large ΔpCO_2 difference of –66 ppm.

At least three shortcomings of the model could be contributing to an overestimate of ΔpCO_2 for the North Atlantic Ocean. Firstly, in contrast to our assumption that the air-sea exchange coefficient over the region of the sink is uniform, actually this coefficient probably increases in magnitude northward, because the wind speed increases northward (see, for example, the map of Heimann and Monfray [1989]). If air-sea exchange were to take place preferentially in higher latitudes rather than uniformly as assumed in the construction of the North Atlantic sink component, then a smaller integrated flux would be sufficient to achieve an optimal fit of the model-predicted mean fields to the observations. Second, underestimation of the interhemispheric transport in the model is likely to have produced an overestimate of the North Atlantic sink by the order of 13 percent, as discussed above in subsection 4.3.7. Third, the model neglects to allow that a substantial fraction of the oceanic northern hemisphere sink may be located in the North Pacific Ocean.

We regret the abandonment of Weather Station P in the North Pacific Ocean in 1981 since that station, located far from interferences of terrestrial sources and sinks of CO_2, would have been of great value in assisting us in deciding on the possibility of a Pacific Ocean CO_2 sink. The observed difference in CO_2 concentration between Ocean Station P and Point Barrow, Alaska, is larger than the predicted difference for both the 1968 and 1980 profiles (see Figures 44 and 45), suggesting a tendency for the North Pacific Ocean to be more of a sink. The 1968 difference is of questionable reliability, however, because it depends on extrapolated data at both stations [I, Appendix A]. Furthermore, the Station P data in general may be biased because of a storage problem with the small volume flasks used there to collect samples of air [Keeling et al. 1985]. Thus we cannot rely on a comparison of data at these two stations to establish a North Pacific sink. With very precise data at alternative stations such as Cold Bay, Alaska, and Weather Station M in the Atlantic Ocean, where the U.S. National Oceanic and Atmospheric Administration (NOAA) currently collects samples [Conway et al., 1988], the division of the sink between the two oceans perhaps could be resolved.

None of the above-mentioned aspects of our model simulation alone is probably sufficient to reduce the implied sea-air ΔpCO_2 difference to acceptable values. If, however, more than one of them contributes to an overestimate of ΔpCO_2 it may be possible to reconcile the discrepancy.

In addition, although we have no basis for suspecting it, errors in modeling the global production of industrial CO_2, and even errors in modeling the seasonal cycle of plant activity (see subsection 2.3.1, above) might contribute to an overestimate of the North Atlantic sink. Finally, it cannot be ruled out that the modeled terrestrial sink of CO_2 associated with biospheric fertilization may be too weak or be incorrectly distributed geographically. For example, if the "high scenario" discussed in subsection 4.3.9 is accepted for the model with variable gas exchange and horizontal diffusion, ΔpCO_2 for the North Atlantic Ocean is computed to be –52 ppm, a gradient which almost approaches a realistic value.

In the higher latitudes of the southern hemisphere the deduced $pCO_{2\,sea}$ field must be such as to compensate for both the northern hemisphere sink and for the opposing equatorial source. As the model indicates, the average $pCO_{2\,sea}$ there is probably so close to equilibrium with the atmosphere that very little net CO_2 exchange occurs. Thus the gas exchange rate at high latitudes can probably be estimated from atmospheric CO_2 data only in the northern hemisphere.

5.2 *Detection of Biospheric Perturbations*

As we noted in subsection 2.7 above, it should be possible to distinguish biospheric and oceanic processes as they affect atmospheric CO_2 because of the much larger shift in annual mean isotopic ratio, δ_{mean}, accompanying terrestrial biospheric exchange compared to the shift accompanying oceanic exchange. Our attempt to do so using the three-dimensional model is hampered, however, by two interfering processes: release to the air of industrial CO_2, isotopically indistinguishable from release of carbon from plants, and a purely isotopic exchange arising from variations in isotopic fractionation with temperature when gaseous CO_2 exchanges with dissolved inorganic carbon in sea water. The Suess Effect (see Figure 27) contributes a small additional oceanic interference. We now examine the effects of these interferences on detecting biospheric fluxes in the light of our analysis of modeling errors discussed in subsection 4.2. Afterwards we add a few final comments regarding the detection of biospheric processes using isotopes.

The detection of the mean annual net primary productivity (NPP) and respiration using isotopes is best accomplished by first studying the seasonal cycle of atmospheric CO_2. Heimann et al. [this volume] demonstrate that it should be possible to distinguish oceanic and biospheric seasonal exchanges by simultaneously examining seasonal variations in CO_2 concentration and reduced isotopic ratio, but they deferred attempting to do so [III.5.4] pending the availability of more isotopic data to reduce the uncertainty in observations of the isotopic seasonal cycle.

The release of CO_2 by destruction of the terrestrial biosphere through deforestation and other human activities takes place largely in the tropics (see subsection 2.3.2, above), where it produces only a weak north-south variation in atmospheric CO_2 along the transect of our observations (see Figure 11 and subsection 4.3.5). The maximum predicted difference in δ_{mean}, along this transect, is found between the tropics and the South Pole. The difference, 0.017‰, is too small to be verified with our existing model and data.

We therefore focus on the detection of the remaining biospheric source component, biospheric fertilization. This process involves the stimulation of plant growth. On the assumption that the rate of stimulation is proportional to NPP, the model for a global source strength of 2.1×10^{12} kgC yr^{-1} predicts maximum concentration differences in the lower atmosphere at the polar extremes of the profile (see Figure 13 and subsection 2.3.2 above). Between Point Barrow, Alaska, (71°N.) and the South Pole the predicted difference is 0.044‰.

In Table 11 we compare the contributions to this difference for each of the model source components. Also listed are isotopic errors in these individual predictions as estimated in subsection 4.2, above. The composite error has been arrived at by assuming that the errors for biospheric and oceanic exchange and for industrial CO_2 release are uncorrelated, and hence that the variances are additive, as discussed in subsection 4.2.3. The individual biospheric components, in contrast, are uncertain in their isotopic composition because the same error applies to each biospheric component. Hence the relative uncertainty in the sum of the biospheric components is the same as that of the individual components. We cannot decide whether the prediction of δ_{mean} for temperature-dependent fractionation is more nearly correct assuming constant or variable air-sea exchange and we have therefore chosen somewhat arbitrarily the average of the two predictions as our best estimate.

The observed difference in δ_{mean} between Point Barrow and the South Pole is –0.183‰ with a standard error of 0.015‰, close to the predicted value of –0.205‰. The contribution of 0.039‰ to this composite owing to the fertilization process is more than twice the observed standard error. Thus the evidence for fertilization from isotopic data would be convincing were it not for the large estimated errors in the model's prediction of the δ_{mean} difference arising from temperature-dependent fractionation (0.041‰) and industrial CO_2 release (0.037‰). Including lesser independent errors of the other components we estimate that the overall error is nearly 0.06‰. Even this estimated error does not include the possible biases caused by incorrect specification of vertical and horizontal subgridscale processes in the model. Thus, it does not appear possible to prove the existence of fertilization with the present model. On the other hand, the model predictions, with adding provisions for variable air-sea exchange and explicit horizontal diffusion (see subsection 4.3.9) suggest that the outlook for deducing biospheric fluxes is likely to improve.

Also, the analysis of Table 11 is helpful in suggesting improvements which are needed to reduce errors in the isotopic specifications of the model. It should be possible to reduce considerably the large error that arises from uncertainties in industrial CO_2 emissions, if direct measurements of the isotopic ratio of atmospheric CO_2 were undertaken downwind from industrial

TABLE 11. Contributions of Model Source Components to Predicted Differences in δ_{mean} between Point Barrow, Alaska (71°N.) and the South Pole in 1980

Component	Difference in δ_{mean} (‰)	Estimated Error Relative	Estimated Error (‰)
Biospheric Exchanges			
Net of NPP and Respiration	–0.036	10%	
Destruction	–0.006	10%	
Fertilization	0.039	10%	
sum	–0.003	10%	± 0.001
Oceanic Exchanges			
Bulk exchanges	0.007	10%	± 0.001
Temperature Dependent Fractionation[a]	0.070	67%	± 0.041
Suess Effect	–0.016	10%	± 0.002
sum	0.061		± 0.041
Industrial CO_2 Release	–0.263	14%	± 0.037
Composite of All Components	–0.205		± 0.055[b]
Observed (1980 and 1984 data combined)	–0.183		± 0.015[c]

[a] Assumes average of predictions with a constant and with a variable air-sea gas exchange coefficient.

[b] Assumes that variances are additive (see text).

[c] Assumes that variances, computed as squares of the individual standard errors listed in Table 3, are additive.

regions. A sampling program carried out in key areas could provide data which would establish the δ of industrial CO_2 for all regions of the world where large emissions occur. More difficult, but also attainable, is to obtain better reports by members of the United Nations of the production of coal, petroleum and natural gas country by country. If the errors in both the isotopic composition and amount of fuel produced could be reduced to about 3 percent from the present 10 percent, the error in predicting the gradient in δ_{mean} for industrial CO_2 between Alaska and the South Pole would drop to 0.02‰.

We assigned a large error to temperature-dependent fractionation because we could not decide the extent to which gas exchange is dependent on wind speed. This dependency should be far better established within a few years, if present studies in wind-wave facilities and measurements and predictions of the CO_2 partial pressure in sea water are vigorously pursued.

Finally, even if the errors in chemical and physical specification of the model cannot be reduced sufficiently to prove the extent of biospheric fertilization, it should be possible to detect *changes* in the strength of fertilization, or, at least, in the net terrestrial biospheric exchange of CO_2 with the atmosphere. The fractionation factors of CO_2 and the parameters characterizing atmospheric transport should not change appreciably over time. Thus a model which is calibrated to predict the field of δ_{mean} based on present observations, if it is used to predict δ_{mean} in future decades, should be adequate to detect net changes in terrestrial biospheric exchange to the order of 0.01‰. As long as biospheric destruction occurs mainly in the tropics, a significant reduction in the difference in δ_{mean} pole to pole over time compared to model predictions should be a basis for establishing changes in fertilization at higher latitudes to an imprecision of about 1×10^{12} kgC yr^{-1}.

6. Large Scale Inferences Regarding the Carbon Cycle

We have up to this point focused on regional aspects of the carbon cycle. We now address how the predictions of our standard model compare with studies of the carbon cycle pursued in terms of only a very limited compartmentalization of the atmosphere and the biospheric and oceanic carbon reservoirs which contact it.

The direct results of our three-dimensional model do not challenge carbon cycle studies in which the atmosphere, surface oceans, and terrestrial biosphere are treated as single compartments or are differentiated solely with respect to function, for example, living and dead carbon on land, because the global integrals of the source components of the model were all estimated independently by means of such a global compartment model, as discussed in section 2, above. The three-dimensional model generates useful information, however, as soon as interest is directed toward any degree of subdivision of the atmosphere, along with its spatially distributed sources and sinks.

For the present discussion, we pass up the simplest case of subdivision into two compartments and focus on four. We distinguish transport occurring between the northern and southern hemispheres and between low and high latitudes in each hemisphere. We set the compartment boundaries within the atmosphere at the equator and at 15.65° in each hemisphere, thus making use of grid boundaries designated in the three-dimensional model. Afterwards, we will further subdivide the extratropical compartments at 39.13° in each hemisphere in order to single out the middle latitude zones where, in the northern hemisphere, the industrial CO_2 source is maximal. This separation into six zones is approximately at the degree of detail employed by Bolin and Keeling [1963, p. 3013] who characterized the atmosphere with a one-dimensional continuous north-south diffusive model in which the diffusion equation was solved using five terms in the Legendre polynomial expansion of the concentration field.

The mean annual fluxes integrated over each of six compartments for each source component are listed in Table 10. Selected composites of these fluxes divided into four compartments, are shown schematically in Figures 68 to 71 for the four historical periods for which fits were made to the data (see subsection 2.3). In each figure, oceanic fluxes (shown as dashed pathways with arrowheads) are inferred to be coupled via subsurface water. One such flux, defined to pass from high northern to high southern latitudes, depicts the model source component hypothesized to represent a sink for atmospheric CO_2 in the North Atlantic Ocean balanced by a source in the southern oceans. Two other fluxes are

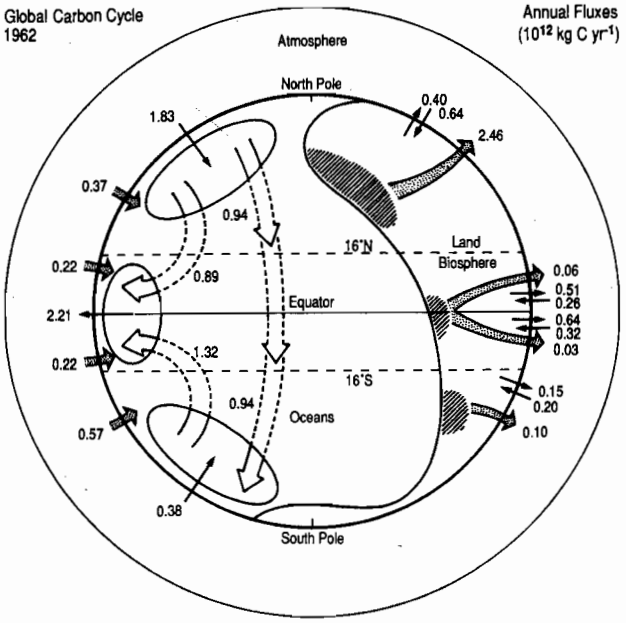

Fig. 68. Schematic representation of the major sources and sinks of atmospheric CO_2 arising from perturbations of the carbon cycle as predicted for 1962 by the three dimensional tracer model. The CO_2 transfers, expressed in units of 10^{12} kgC yr^{-1}, are averages over one year centered on January 1, 1962 and are for zonal compartments of the earth's surface as described in the text. The transfers are divided into categories as follows: open dashed arrows, subsurface oceanic transfers with their sums for each region shown as line arrows; shaded arrows, CO_2 entering the atmosphere from fossil fuel combustion (shown on the right) and absorption of a fraction of this CO_2 by the oceans (shown on the left); line arrows on the right, CO_2 exchange with the biosphere, "biospheric fertilization" and "biospheric destruction".

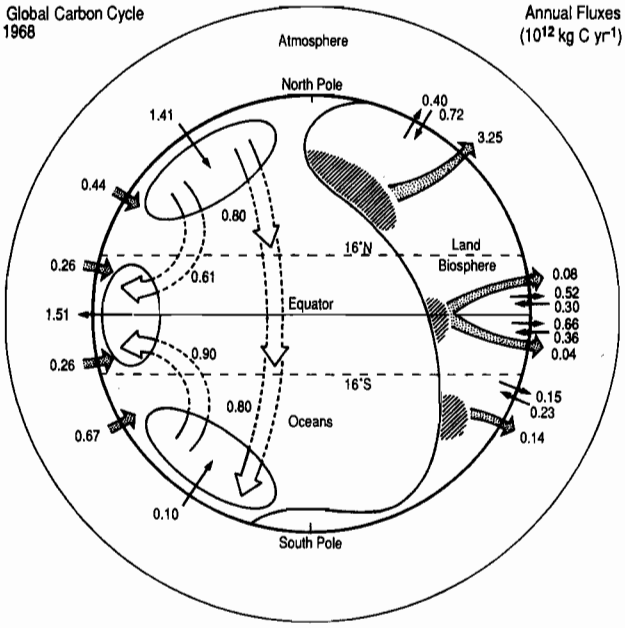

Fig. 69. Same as Figure 68, but for 1968.

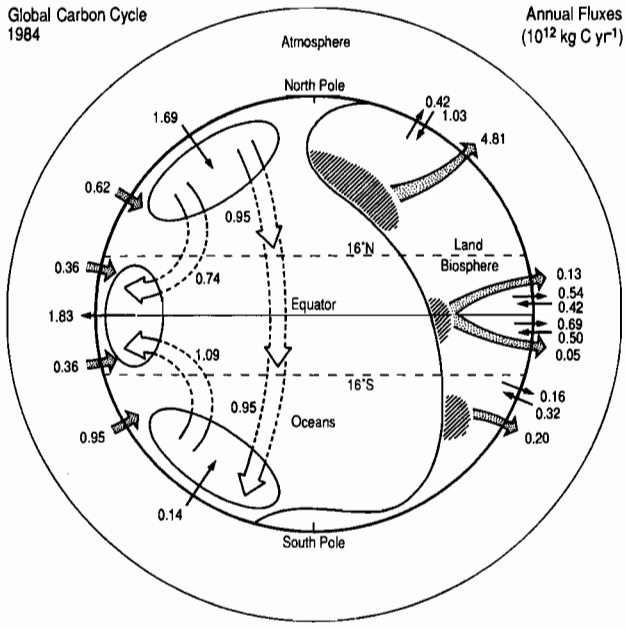

Fig. 71. Same as Figure 68, but for 1984, centered on May 15 instead of January 1.

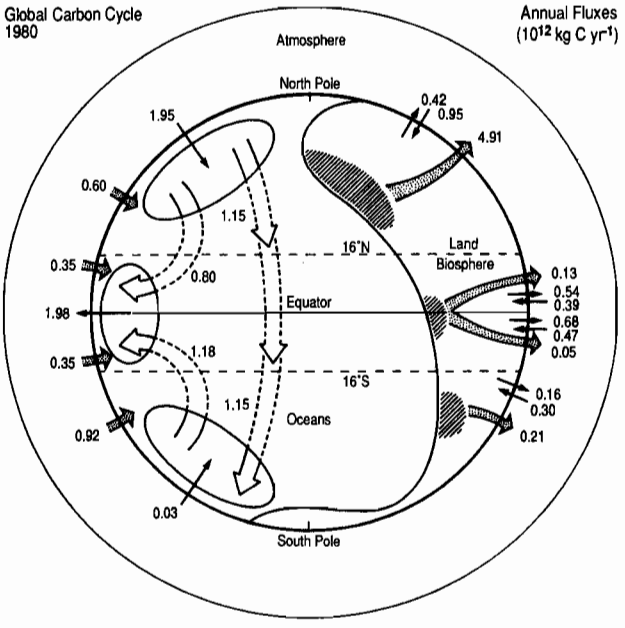

Fig. 70. Same as Figure 68, but for 1980.

directed from high to low latitudes in each hemisphere. These together reflect the equatorial source component, identified by high CO_2 partial pressure (pCO_2) in the surface waters of the tropics, and by low pCO_2 in surface waters at high latitudes, such that the transport of CO_2 within the oceans is separately balanced in each hemisphere.

The North Atlantic sink component of the model is computed to be approximately the same strength in 1962 and 1984 (about 0.9×10^{12} kgC yr^{-1}), but somewhat smaller in 1968 and larger in 1980 (about 0.8 and 1.1×10^{12} kgC yr^{-1} respectively). Thus a cross-equatorial flux of the order of 1.0×10^{12} kgC yr^{-1} appears to be a persistent feature of the air-sea exchange of CO_2 as previously noted in sections 2 and 4.

The oceanic fluxes which transport CO_2 from high to low latitudes within each hemisphere reflect the known upwelling of CO_2-rich waters in the tropical oceans. This upwelling is especially prominent in the Pacific Ocean where waters at high latitudes in both hemispheres sink to intermediate depths and return to the surface near the equator. For all four historical years for which the carbon cycle is depicted here, the flux in the southern hemisphere is computed to be slightly larger than in the northern, as a result of the cross-equatorial asymmetry of the data for the oceanic CO_2 partial pressure, $pCO_{2\,sea}$, used in the computations. Since these data are based on only one composite set of observations for the Pacific Ocean near 150°W., one should not attach too much significance to the predicted difference. Nevertheless, the north-south profiles of the mean annual atmospheric CO_2 concentration, C_{mean}, in Figures 43 to 46 indicate that the model predictions fit the concentration data well, except in the southern tropics where the predictions, for all years but 1968, appear to be slightly too low. This mismatch suggests an even greater asymmetry in $pCO_{2\,sea}$ in the south near the time of these two profiles and thus a consistently stronger oceanic CO_2 source south of the equator.

The CO_2 emitted near the equator by the sum of the two oceanic fluxes, as indicated on each schematic plot, varies only slightly from period to period. Since the atmospheric data for each period are independent, this near agreement in model prediction suggests a persistent feature of the oceanic carbon cycle. The rather poor fit

for the mean annual isotopic ratio of CO_2, δ_{mean}, in the tropics in 1980 for either constant or variable air-sea exchange (see Figure 51) does not challenge this conclusion, because the equatorial oceanic source contributes only negligibly to the isotopic distribution, and because the source components that do affect δ_{mean} near the equator have only a small impact on the shape of the concentration profile near the equatorial peak.

With respect to the terrestrial biospheric fluxes only perturbations are shown in Figures 68 to 71. These are divided into an uptake flux owing to stimulated biospheric growth and a release flux owing to biospheric destruction arising from land use practices, as previously discussed in subsection 2.4. The annually balanced fluxes in the model from NPP and respiration are not shown on the plots, although they are listed for each of the four compartments in Table 10. (They are prescribed to increase slightly with time as the peak-to-peak amplitudes in the annual cycle increase from one historical period to the next, as noted in subsection 2.3.1). These fluxes are much larger than the perturbation fluxes, but have only a small, indirect impact on the mean annual atmospheric CO_2 field, as discussed previously in section 2.

A principal conclusion to be drawn from the schematic plots, and from Table 10, is that the separately prescribed biospheric perturbation fluxes of CO_2 are small compared to the globally balanced oceanic fluxes. Their combined net impact on the mean field of atmospheric CO_2 is still smaller. On this account we are evidently justified in not attempting to adjust their global strengths to observations of CO_2 concentration in our fitting procedure.

Release of industrial CO_2 from fossil fuel combustion, as noted in subsection 2.6, is clearly a dominant flux in the extratropical northern hemisphere. For 1980 and 1984, as shown on the schematic plots, the industrial CO_2 flux was nearly 5×10^{12} kgC yr^{-1} for this zone alone. A comparison of the CO_2 concentration field produced by industrial CO_2 emissions (Figure 23) with the field produced by the sum of all of the biospheric fluxes (Figure 20) and that of all of the oceanic fluxes (Figure 22) argues strongly for the dominant role of fuel emissions in producing CO_2 gradients generally.

The notion has sometimes been advanced that the rise in atmospheric CO_2 cannot be identified as due to fossil fuel combustion, because these industrial emissions are blended into much larger, natural fluxes of CO_2 between the atmosphere, the oceans, and the terrestrial biosphere. The fossil fuel emissions are, indeed, small compared to NPP and respiration which separately transfer the order of 60×10^{12} kgC yr^{-1} of CO_2 between the atmosphere and the terrestrial biosphere. Similarly, the transfers of CO_2 between the air and the sea which arise from the gross exchange of CO_2 molecules are still larger, of the order of 90×10^{12} kgC yr^{-1} in each direction [Bolin, 1983, Figure 2.1].

Nevertheless, the combination of NPP and respiration produces much smaller gradients in atmospheric CO_2 concentration (Figures 8 and 9) than are produced by industrial CO_2 (Figure 23), while the gross oceanic exchange has no influence on this concentration at all, except where the exchange is regionally or seasonally imbalanced, as already addressed. Even these imbalances produce smaller atmospheric gradients than does industrial CO_2. The oceanic fluxes of the model cannot be grossly in error, because they are constrained by some knowledge of $pCO_{2\,sea}$ and the rate of exchange of gases at the sea surface, as discussed earlier. Unless the biospheric perturbation fluxes in the model are seriously underestimated, it is justified to conclude that the fossil fuel flux in recent years is the dominant cause of the mean annual gradients of atmospheric CO_2.

7. Conclusions

Although broad, general features of the carbon cycle have been understood for many years, the cycle must receive far more study if we are to appreciate how it may be impacted by human activity during the coming decades. The present study has sought to advance our understanding of the contemporary cycle on the global scale by means of a three-dimensional transport model that predicts variations in atmospheric CO_2 arising from identified physical, chemical, and biological processes occurring near the interfaces of the atmosphere with land and water. The realism of the model has been tested by comparing its predictions of atmospheric CO_2 with measurements made during the past 25 years almost from pole to pole near the north-south axis of the Pacific Ocean. This article, the final in a series of four, has focused on the mean annual cycle and on its interannual variations. The measurements and model simulations cover a period in which human activities have increasingly altered the carbon cycle.

To identify these anthropogenic impacts, and the natural cycle as it would have operated in their absence, we have divided the carbon cycle conceptually into a set of model components which represent selected processes involving the metabolic activity of the terrestrial biosphere and the chemistry of near-surface ocean water. These processes, expressed as regionally varying sources or sinks of atmospheric CO_2, take place in proximity to the atmosphere where most living matter resides and where most of these activities take place. In the model, as consequences of human activities, we have included the release of CO_2 from fossil fuel combustion and from deforestation and land use changes. We have also hypothesized that plants on land are growing more rapidly today than in the past in response to the recent build-up of atmospheric CO_2 which itself is largely caused by man's industry. We have devoted much of our four-part study to describing how the model, component by component, prescribes these processes and predicts their effect on atmospheric CO_2.

The model is sufficiently realistic to reveal hitherto unexplained features of the atmospheric CO_2 distribution, especially regional features on synoptic and seasonal times scales, as discussed in the third article in this series by Heimann et al. [this volume]. In this final article we have continued to address regional details of the carbon cycle, but we have also addressed broader, even global-scale, features.

The combustion of fossil fuel influences not only the long-term time trend in atmospheric CO_2 but the spatial patterns of the mean annual field as well. It especially affects the meridional gradient of atmospheric CO_2, because emissions occur mainly in the northern hemisphere. According to the model, fossil fuel combustion makes a larger imprint on meridional gradients than either terrestrial biospheric activity or oceanic CO_2 exchange, or even both of these predominantly natural processes combined. Given that the annual release of industrial CO_2 has recently been about 5.5×10^{12} kgC, we infer that the global net exchanges of the biosphere and oceans with the atmosphere cannot be more than a few times 10^{12} kgC yr^{-1}, except for components distributed so nearly symmetrically with respect to the equator that they escape our attention

because they produce no well defined north-south gradients in atmospheric CO_2.

Having mapped the industrial CO_2 source and predicted its influence on the atmospheric CO_2 distribution, we have sought to discern, through the noise in the atmospheric CO_2 measurements and the errors in the model predictions, the weaker residual patterns in atmospheric CO_2 produced by the terrestrial biosphere and the oceans. The predominance of the industrial source makes our task more difficult than it would have been in preindustrial times, or even in the first half of this century, but we have nevertheless been able to establish, within broad limits, the strengths of the sources and sinks generated by the biosphere and the oceans.

The most clearly established source of CO_2 arises from the tropical oceans in a band approximately 30° wide centered on the equator. This oceanic flux, which introduces between 1½ and 2×10^{12} kgC yr^{-1} of CO_2 into the atmosphere, shows little interannual variation from the early 1960's to the mid-1980's. Because this flux is produced in a region where the CO_2 partial pressure in surface sea water, $pCO_{2\,sea}$, is relatively well known, we have been able to estimate the average gas exchange coefficient, k_{equ}, in tropical sea water by comparing our estimate of the flux with a map of mean annual $pCO_{2\,sea}$. We find k_{equ} to be about two-thirds (64 percent) of the global value computed from radiocarbon data.

The model further establishes a CO_2 sink of about 1×10^{12} kgC yr^{-1} in the North Atlantic Ocean, or more correctly *somewhere* in the higher latitudes of the northern hemisphere. Although we lack reliable data on the mean annual $pCO_{2\,sea}$ in this region of high seasonal variability to substantiate such a flux, the model results leave little doubt that this component is required to explain why the observed meridional gradient in CO_2 concentration is substantially less than as predicted solely from industrial CO_2 emissions in the northern hemisphere.

Our estimate of the equatorial source is sensitive to the model's parameterization of vertical transport in the tropics. An unrealistically large increase in subgridscale vertical convection would be required, however, for the model to be compatible with the global average gas exchange coefficient, k_{ex}, deduced from radiocarbon data. Alternatively it is possible that vertical convection was modeled to be too strong in the tropics, leading to an overestimate in k_{equ}, perhaps by nearly one half. The model's lack of an explicit boundary layer is unlikely to have contributed to an underestimate of k_{equ}, but, it may have further contributed to an overestimate. Thus, unless gaps in our observations have seriously biased our estimates of the $pCO_{2\,sea}$ in tropical waters, the model result strongly suggests that the rate of air-sea exchange of CO_2 in the tropics is less than the global average.

The computed strength of the North Atlantic sink is insensitive to model errors in vertical transport and air-sea exchange, and is influenced to only a minor extent by the presumed strength of interhemispheric exchange. Measurements of the passive tracer, krypton-85, suggest that the interhemispheric exchange time in the model may be overestimated by as much as 20 percent. If so, the North Atlantic sink, including contributions associated with the equatorial source and industrial CO_2 sink, is overestimated by about 8 percent.

Further confirmation of this oceanic sink is afforded by our attempt to replace it in the model with a hypothetical terrestrial biospheric sink. Owing to the isotopic signature of terrestrial carbon, such a sink, irrespective of its precise location, must produce an appreciable meridional gradient in the annual mean of the reduced isotopic ratio, δ_{mean}. The model prediction of δ_{mean} with such a biospheric sink is distinctly less realistic than if the sink is oceanic.

We analyzed the possible errors in the formulation of the isotopic fields of the model, especially those arising from uncertainties in the average isotopic ratios and the source strength of industrial CO_2. These errors weaken our conclusion regarding a North Atlantic sink, but do not dismiss it. We note that it should be possible, with additional field studies, to obtain much better estimates of the isotopic composition of fossil fuel CO_2, and we urge that attempts be made to report rates of production of fossil fuels more accurately world-wide.

Given the uncertainties in estimating the strength and location of the North Atlantic sink and inadequate measurements of $pCO_{2\,sea}$ for all seasons in the northern oceans, we did not attempt to compute the average gas exchange coefficient for the region of this presumed sink. We indicated, however, that very large gas exchange rates or suspiciously large deficits in in $pCO_{2\,sea}$ would be needed to sustain a flux of the order of 1×10^{12} kgC yr^{-1}, if it operates only in the Atlantic Ocean as modeled.

The north-south gradient in atmospheric CO_2 would be easier to explain if an oceanic sink were to exist in the North Pacific Ocean as well as in the Atlantic. The mean annual $pCO_{2\,sea}$ fields in both northern oceans are poorly known, and we chose to assume a sink in the Atlantic Ocean on the general grounds that the large scale circulation of the oceans indicates that a sink should exist there. With more extensive direct oceanic measurements to establish regional means of $pCO_{2\,sea}$ in both oceans, and with additional very precise atmospheric CO_2 measurements near each ocean basin to establish the partitioning of the sink between the two oceans, it should be possible to provide a second critical test of the spatial variability of the gas exchange coefficient to complement our estimate for the tropical oceans. Given the small annual average air-sea gradients in CO_2 partial pressure which probably exist at the sea surface in high southern latitudes, the gas exchange rate in high latitudes can probably be estimated from CO_2 data only in the North Pacific and North Atlantic regions.

The strengths and locations of nonseasonal terrestrial biospheric sources and sinks of atmospheric CO_2 are less readily established by the model than are oceanic sources and sinks, because they are weaker and produce relatively still weaker patterns at our array of Pacific Ocean basin stations than do the oceanic sources and sinks. These patterns are also partially masked by spatial variations in atmospheric CO_2 produced as a consequence of the pronounced seasonal cycle of plants in the northern hemisphere. As our model indicates, the seasonality of plant growth produces CO_2 fluxes which interact with seasonal variations in atmospheric tracer transport so as to contribute significantly to the mean annual field of atmospheric CO_2.

We experienced particular difficulty in identifying releases of CO_2 by deforestation, agriculture, land use changes and other human activities because these releases which, together, we call "biospheric destruction", evidently occur mainly in the tropics and produce a nearly symmetric north-south pattern in atmospheric CO_2 with respect to the equator. From a comparison of the predicted and observed patterns of atmospheric CO_2 concentration and isotopic ratio at our array of observing stations in the Pacific Ocean basin, we were unable to distinguish between global bios-

pheric releases ranging from 2 to 5 $\times$ 10^{12} kgC yr^{-1}. We do not expect that data from a few additional observing stations situated close to where these fluxes principally occur would greatly improve our release estimates because, as the model predictions indicate, strong spatial gradients in atmospheric CO_2 and masking by industrial CO_2 emissions are likely to confuse the biospheric signals close to their sources.

Addressing the global carbon cycle balance in the first article in this series, Keeling et al. [this volume] showed that an examination of time series of atmospheric CO_2 offer an alternative approach to finding the global integral of destruction by providing evidence of how the net exchange of CO_2 between the biosphere and atmosphere has changed over the past century. In addition to destruction there must have been a transfer of CO_2 from the atmosphere to vegetation on land, large enough to explain both the observed rise in atmospheric CO_2 and a time progression in biospheric destruction that is positive and generally rising. By requiring that destruction increase in magnitude as indicated by direct evidence of deforestation and changing agricultural practices, one can estimate the global magnitudes of both fluxes. It is thus likely that further studies of the interannual variations in atmospheric CO_2, rather than three-dimensional modeling, will continue to provide a better means to establish this anthropogenic flux, second in importance to fossil fuel combustion.

The three-dimensional model was more successful in establishing that plant growth is being increasingly stimulated by a process which we call "biospheric fertilization". The CO_2 patterns produced by this stimulation, if proportional to mean annual net primary productivity (NPP) as we assumed, are asymmetrical with respect to the equator and are less attenuated than those of biospheric destruction in oceanic regions. If we eliminate this assumed stimulation flux from the model and augment oceanic CO_2 uptake by the same amount (2.1 $\times$ 10^{12} kgC yr^{-1}) so as to preserve the global atmospheric CO_2 budget for 1980, we noticeably degrade the model prediction of δ_{mean}. On the other hand, if we augment fertilization to twice the standard value (to 4.2 $\times$ 10^{12} kgC yr^{-1}), and also raise destruction to maintain the same net biospheric flux, the model prediction of δ_{mean} is improved in the tropics and only slightly degraded elsewhere. Furthermore with augmented fertilization the predicted deficit in $pCO_{2\,sea}$ in the North Atlantic is reduced by about 20 percent to a value that is better agreement with chemical oceanographic observations.

It seems likely that the three-dimensional model could be improved enough to provide a significantly more reliable test for fertilization. Our sensitivity tests indicate that the model prediction of δ_{mean} improves when we assume a variable gas exchange coefficient correlated with wind speed data rather than a constant exchange, and becomes still better (a reduced chi square of about 4), if we also assume a 20 percent decrease in interhemispheric exchange time effected by including subgridscale horizontal diffusion in the model.

The test for fertilization might also be more decisive if more extensive isotopic data were available. The data which we compared to model predictions were derived from measurements made during 1980 and 1984 combined into a single data set, because we lack sufficiently extensive data for either year alone to construct a good pole-to-pole profile of δ_{mean}. Measurements made since 1984 will soon result in an improved isotopic data base, but even longer records as well as records are needed, including isotopic data from additional observing stations.

Even if three-dimensional transport models calibrated with better data should prove to be inadequate to establish the strength of CO_2 fertilization, investigators in future years may be able to detect *changes* in fertilization by identifying *changes* in the isotopic field of CO_2 that are not explained by documented changes in fossil fuel combustion or in human activities affecting the terrestrial biosphere. Imperfections in the model formulations should not be so serious as to introduce significant errors in assessing *changes* from one period to another. Modeling errors could be made still smaller if account were taken of the interannual variability in the wind field and in NPP, by using meteorological and remote sensing satellite data for all recent years rather than for just the period of the Global Weather Experiment of 1978 and 1979.

It is important to establish the extent of fertilization in order to deduce the budget of atmospheric CO_2 correctly. All attempts so far to establish biospheric destruction have, in fact, addressed only the *net* exchange of CO_2 between the atmosphere and terrestrial biosphere. To determine the global integral of biospheric destruction, defined as the release of CO_2 occurring in direct response to human activities, one must know whether inadvertent fertilization by high atmospheric CO_2 concentrations is actually occurring, and, if so, precisely how much atmospheric CO_2 is being sequestered as a result. Even if three-dimensional atmospheric tracer transport modeling cannot establish the global magnitude of biospheric destruction, it may provide evidence to help distinguish between destruction and fertilization.

Improvements in three-dimensional modeling of the nonseasonal carbon cycle are likely to increase our understanding of oceanic processes more rapidly than of biospheric processes, because of the inherently lesser difficulty in sensing these oceanic signals at background stations monitoring atmospheric CO_2. Broad stationary patterns produced by oceanic CO_2 exchange have been deduced in this study with only minimal use of direct oceanic data. Although only briefly considered in the present study [see I.6], three-dimensional oceanic tracer transport models, analogous to the three-dimensional atmospheric model used in the present study, offer a potentially powerful additional tool to verify regional patterns in atmospheric CO_2. These models, only recently brought under development, if calibrated with precise oceanic carbon data in a manner similar to the calibration of our atmospheric transport model with our atmospheric CO_2 data, could provide a reliable, independent prediction of the air-sea exchange fluxes of CO_2 and a correct explanation of how this exchange is driven by the circulation of the oceans and by biological processes within the sea.

Eventually such oceanic models, if repeatedly verified with precise measurements of oceanic carbon, could also provide reliable determinations of the global uptake of industrial CO_2 by the oceans, even though this is a formidable undertaking, given the large background concentration of carbon compounds in ocean water. If this global uptake could be established, it would be possible to corroborate estimates of the global average biospheric contribution to the atmospheric CO_2 budget by difference.

The outlook for modeling of the terrestrial biosphere to deduce large scale and global scale behavior would become more favorable if remote sensing of the biosphere should later on provide demonstrably reliable estimates of regional CO_2 fluxes, for example, through improvements in the Kumar-Monteith model which we used to simulate NPP. Particularly valuable would be continued global coverage of the normalized difference vegetative index (NDVI), an essential parameter of this model.

To establish unambiguously how the natural carbon cycle is being altered on a global scale will require intense, sustained research efforts for many years. Modeling alone, however ingenious, will not be enough; there must be extensive gathering of oceanic, biospheric, and atmospheric data to corroborate model predictions as well.

The need to sustain both modeling studies and data collection over many decades, perhaps even over centuries, poses an unprecedented challenge to the scientific community and to human society, especially because much of the effort must be repetitious, some of it even boring. Nevertheless, the life support system of the human race, and indeed the fate of terrestrial life, is intimately linked to a carbon cycle that is likely to be profoundly altered in the coming decades by human activities. Recognizing this possibility, we may hope for continuing, even intensified efforts, to determine how that carbon cycle is changing.

Appendix

As an aid to readers of all four articles in this series, we append here an outline of these articles in the manner of a table of contents.

A THREE-DIMENSIONAL MODEL OF ATMOSPHERIC CO_2 TRANSPORT BASED ON OBSERVED WINDS: 1. ANALYSIS OF OBSERVATIONAL DATA

Charles D. Keeling, R. B. Bacastow, A. F. Carter, S. C. Piper, Timothy P. Whorf, Martin Heimann, Willem G. Mook, and Hans Roeloffzen

A THREE-DIMENSIONAL MODEL OF ATMOSPHERIC CO_2 TRANSPORT BASED ON OBSERVED WINDS: 2. MODEL DESCRIPTION AND SIMULATED TRACER EXPERIMENTS

Martin Heimann and Charles D. Keeling

A THREE DIMENSIONAL MODEL OF ATMOSPHERIC CO_2 TRANSPORT BASED ON OBSERVED WINDS: 3. SEASONAL CYCLE AND SYNOPTIC TIME SCALE VARIATIONS

Martin Heimann, Charles D. Keeling, and Compton J. Tucker

A THREE-DIMENSIONAL MODEL OF ATMOSPHERIC CO_2 TRANSPORT BASED ON OBSERVED WINDS: 4. MEAN ANNUAL GRADIENTS AND INTERANNUAL VARIATIONS

Charles D. Keeling, Stephen C. Piper, and Martin Heimann

Acknowledgments. Acknowledgments to the full study, of which this is the fourth part, are provided by Keeling et al. [this volume]. This work was supported financially by the Electric Power Research Institute under contracts RP2333 and RP8000 and by the National Science Foundation under grant ATM85–16939. The principal computations for this paper were carried out on the San Diego Supercomputer Center Cray X-MP.

References

Bevington, P. R., *Data Reduction and Error Analysis for the Physical Sciences,* 336 p., McGraw-Hill Book Co., NY, 1969.

Bolin, B, editor, *SCOPE 16: Carbon Cycle Modelling,* 390 p., John Wiley and Sons, New York, 1981.

Bolin, B., The Carbon Cycle, in *SCOPE 21: The Major Biogeochemical Cycles and Their Interactions,* edited by B. Bolin and R. B. Cook, p. 41–45, John Wiley and Sons, New York, 1983.

Bolin, B., How much CO_2 will remain in the atmosphere?, in *SCOPE 29: The Greenhouse Effect, Climatic Change, and Ecosystems,* edited by B. Bolin, B. R. Döös, J. Jäger, and R. A. Warrick, p. 93–155, John Wiley and Sons, New York, 1986.

Bolin, B., and Keeling, C. D., Large-scale atmospheric mixing as deduced from the seasonal and meridional variations of carbon dioxide, *Journal of Geophysical Research,* v. 68, p. 3899–3920, 1963.

Bolin, B., Degens, E. T., Duvigneaud, P., and Kempe, S., The global biogeochemical carbon cycle, in *SCOPE 13: The Global Carbon Cycle,* edited by B. Bolin, E. T. Degens, S. Kempe, and P. Ketner, p. 1–56, John Wiley and Sons, New York, 1979.

Broecker, W. S., Li, Y. H., and Peng, T. H., Carbon dioxide-Man's unseen artifact, in *Impingement of Man on the Oceans,* edited by D. W. Hood, p. 287–324, Wiley-Interscience, New York, 1971.

Broecker, W. S., and Takahashi, T., Is there a tie between atmospheric CO_2 content and ocean circulation, in *Climate Processes and Climate Sensitivity,* edited by J. E. Hansen and T. Takahashi, p. 314–326, Geophysical Monograph, v. 29, American Geophysical Union, Washington, DC, 1984.

Broecker, W. S., Ledwell, J. R., Takahashi, T., Weiss, R., Merlivat, L., Memery, L., Peng, T.-H., Jähne, B., and Münnich, K. O., Isotopic versus micrometeorologic ocean CO_2 fluxes: A serious conflict, *Journal of Geophysical Research,* v. 91, p. 10517–10527, 1986.

Conway, T. J., Tans, P., Waterman, L. S., Thoning, K. W., Masarie, K. A., and Gammon, R. H., Atmospheric carbon dioxide measurements in the remote global troposphere, 1981–1984, *Tellus,* v. 40B, p. 81–115, 1988.

Detwiler, R. P., and Hall, C. A. S., Tropical forests and the global carbon cycle, *Science,* v. 239, p. 42–47, 1988.

Eriksson, E., and Welander, P., On a mathematical model of the carbon cycle in nature, *Tellus,* v. 8, p. 155–175, 1956.

Fung, I., Prentice, K., Matthews, E., Lerner, J., and Russell, G., Three- dimensional tracer model study of atmospheric CO_2: Response to seasonal exchanges with the terrestrial biosphere, *Journal of Geophysical Research,* v. 88, p. 1281–1294, 1983.

Garrels, R. M., Mackenzie, F. T., and Hunt, C., *Chemical Cycles and the Global Environment: Assessing Human Influence,* 206 p., William Kaufmann, Inc., Los Altos, CA, 1975.

Goldschmidt, V. M., Carbon, in *Geochemistry,* edited by A. Muir, p. 340–719, Clarendon Press, Oxford, 1954.

Heimann, M., and Keeling, C. D., A three dimensional model of atmospheric CO_2 transport based on observed winds: 2. Model description and simulated tracer experiments, in *Aspects of Climate Variability in the Pacific and the Western Americas,* edited by D. H. Peterson, this volume, American Geophysical Union, Washington, DC, 1989.

Heimann, M., and Monfray, P., Spatial and temporal variations of the gas- exchange coefficient for CO_2: 1. Data analysis, to be submitted to *Journal of Geophysical Research,* 1989.

Heimann, M., Keeling, C. D., and Fung, I. Y., Simulating the atmospheric carbon dioxide distribution with a three-dimensional tracer model, in *The Changing Carbon Cycle: A Global Analysis,* edited by J. R. Trabalka and D. E. Reichle, p. 16–49, Springer-Verlag, New York, 1986.

Heimann, M., Keeling, C. D., and Tucker, C. J., A three dimensional model of atmospheric CO_2 transport based on observed winds: 3. Seasonal cycle and synoptic time scale variations, in *Aspects of Climate Variability in the Pacific and the Western Americas,* edited by D. H. Peterson, this volume, American Geophysical Union, Washington, DC, 1989.

Houghton, R. A., The global carbon cycle, *Science,* v. 241, p. 1736, 1988.

Houghton, R. A., Boone, R. D., Fruci, J. R., Hobbie, J. E., Melillo, J. M., Palm, C. A., Peterson, B. J., Shaver, G. R., and Woodwell, G. M., The flux of carbon from terrestrial ecosystems to the atmosphere in 1980 due to changes in land use: Geographic distribution of the global flux, *Tellus,* v. 39B, p. 122–139, 1987.

Hyson, P., and Pearman, G. I., Aspects of atmospheric CO_2 observations and modelling, *Carbon Dioxide and Climate: Australian Research,* publication compiled from papers presented at symposium entitled The Carbon Dioxide Climate Problem held in Canberra, Australia, September 15–17, 1980, p. 65–77, 1980.

Hyson, P., Fraser, P. J., and Pearman, G. I., A two dimensional transport simulation model for trace atmospheric constituents, *Journal of Geophysical Research,* v. 85, p. 4443–4456, 1980.

Jacob, D. J., Prather, M. J., Wofsy, S.C., and McElroy, M. B.,

Atmospheric distribution of ^{85}Kr simulated with a general circulation model, *Journal of Geophysical Research,* v. 92, p. 6614–6626, 1987.

Junge, C. E., Note on the exchange rate between the northern and southern hemisphere, *Tellus,* v. 14, p. 242–246, 1962.

Junge, C. E., and Czeplak, G., Some aspects of the seasonal variation of carbon dioxide and ozone, *Tellus,* v. 20, p. 422–434, 1968.

Keeling, C. D., Carbon dioxide in surface ocean waters: 4. Global distribution, *Journal of Geophysical Research,* v. 73, p. 4543–4553, 1968.

Keeling, C. D., and Heimann, M., Meridional eddy diffusion model of the transport of atmospheric carbon dioxide: 2. Mean annual carbon cycle, *Journal of Geophysical Research,* v. 91, p. 7782–7796, 1986.

Keeling, C. D., Carter, A. F., and Mook, W. G., Seasonal, latitudinal, and secular variations in the abundance and isotopic ratios of atmospheric CO_2: 2. Results from oceanographic cruises in the tropical Pacific ocean, *Journal of Geophysical Research,* v. 89, p. 4615–4628, 1984.

Keeling, C. D., Whorf, T. P., Wong, C. S., and Bellagay, R. D., The concentration of atmospheric carbon dioxide at Ocean Weather Station P from 1969 to 1981, *Journal of Geophysical Research,* v. 90, p. 10511–10528, 1985.

Keeling, C. D., Bacastow, R. B., Carter, A. F., Piper, S. C., Whorf, T. P., Heimann, M., Mook, W. G., and Roeloffzen, H., A three dimensional model of atmospheric CO_2 transport based on observed winds: 1. Analysis of observational data, in *Aspects of Climate Variability in the Pacific and the Western Americas,* edited by D. H. Peterson, this volume, American Geophysical Union, Washington, DC, 1989.

Liss, P. S., and Merlivat, L., Air-sea gas exchange rates: Introduction and synthesis, in *The Role of Air-Sea Exchange in Geochemical Cycling,* edited by P. Buat-Ménard, p. 113–127, D. Reidel Publishing Company, London, 1986.

Machta, L., Global scale atmospheric mixing, *Advances in Geophysics,* v. 18B, p. 33–56, 1974.

Marland, G., and Rotty, R. M., Carbon dioxide emissions from fossil fuels: A procedure for estimation and results for 1950–1982, *Tellus,* v. 36B, p. 232–261, 1984.

Marland, G., Rotty, R. M., and Treat, N. L., CO_2 from fossil fuel burning: Global distribution of emissions, *Tellus,* v. 37B, p. 243–258, 1985.

Mook, W. G., ^{13}C in atmospheric CO_2, *Netherlands Journal of Sea Research,* v. 20, p. 211–223, 1986.

Mook, W. G., Bommerson, J. C., and Staverman, W. H., Carbon isotope fractionation between dissolved bicarbonate and gaseous carbon dioxide, *Earth and Planetary Science Letters,* v. 22, p. 169–176, 1974.

Parratt, L. G., *Probability and Experimental Errors in Science,* 255 p., Dover Publications, Inc., New York, 1961.

Pearman, G. I., and Hyson, P., Global transport and inter-reservoir exchange of carbon dioxide with particular reference to stable isotopic distributions, *Journal of Atmospheric Chemistry,* v. 4, p. 81–124, 1986.

Pearman, G. I., Hyson, P., and Fraser, P. J., The global distribution of atmospheric carbon dioxide: 1. Aspects of observations and modeling, *Journal of Geophysical Research,* v. 88, p. 3581–3590, 1983.

Peng, T.-H., Takahashi, T., and Broecker, W. S., Seasonal variability of carbon dioxide, nutrients and oxygen in the northern North Atlantic surface water: Observations and a model, *Tellus,* v. 39B, p. 439–458, 1987.

Pond, S., and Pickard, G. L., *Introductory Dynamic Oceanography,* 329 p., Pergamon Press, New York, 1983.

Prather, M., McElroy, M., Wofsy, S., Russell, G., and Rind, D., Chemistry of the global troposphere: Fluorocarbons as tracers of air motion, *Journal of Geophysical Research,* v. 92, p. 6579–6613, 1987.

Rankama, K., and Sahama, T. G., *Geochemistry,* 912 p. University of Chicago Press, Chicago, 1950.

Revelle, R., and Suess, H. E., Carbon dioxide exchange between atmosphere and ocean, and the question of an increase of atmospheric CO_2 during the past decades, *Tellus,* v. 9, p. 18–27, 1957.

Rotty, R. M., A look at 1983 CO_2 emissions from fossil fuels, *Tellus,* v. 39B, p. 203–208, 1987a.

Rotty, R., Estimates of seasonal variation in fossil fuel CO_2 emissions, *Tellus,* v. 39B, p. 184–208, 1987b.

Skirrow, G., The Dissolved Gases-Carbon Dioxide, in *Chemical Oceanography,* Volume 2, edited by J. P. Riley and G. Skirrow, p. 1–192, Academic Press, New York, 1975.

Strain, B. R., and Cure, J. D., editors, *Direct Effects of Increasing Carbon Dioxide on Vegetation,* Report ER–0238, 286 p., U.S. Department of Energy, 1985.

Sundquist, E. T., Geological perspectives on carbon dioxide and the carbon cycle, in *The Carbon Cycle and Atmospheric CO_2: Natural Variations Archean to Present,* edited by E. T. Sundquist and W. S. Broecker, p. 5–59, American Geophysical Union, Washington, DC, 1985.

Takahashi, T., Chipman, D., and Volk, T., Geographical, seasonal and secular variations of the partial pressure of CO_2 in surface waters of North Atlantic Ocean: The results of the North Atlantic TTO Program, Proceedings, Carbon Dioxide Research Conference: Carbon Dioxide, Science, and Consensus, Office of Energy Research, U.S. Department of Energy, Washington, DC, p. II.123–II.145, 1983.

Takahashi, T., Ólafsson, J., Broecker, W. S., Goddard, J., Chipman, D. W., and White, J., Seasonal variability of the carbon-nutrient chemistry in the ocean areas west and north of Iceland, *Rit Fiskideildar,* v. 9, p. 20–36, 1985.

Tans, P., $^{13}C/^{12}C$ of industrial CO_2, in *SCOPE 16, Carbon Cycle Modelling,* edited by B. Bolin, p. 127–129, John Wiley and Sons, Chichester, 1981.

Weiss, R. F., Carbon dioxide in water and seawater: The solubility of a non- ideal gas, *Marine Chemistry,* v. 2, p. 203–215, 1974.

Woodwell, G. M., Whittaker, R. H., Reiners, W. A., Likens, G. E., Delwiche, C. C., and Botkin, D. B., The biota and the world carbon budget, *Science,* v. 199, p. 141–146, 1978.

Woodwell, G. M., Hobbie, J. E., Houghton, R. A., Melillo, J. M., Moore, B., Peterson, B. J., and Shaver, G. R., Global deforestation: Contribution to atmospheric carbon dioxide, *Science,* v. 222, p. 1081–1086, 1983.